

Christian-Albrechts-Universität zu Kiel

**Spring bloom dynamics in a coastal  
marine ecosystem:  
identification of key processes**

DISSERTATION

in fulfilment of the requirements for the degree “Dr. rer. nat.”  
of the Faculty of Mathematics and Natural Sciences  
at Kiel University

submitted by

**Tian Tian**

Kiel, 2011

First referee: Prof. Dr. Kai W. WIRTZ

Second referee: Prof. Dr. Andreas OSCHLIES

Date of the oral examination: 09 February 2011

Approved for publication: 09 February 2011

Prof. Dr. Lutz KIPP

Dean of the Faculty of Mathematics and Natural Sciences

---

## Spring bloom dynamics in a coastal marine ecosystem: identification of key processes

**Abstract:** The strong variability of coastal phytoplankton on many time and spatial scales still challenges our understanding of temperate shallow-water ecosystems. It is often believed that, in the absence of nutrient limitation and grazing pressure, underwater irradiance and lateral advection control the spatial distribution of phytoplankton and also the inter-annual variability of spring bloom timing. However, our quantitative knowledge about how light climate shapes spatio-temporal patterns in coastal-offshore Chlorophyll-*a* (Chl-*a*) concentrations and how algal blooms and related secondary production respond to meteorological and hydrographic variability, in space and time, is yet much limited. This study therefore aims at an integrated and quantitative understanding of coastal spring blooms. These not only constitute the major biological event in coastal marine ecosystems. Spring blooms also should facilitate a comprehensive factor analysis given their independence from complex nutrient dynamics in coastal seas. Given the high amount of related information available for the German Bight (GB), the study refers to the GB ecosystem as a representative case. Using an integrated data-modelling approach, the study illustrates (i) how typical bathymetric variations or local mixing and turbidity conditions shape the distribution of phytoplankton growth and loss (local factors), and (ii) how transport-related mechanisms control the bloom dynamics (non-local factors). A central question then will be how the relative importance of individual local and non-local factors vary across the GB and at seasonal to inter-annual scales.

The thesis is organised along three interlinked chapters. The first chapter addresses different formulas of light attenuation ( $K_d$ ) which are integrated into a coupled physical-biological model to obtain a more realistic light forcing for phytoplankton growth. A novel application using MERIS-derived  $K_d$  fields is proposed to constrain the parameterization. The coupled ecosystem model is calibrated and validated by in situ measured phytoplankton biomass and remotely sensed Chl-*a* concentrations. The contribution of suspended particulate matter (SPM) to variations in  $K_d$  is found to be crucial to reproduce the Chl-*a* spatial variability at the onset of the spring bloom. Secondly an integrated data set along a nearshore-offshore gradient is analysed to investigate how interannual changes in light, wind and frontal dynamics affected the timing and intensity of spring blooms during 2002–2005. A critical role of mesoscale spatial variations on coastal plankton dynamics in spring is demonstrated. Further, numerical experiments facilitate decomposing the relative importance of local production-loss balance (given changing light, mixing and temperature regimes) and lateral advection (under different circulation patterns) in determining the interannual variability of the spring bloom. Sensitivity tests examine how spring bloom dynamics respond to changing light and temperature with special focus on the fate of diatom production at contrasting sites, nearshore and offshore.

In coastal marine ecosystems, usually large spatial gradients in Chl-*a* are observed in the early and mid-bloom phase. Physical processes (wind induced vertical shear, tides, circulation, etc) determine underwater irradiance and lateral advection, which are bound to be responsible for the spatial variability in the early and mid-bloom. Bloom termination is regulated by an ensemble of mechanisms which differ between well-mixed coastal and stratified offshore waters. These determine the net rates of carbon export and recycling in the pelagic system. However, this spatial difference in production-loss balance can, in my model simulations, be impaired by temperature-mediated grazing, especially under a warming climate. This prediction needs further investigation by resolving the adaptive behaviour of a phytoplankton population under the stress by light- or nutrient-limitation like nearshore and offshore habitats. This work, based on both data-analysis and numerical experiments, underlines the demand for a realistic and mechanistic representation of marine (near-shore) ecosystems, which requires not only an accurate description of the spatial variations in physical processes but also how individual ecosystem components are affected by those factors. The integrated data-modelling approach provides a methodical basis for future models which resolve variability in key ecosystem variables on a larger spectrum of spatial and temporal scales in temperate coastal environments.

**Keywords:** physical-biological model; spring bloom dynamics; coastal marine ecosystem; nearshore-offshore gradient; interannual variability

---

## Die Frühlingsblüte in einem marinen, küstennahen Ökosystem: Identifikation von Schlüsselprozessen

### Kurzzusammenfassung:

Die große, in Raum und Zeit multi-skalige Variabilität in der Abundanz des küstennahen Phytoplanktons fordert immer noch unser Verständnis gemäßigter Flachwasser-Ökosysteme heraus. Es wird oft vermutet, daß bei Vernachlässigung von Nährstofflimitierung und Beweidungsdruck vor allem zwei Prozesse die räumliche Phytoplanktonverteilung und damit auch die Jahr-zu-Jahr Variabilität des Einsetzens der Frühlingsblüte kontrollieren: die Unterwasser-Strahlungsdichte und die laterale Advektion. Darüber hinaus ist das quantitative Wissen über die Wirkungsweise der lichtklimatischen Beeinflussung der raum-zeitlichen Muster küstennaher Chl-a Verteilungen sehr begrenzt und damit auch die Art und Weise, wie die Frühlingsblüte und die mit ihr verbundene Sekundärproduktion auf die räumliche und zeitliche Variabilität meteorologischer und hydrodynamischer Prozesse reagieren. Die vorliegende Studie zielt auf eine Integration des quantitativen Verständnisses der küstennahen Frühlingsblüte. Letztere wird dabei nicht nur als einzelnes biologisches Ereignis angesehen. Ihre Unabhängigkeit von der (in küstennahen Gewässern extrem komplexen) Nährstoffdynamik ermöglicht eine generalisierende wie auch auf Vollständigkeit bedachte Faktorenanalyse. Aufgrund der hohen Verfügbarkeit relevanter Information für die Deutschen Bucht (German Bight, GB), wurde das GB Ökosystem für diese Studie als charakteristisches Fallbeispiel ausgewählt. Die Verwendung von integrierte Modell-Daten Ansatz illustriert, (i) wie Variationen in der Meerestiefe, lokale Vermischungs- und Trübungsverhältnisse das Wachstum und Absterben von Phytoplankton (lokale Faktoren) beeinflussen und (ii) wie transportabhängige Mechanismen die Dynamik der Frühlingsblüte beeinflussen (nicht-lokale Faktoren). Eine zentrale Fragestellung der Arbeit ist die relative Bedeutung lokaler und nicht-lokaler Faktoren als Funktion relevanter räumlicher und zeitlicher (physikalischer) Gradienten in der Deutschen Bucht.

Die vorliegende Arbeit besteht aus drei Kapiteln. Das erste Kapitel behandelt die verschiedenen Formulierungen der Unterwasser-Lichtattenuation ( $K_d$ ). Ihre Integration in physikalisch-biologische Modelle ist notwendig, um eine realistischere Beschreibung der Lichteinwirkung auf das Phytoplanktonwachstum zu erhalten. Es wird eine neuartige Anwendung vorgestellt, welche auf MERIS-abgeleiteten  $K_d$  Feldern basiert und die Einschränkung von Freiheitsgraden bei der Parametrisierungen erlaubt. Das gekoppelte Ökosystemmodell wurde unter Verwendung von (in-situ) gemessenen Phytoplankton-Biomassen und fernerkundeten Chl-a Konzentrationen kalibriert und validiert. Die Ergebnisse zeigen, daß der Schwebstoffanteil an den  $K_d$  Schwankungen besonders während der Frühlingsblüte entscheidend für die richtige Vorhersage der räumlichen Variabilität

---

von Chl-*a* ist. Entlang eines küstennah-zu-küstenvorgelagerten Gradienten wurden verschiedene Datensätze integriert und ausgewertet, und somit der Einfluss jährlicher Schwankungen von Licht, Wind und Frontendynamik auf den Start-Zeitpunkt und die Intensität der Frühlingsblüte bestimmt. Die Ergebnisse untermauern die entscheidende Bedeutung von räumlichen Mesoskalen-Variationen für die küstennahe Planktodynamik während des Frühlings. Numerische Experimente erlauben zudem die Bestimmung der Relevanz lokaler Faktoren (Licht-, Vermischungs- und Temperatur Regimes) und der lateralen Advektion (verschiedene Zirkulationszustände) für verschiedene Jahre. Sensitivitätsstudien zeigen, inwieweit speziell die Dynamik der Frühlingsblüte von den Licht und Temperaturverhältnissen abhängt. Besonderer Fokus wird dabei auf die Diatomeen-Produktion im küstennahen Raum und in den küstenvorgelagerten Gebieten gelegt.

Küstennahe Ökosysteme im Meer weisen für gewöhnlich große räumliche Chl-*a* Gradienten auf, welche besonders zu den Zeiten der frühen bis mittleren Blüte zu beobachten sind. Physikalische Prozesse (windinduzierte vertikale Schubspannungen, Gezeiten, Zirkulation, etc.) steuern sowohl die Unterwasser-Strahlungsdichte, die Balance aus Resuspension und Sedimentation, wie auch den lateralen Transport, und beeinflussen daher die räumliche Variabilität während der frühen bis mittleren Blüte erheblich. Das Einsetzen der Blüte wird durch ein Ensemble von Mechanismen reguliert, welche sich in ihrer Wirksamkeit zwischen den gut gemischten küstennahen und den stratifizierten küstenvorgelagerten Gebieten unterscheiden. Diese Mechanismen prägen vor allem die Netto-Rate des Kohlenstoffexports und -Recyclings im Pelagial. Meine Modellsimulationen zeigen, daß räumliche Unterschiede in der Balance von Produktion und Verlustprozessen (Absinken, etc) vor allem in einem wärmeren Klimaszenario durch temperaturbedingt erhöhte Beweidung ausgeglichen werden können. Die Bestätigung dieser Prognose benötigt noch weitere Forschungsarbeit, insbesondere hinsichtlich der Einbeziehung des adaptiven Verhaltens von Phytoplankton-Populationen unter der Einwirkung von Licht- oder Nährstoffbelastung. Die vorliegende Arbeit basiert auf Analyse von Daten und numerischer Experimente. Sie unterstreicht den großen Bedarf einer realistischen und mechanistischen Beschreibung des (küstennahen) Meeres-Ökosystems. Diese Beschreibung beinhaltet nicht nur eine akkurate Reproduktion der räumlichen Variationen physikalischer Prozesse, sondern muss auch darstellen, wie die individuellen Ökosystem-Komponenten von diesen Faktoren beeinflusst werden. Der integrierte Modell-Daten Ansatz bietet eine methodische Basis für weitere Modellbeschreibungen, welche die große Variabilität in den Schlüsselvariablen küstennaher, gemäßigter Ökosysteme auf einem sehr breiten Spektrum räumlicher und zeitlicher Skalen beschreiben.

**Schlüsselwörter:**

Physikalisch-biologisches Modell; Dynamik der Frühlingsblüte; Primärproduktion; Küstennahes Meeres-Ökosystem; Jährliche Variabilität

# Contents

<b>Abstract</b>	<b>i</b>
<b>Kurzzusammenfassung</b>	<b>iii</b>
<b>Table of Contents</b>	<b>v</b>
<b>1 Overview</b>	<b>1</b>
1.1 Introduction . . . . .	1
1.1.1 The German Bight . . . . .	2
1.1.2 Phytoplankton spring blooms . . . . .	3
1.1.3 Factors controlling the spring bloom . . . . .	4
1.1.4 Integrated data-modelling approach . . . . .	7
1.2 Objectives . . . . .	8
1.3 Thesis outline . . . . .	8
<b>2 Importance of resuspended sediment dynamics for the phytoplankton spring bloom in a coastal marine ecosystem</b>	<b>11</b>
2.1 Introduction . . . . .	12
2.2 Methods . . . . .	14
2.2.1 Characteristics of the German Bight ecosystem . . . . .	14
2.2.2 Model description . . . . .	15
2.2.3 Light forcing . . . . .	17
2.2.4 Parameterization of the biological model . . . . .	19
2.3 Observations . . . . .	20
2.3.1 Satellite imagery . . . . .	20
2.3.2 Cruise observations . . . . .	22
2.3.3 Helgoland Roads data . . . . .	23
2.4 Results . . . . .	24
2.4.1 Spring bloom timing . . . . .	24
2.4.2 Horizontal and vertical gradients in Chl- <i>a</i> . . . . .	26
2.4.3 Mesoscale variabilities in $K_d$ and Chl- <i>a</i> . . . . .	28
2.5 Discussion . . . . .	31
2.5.1 Implications for spatial gradients of Chl- <i>a</i> . . . . .	31
2.5.2 SPM dynamics and spring bloom timing . . . . .	32
2.5.3 High frequency light fluctuations . . . . .	33
2.5.4 Data-model integration . . . . .	34
2.6 Conclusions . . . . .	35

<b>3</b>	<b>Factors controlling the onset of spring blooms in the German Bight 2002–2005: light, wind and stratification</b>	<b>37</b>
3.1	Introduction . . . . .	38
3.2	Data and methods . . . . .	39
3.2.1	Study area . . . . .	39
3.2.2	Station data sets . . . . .	40
3.2.3	Remote sensed SST and identification of tidal front . . . . .	42
3.3	Results . . . . .	43
3.3.1	Interannual changes in the onset of spring bloom . . . . .	43
3.3.2	Processes related to the observed bloom onset . . . . .	43
3.3.3	Variations of Chl:C ratio in mixing/light regimes . . . . .	48
3.3.4	Two effects of alterations in wind intensity . . . . .	48
3.4	Discussion . . . . .	50
3.4.1	Chl:C ratio as a proxy for algal eco-physiology . . . . .	51
3.4.2	Wind slack as a spring bloom trigger . . . . .	52
3.5	Conclusions . . . . .	53
<b>4</b>	<b>The sensitivity of coastal diatom spring bloom dynamics to meteorological and hydrographic variability</b>	<b>55</b>
4.1	Introduction . . . . .	56
4.2	Methods . . . . .	58
4.2.1	Characteristics of the German Bight ecosystem . . . . .	58
4.2.2	Model description . . . . .	59
4.2.3	Data integration . . . . .	61
4.2.4	Sensitivity tests . . . . .	64
4.3	Results . . . . .	65
4.3.1	Sensitivity of the HR bloom to local light and temperature variations . . . . .	65
4.3.2	Sensitivity of spatial gradients in Chl- <i>a</i> to light and lateral advection . . . . .	67
4.3.3	Sensitivity of diatom production to a warm climate . . . . .	70
4.4	Discussion . . . . .	72
4.4.1	Modelling environmental drivers . . . . .	72
4.4.2	What governs the HR bloom formation and affects the sensitivity to local forcing? . . . . .	73
4.4.3	Can temperature-mediated grazing modify the spatial sensitivity? . . . . .	75
4.5	Conclusions . . . . .	76
<b>5</b>	<b>Conclusions and perspectives</b>	<b>79</b>
<b>A</b>	<b>Biological model equations</b>	<b>83</b>
<b>B</b>	<b>Abbreviations</b>	<b>87</b>
	<b>Bibliography</b>	<b>89</b>
	<b>Acknowledgements</b>	<b>105</b>
	<b>Curriculum Vitae</b>	<b>107</b>
	<b>Erklärung</b>	<b>109</b>



# Chapter 1

## Overview

---

### 1.1 Introduction

Phytoplankton spring blooms start the production cycle in most temperate aquatic ecosystems. The role of phytoplankton primary production is to transform solar energy and nutrients into organic matter and provide food for higher trophic levels. Interannual changes in the timing of spring blooms may therefore cause a matching or mismatching of the energy flow from primary to herbivorous secondary producers and appear to be of crucial importance to the dynamics of the whole ecosystem (Cushing, 1990). The strong spatio-temporal variability of phytoplankton are prominent biological characteristics of coastal environments, documented by many long-term observation and research in a large class of estuaries and coastal systems, such as San Francisco Bay, Chesapeake Bay and the continental coastal areas of the North Sea (NS) (Harding and Program, 1994; Cloern, 1996; Patsch and Radach, 1997; Edwards and Richardson, 2004; Wiltshire et al., 2008). However, quantitative understanding of how algal spring blooms and related secondary production are sensitive to meteorological and hydrographic variability is yet much limited by the presence of changing physical forcings (e.g., tides, wind, precipitation and river runoff) on various spatio-temporal scales and the lack of sustained-high quality-real-time observations (Rixen et al., 2009). The predictive success of ecosystem models relies on if observations are available to constrain their parameterization (Murray, 2001; Schartau and Oschlies, 2003; Losa et al., 2004). Limited by monitoring capabilities and prediction skills, accurate representation of spring bloom dynamics along a coastal-ocean gradient is one of the most challenging aspects of ecosystem models (Tiedje et al., 2010).

The GB has been the focus of sustained investigation because it has high biological productivity and common features of many shallow coastal ecosystems that are influenced by natural and anthropogenic sources of variability (Radach et al., 1990; Hickel et al., 1993; Sündermann et al., 1999; Moll and Radach, 2003; Cloern and Jassby, 2009; Wiltshire et al., 2010). During preceding studies in the GB an integrated methodology has been developed by which field experiments, remote sensing, laboratory experiments and

numerical modelling were already (tentatively) combined. These studies contributed to a comprehensive understanding of recurrent seasonal features in coastal mass fluxes, nutrient cycles, as well as primary production (Moll, 1997; Pohlmann et al., 1999; Sündermann et al., 1999). In spite of these successes, an important ecological feature of this region, how environmental gradients in light, nutrients and temperature can drive physiological responses, shape spatio-temporal patterns in nearshore-offshore algal blooms and give rise to the inter-annual variation has been rarely addressed.

This study seeks an integrated and quantitative understanding of coastal spring blooms, as also briefly outlined in section 1.1.2. It will refer to the GB ecosystem as a representative case. Using an integrated data-modelling approach the study should illustrate (i) how typical bathymetric variations shape the distribution of phytoplankton growth and loss (local factors), and (ii) how representative transport-related mechanisms control the bloom dynamics (non-local factors). A short literature review in section 1.1.3 will introduce relevant physical, physiological and ecological factors that are relevant for the onset, intensity and the termination of the algal spring bloom. Although I will make use of physical forcing and biological parameter ranges characteristic for the GB, the purpose of this study is to develop more general insights into physical-biological mechanisms relevant for coastal marine systems. In this study I do not aim to systematically investigate errors and uncertainties in model simulations. Instead, available observations are rather qualitatively compared to model simulations to assess model validity ranges as a prerequisite for quantifying the time variable relevance of different processes as a mean to understand the often complex interaction between multiple factors and the apparent variations of their impacts. With this approach, I also attempt to highlight possible improvements of future models applied to coastal ecosystems.

### 1.1.1 The German Bight

The GB is a semi-enclosed marine area in the southeast of the NS with a mean depth of about 22 m and a total area of about 25000 km<sup>2</sup> (Sündermann et al., 1999). Inshore, the GB includes the Wadden Sea, characterized by tidal flats and shallow water depths. Large freshwater discharges arrive from the rivers Elbe (700 m<sup>3</sup> s<sup>-1</sup>), Weser (327 m<sup>3</sup> s<sup>-1</sup>), Ems (80 m<sup>3</sup> s<sup>-1</sup>) and several smaller rivers which together contribute a substantial load of particulate and dissolved substances to the ecosystem. The mean current pattern is anticlockwise driven by prevailing wind. Oceanic water masses enter the GB from the west and flow northward along the North Frisian coast. Circulation patterns can vary significantly, depending on wind forcing (Becker et al., 1999). Strong tidal currents (up to 2.5 m s<sup>-1</sup>) generate high kinetic energy dissipation and induce turbulent mixing and erosion of bottom sediments (Gayer et al., 2006). The horizontal transport of tidal currents contributes to a steady exchange of particulate and dissolved matter between the offshore waters and the Wadden Sea (Staneva et al., 2009). Changing wind, bottom

topography, buoyancy and flow-induced turbulence form a fragile balance, evoking considerable variability in dynamical features such as fronts, meanders and eddies (Dippner, 1993; Schrum, 1997; Langenberg, 1998). Water masses in the GB have a rather long residence time. Taken together, the GB is able to produce intense algal blooms. This capacity yields an extremely high net input of labile organic matter into the sediment (Luff and Pohlmann, 1995; Luff and Moll, 2004), which in part is even buried in deeper sediments, evading a fast turnover and remineralization (Beck et al., 2009; Holstein and Wirz, 2010).

### 1.1.2 Phytoplankton spring blooms

Spring blooms appear as rapid production and accumulation of phytoplankton biomass in most temperate aquatic ecosystems. Blooms are generally formed by one single species (Reid et al., 1990). In the NS, phytoplankton communities are dominated by diatoms (*Bacillariophyceae*) ranging in size from ca. 3–300  $\mu\text{m}$  in diameter, especially during the spring bloom (Reid et al., 1990; Wiltshire and Dürselen, 2004). Some important genera of diatoms are *Chaetoceros*, *Thalassiosira*, *Coscinodiscus*, *Rhizosolenia*, *Odontella*, *Leptocylindrus* and *Skeletonema* (Hoppenrath, 2004). The spring and presummer phytoplankton community sampled at the offshore station “Helgoland Roads” (HR) consists of over 90% diatoms (Wiltshire et al., 2008).

An accurate estimate of phytoplankton growth is essential because from a biogeochemical point of view it drives major element cycles and from an ecological point of view it determines the amount of food available for higher trophic levels. There are no direct in situ measurements of phytoplankton carbon biomass. It is usually estimated on the base of cell counts at species level. This approach is time-consuming and subject to inaccuracies (Wiltshire and Dürselen, 2004). Alternatively, Chl-*a* can be easily measured in the field and remotely sensed. Therefore, the concentration of Chl-*a* is used as the most common proxy variable of phytoplankton biomass. The C:Chl ratio of phytoplankton usually ranges from 25–50 g C:g Chl in healthy diatoms, microflagellates and dinoflagellates (Reid et al., 1990; Geider et al., 1998), but larger seasonal deviations are observed for the southern NS (Llewellyn et al., 2005).

The spatial distribution of phytoplankton biomass is governed by a variety of factors. Physical processes determine the light environment, water column stability and temperature. Chemical processes define the level of macro- and micro-nutrients. Finally, physiological or community level adaptation alters the sensitivity of cells or algae as a whole to environmental factors, and to ecological interactions (e.g. with grazers) (Reid et al., 1990). Thus, the development of a bloom results from a delicate balance between the amount of solar radiation received by a phytoplankton population, the availability of dissolved inorganic nutrients, and phytoplankton biomass losses associated with death, grazing and sedimentation (Smetacek and Passow, 1990; Platt et al., 1991; Townsend

*et al.*, 1994). In addition to local production-loss balance, lateral advection also seems to be an important loss/gain factor for net phytoplankton growth (*Lucas et al.*, 1999b).

In shallow coastal ecosystems, phytoplankton dynamics is especially variable because the water body is open to various external forcing originating from the adjacent open ocean, the seafloor, the atmosphere, or from terrestrial inputs. Therefore, spring bloom variability (in terms of timing, duration, and magnitude) occurs on many spatial and temporal scales. However, it is difficult to sort out the primary cause responsible for each blooming event because of the multitude of factors that are apparently involved. In the following, I discuss four major factors.

### 1.1.3 Factors controlling the spring bloom

#### Advection and turbulence

There are two distinct frontal systems in the GB: a seasonal tidal mixing front (thermal as well as haline) within the 25 m isobath and a permanent river plume front deriving mainly from the Elbe river in the southeast (*Dippner*, 1993). The intensity of the permanent salinity front reveals a strong seasonality with horizontal gradients increasing in spring, weakening in summer and again re-building in winter (*Becker et al.*, 1999). Between April and May, the weakening haline front initiates thermal stratification. Due to tidal mixing and often low wind speeds the front is strengthened in May along the 25 m isobath (*Becker et al.*, 1999), which separates well mixed coastal waters from stratified off-shore waters (*Dippner*, 1993). The dynamics and intensity of fronts are of great ecological importance in the GB because the spreading and dilution of nutrient-rich freshwater strongly depends on the frontal structure and the tidal-front entrainment and retention of plankton eventually enhances algal blooms (*Becker et al.*, 1999).

Wind field variability is largely responsible for the mesoscale variability of the frontal position and is the main factor influencing the inclination of the front and thus haline stratification. In contrast to south-westerly wind, which drives a more or less vertically uniform current, winds from other directions result in a much stronger vertical shear and support the development of haline stratification in the GB by differential advection (*Schrum*, 1997). Hydrological and meteorological conditions favour an intensification/weakening of advection primarily from the north-west NS towards Helgoland (*Schrum*, 1997; *Becker et al.*, 1999). As a consequence, Helgoland, a location relevant to this study as explained below, is subject to considerable shifts between offshore and coastal water influence (*Greve et al.*, 1996; *Wiltshire et al.*, 2010).

The GB is characterized by strong variability in wind stress since high and low wind speeds frequently alternate (*Sündermann et al.*, 1999). In shallow water tides or wind-induced sediment resuspension directly affects light penetration (*May et al.*, 2003). In

deeper water phytoplankton can begin to bloom prior to the vernal development of stratification, given a rapidly increasing solar radiation and a drop in wind speeds under a specific threshold which allow light penetrate deeper in the relatively clear and calm late-winter waters (Townsend et al., 1994).

### **Average light intensity**

In spring, light controls algal growth rather than nutrient availability, particularly near the coast and in estuaries (Postma, 1982; Cloern, 1987; Gallegos et al., 1990). According to classical theory, the spring bloom starts only when depth-integrated photosynthesis rate exceeds depth-integrated loss rate (e.g. Sverdrup, 1953; Smetacek and Passow, 1990). This requires that, in deep water systems, the upper mixed layer depth becomes shallower than some critical depth, or in turbid well-mixed waters, that the ratio of euphotic zone depth to water column depth exceeds a threshold value.

In the coastal ecosystem of the GB, the interannual variability in the timing of the spring bloom is mainly controlled by year-to-year differences in the amount of light energy penetrating the water column, either driven by cloud cover (Townsend et al., 1994; Byun et al., 2007) or by water turbidity (Colijn, 1982). The variation in turbidity is caused by river inputs of dissolved loads (humic substances), and by changes in the concentrations of SPM including particulate organic matter and/or resuspension of bottom sediments. In this shallow marine region, underwater light intensity is therefore horizontally dependent on the spatial SPM distribution and rapidly declines with depth (May et al., 2003; Xu et al., 2005). Indeed, first modelling studies suggested that integrating SPM fields to recalibrate water column light availability can considerably improve the prediction capability with respect to the spatial variability of the spring bloom (Muylaert et al., 2005; Byun et al., 2007).

### **Sedimentation**

Direct sedimentation of phytoplankton cells has been shown to be important during the spring bloom and tend to be enhanced by the formation of aggregates towards the end of the blooming period (Riebesell, 1991a; Brussaard et al., 1995; Smetacek, 1999; Passow and Alldredge, 1995). Early in a bloom, large cells of marine diatoms are able to avoid the theoretically high sinking rate, at least under optimal light and nutrient availability (Waite et al., 1992a). However, when nutrients become depleted, large cells approach the high sinking velocities as predicted by Stokes's law for which several physiological processes have been proposed (Waite et al., 1992a; Reynolds, 2006). Hence, nutrient exhaustion has been proposed to frequently terminate coastal spring blooms (Waite et al., 1992a).

In highly energetic environments like the GB, where turbulent energy in the water column is repeatedly generated by tidal currents and wind stress, shear can become the dominant mechanism controlling both particle aggregation and break-up (Riebesell, 1991a; Mäerz and Wirtz, 2009). Strong turbulence can also keep particles suspended or increase their concentration through resuspension of material from the bottom. However, in deeper offshore areas, after stratification of the water column, turbulent mixing in the upper mixed layer does not prevent diatoms move to deeper water column (Raven and Waite, 2004) and tidal mixing becomes largely restrained to the bottom layer (Riebesell, 1991a). Spatial gradients in diatoms sedimentation, therefore, mainly result from local geographic and hydrodynamic differences (Ehrenhauss et al., 2004).

### Herbivorous grazing

Copepod biomass usually starts to increase in the coastal area of the southern NS after the diatom spring bloom (Krause et al., 2003; Renz et al., 2008). Planktonic copepods comprise a major fraction of marine pelagic zooplankton biomass (larger than 0.2 mm) and form a crucial link between autotrophs and fish in the marine food web (Cushing, 1990). Small copepods of 0.5 to 1.5 mm length dominate the shallow area of the NS. The dominant species off the island of Helgoland are *Temora longicornis*, *Acartia clausi*, *Pseudocalanus elongatus*, *Paracalanus parvus* and *Centropages* spp. (Greve et al., 2004). In contrast to larger copepods from high latitudes, these species rely on a continuous food supply owing to limited capability of storing energy. When the primary food source becomes scarce in winter-spring, they adjust their feeding mode to utilize other prey with strong selection for cell  $> 12\mu\text{m}$ . Generally these are ciliates or other microzooplankton (Gentsch et al., 2009).

Microzooplankton is vigorously grazing nearshore in diatom-dominated waters in the shallow parts of the southern NS in spring (Stelfox-Widdicombe et al., 2004; Calbet, 2008). Microzooplankton (20–200 $\mu\text{m}$ ) is, at the same time, a competitor as well as a food source for copepods. Ciliates and non-pigmented dinoflagellates often dominate the microzooplankton community, in terms of numbers and biomass, and often occur at high abundance during diatom blooms (Tillmann and Hesse, 1998; Stelfox-Widdicombe et al., 2004; Sherr and Sherr, 2008). Ciliates are known to feed selectively at a predator-prey size ratio of 10 : 1 (Jonsson, 1986), while a number of heterotrophic dinoflagellate species can consume prey cells as large as themselves, or even larger (Hansen, 1992). This ability indicates a great potential grazing impact on large diatoms.

Many traditional food-web models proposed a direct energy transfer from phytoplankton to mesozooplankton (Cushing, 1990). It has recently become clear that microzooplankton, and especially ciliates, can contribute considerably to the diets of mesozooplankton (Aberle et al., 2007). Heterotrophic dinoflagellates may be able to survive during

non-bloom conditions and then grow up when phytoplankton is blooming. Due to fundamental differences in growth and grazing rates, accurate modelling of planktonic food webs needs to distinguish between grazing by micro- and meso-zooplankton (Calbet, 2008; Sherr and Sherr, 2008).

It was hypothesized that the spring bloom may be delayed because of grazing by overwintering copepod, in particular after relatively warm winters (Wiltshire and Manly, 2004). However, there is no significant relation between the increased copepod density at high temperatures and bloom phenology from the HR long term data sets (Wiltshire et al., 2008). One main obstacle in the analysis of plankton dynamics is the difficulty to separate between the influences of various external forcings like light and lateral advection in a highly dynamic area (Wiltshire et al., 2010).

#### 1.1.4 Integrated data-modelling approach

The GB belongs to the best monitored ecosystems worldwide. A long-term time series collected at HR since the 1960s is outstanding with respect to its length, measurement frequency, and the number of parameters determined. The time series allow for analysing short-term and seasonal phenomena and, most importantly, also long-term trends in meteorological, hydrographic, biogeochemical, and ecological key variables (Radach et al., 1990; Hickel et al., 1993; Greve et al., 1996; Raabe and Wiltshire, 2009; Wiltshire et al., 2010). In addition, a rapidly growing amount of in situ measurements at high temporal resolution and remotely sensed Chl becomes available for the coastal GB (Petersen et al., 2008). Time continuous observations derive from platforms of opportunities, regular transect cruises, or fixed pile stations across the GB. Especially, the Medium Resolution Imaging Spectrometer (MERIS), launched in 2002 (Rast et al., 1999), provided water-leaving radiance in nine visible channels (Bricaud et al., 1999). The main benefit from this increased spectral information is the product of the concentrations of Chl-*a* and total suspended matter (TSM) dry weight in case 2 waters, which are the key parameters to monitor the coastal ecosystem (Gons et al., 2005; Doerffer, 2007). Many of these observation platforms have recently been bundled within the “Coastal Observing System for Northern and Arctic Seas” (COSYNA). COSYNA has been started to construct a long-term observatory for the German part of the NS which via data assimilation should lead to various model-based products and synoptic assessments.

A central part of the COSYNA model system is the General Estuarine Transport Model (GETM). Advancing earlier hydrodynamic models for the GB, GETM has been used with nested grids and a spatial resolution of 1 km for the GB circulation between 2002 and 2005 (Stanev et al., 2009). Another primary application of models and data assimilation is the integration of MERIS TSM data into a numerical sediment transport model, which provides the state-of-the-art product of continuous SPM distribution for 2002 and 2003 in the NS (Dobrynin, 2009). The combination of numerical models with

high resolution (in space and time) observation systems, has raised opportunities to further the study of the GB ecosystems.

Comprehensive high-resolution information from observational and simulated data forms the basis of this work as it attempts to reconstruct the spring bloom dynamics of this shallow (tidal) ecosystem over the period of 2002–2005. With the model-based coupling of physical atmosphere-ocean processes and planktonic ecosystem dynamics, I aim to disentangle some of the complex interactions on short spatio-temporal scales. These generally evade direct assessment by current observation systems.

## 1.2 Objectives

The aim of this thesis is to obtain more insights into the evolution of coastal spring blooms and how it copes with currents, turbulence, temperature as well as SPM dynamics related underwater light climate. To this end, the primary drivers controlling the variability of spring blooms, in space and time, should be first determined and quantified from extensive observations. Various important physical characteristics of coastal environments such as tides, thermocline stratification as well as SPM dynamics should be taken into account to force the coupled ecosystem model. More specifically, the main objectives are:

1. to develop and test a coupled ecosystem model with special focus on the role of SPM and related light intensity as a trigger for spring blooms
2. to understand interannual changes in the timing and intensity of spring phytoplankton dynamics with special focus on the physical drivers, e.g., light, wind and frontal dynamics
3. to hindcast interannual variability of the GB spring bloom and examine the sensitivity of the ecosystem dynamics to meteorological and hydrographic variability and to quantify of the time- and space variable relative importance of physical, physiological and ecological factors

## 1.3 Thesis outline

This thesis is about data-analysis and modelling addressing the spring bloom dynamics in the GB. It consists of three manuscripts, original publications or submissions to scientific journals, in respective chapters. Each manuscript is stand-alone having it's own research question, methods and results.

**Chapter 2** demonstrates the importance of SPM on the phytoplankton spring bloom in the GB ecosystem. A major concern is the mechanism determining the onset of the



spring bloom. The chapter describes a depth-averaged coupled physical-biological model which is validated for the year 2003 when remote sensed data and in situ measurements are of high quality. A novelty in this study is the use of MERIS-derived data to constrain the parameterization of light attenuation. A comparison between data and simulations shows that the model, despite its simplicity, is capable of reproducing the development of the spring bloom. The chapter then highlights sensitivities of calculated phytoplankton growth to water depth, salinity fronts and SPM transport. It includes to assess the effect of different parameterizations of light attenuation by SPM and of high-frequency fluctuations in SPM on the spring bloom development.

A spatially resolved SPM distribution considerably improves model predictions for Chl-*a* spatial variability at the onset of the spring bloom. It is shown that a correct representation of water turbidity can be achieved either as a function of SPM concentration or of salinity. This outcome substantially facilitates future model studies for shallow coastal seas insofar as an approximation of light attenuation may be obtained from salinity fields.

**Chapter 3** presents data analysis on the spring bloom dynamics from 2002 to 2005 along a nearshore-offshore gradient in the GB. This study uses (offshore) long-term observations at HR, data from near-shore stations of the COSYNA observatory as well as satellite SST fields. Those data enable to assess the role of atmospheric and hydrographic forcing on the spring bloom dynamics. Phytoplankton Chl:C variations represent a highly variable biological response to mesoscale physical forcing. The analysis shows a predominant role of wind alterations in the bloom dynamics. This control ranges from event-scale to seasonal effects, as expressed in the locations of tidal fronts, or fluctuations in light penetration critical to algal growth. To my knowledge, this is the first study that combines information along a continuous transect representing a shallow (tidal) ecosystem. The interconnection between strong physical and biological variability underlines the importance of integrated monitoring systems, which provide a continuous and synoptic environmental state description, for model development and validations.

**Chapter 4** presents a numerical study on how local- and transport-related processes can influence bloom formation and patchiness (i.e. whether and where a bloom occurs) in a highly variable coastal marine environment. Referring to chapter 3, the study focuses on two consecutive years (2003, 2004) as representative cases for a strong coastal and a strong offshore influence on bloom development, respectively. Two major questions are: 1) how is the temporal and spatial variability of spring blooms affected by interannual changes in light climate and lateral advection? And, 2) how do predator-prey interactions respond to locally enhanced light intensities and temperatures along a nearshore-offshore transect? Sensitivity tests are performed to decompose the various environmental impacts on individual ecosystem components. The integration of observations and a numerical model not only demonstrates a critical role of mesoscale spatial variations in coastal plankton but also points to changing sensitivities of coastal

phytoplankton (i.e. species succession) to environmental drivers. This work provides a methodical basis for future models which resolve variability in key ecosystem variables on a larger spectrum of spatial and temporal scales in temperate coastal environments.

**Chapter 5** consists of a short comprehensive conclusion and perspectives on how to improve future coastal ecosystem models.

**Appendix** originally included in the publication of [Tian et al. \(2009\)](#).

## List of contained manuscripts

**Tian, T., Merico, A., Su, J., Staneva, J., Wiltshire, K., Wirtz, K., 2009. Importance of resuspended sediment dynamics for the phytoplankton spring bloom in a coastal marine ecosystem. *J. Sea Res.* 62 (4), 214–228**

The initial idea originates from the last author and myself. The model development, including coding, parameterization and validation, numerical experiments and interpretation of model results were done by myself. I wrote the manuscript, which was improved mainly by the second author. The physical forcing and model set-up were provided by the third and fourth authors. HR time series were provided by the fifth author.

**Tian, T., Su, J., Flöser, G., Wiltshire, K., Wirtz, K., 2010. Factors controlling the onset of spring blooms in the German Bight 2002–2005: light, wind and stratification. *Continental Shelf Res.*, under the 2nd round of reviews**

The initial idea originates from myself. Analysing and interpretation of the data were done by myself. I wrote the manuscript, which was improved by the co-authors. Pre-processed datasets of satellite SST, near-shore stations and HR samples were provided by the second, third and fourth authors, respectively.

**Tian, T., Wirtz, K., 2010. The sensitivity of coastal diatom spring bloom dynamics to meteorological and hydrographic variability. *Manuscript***

The initial idea originates from the co-author and myself. The numerical experiment and interpretation of the model results were done by myself. I wrote the manuscript, which was improved by the co-author.

## Chapter 2

# Importance of resuspended sediment dynamics for the phytoplankton spring bloom in a coastal marine ecosystem

---

**Abstract:** Accurate model estimates of primary production in coastal and shelf waters are challenged by the high temporal and spatial variability of suspended sediment dynamics. It is therefore still unclear how light climate shapes spatio-temporal patterns in near-coast Chlorophyll-*a* (Chl-*a*) concentration. In order to identify an effective representation of light extinction due to suspended particulate matter (SPM) in ecosystem models, we integrate different formulations of light attenuation into a coupled physical-biological model of the German Bight. The model describes Chl-*a* as well as phytoplankton-zooplankton interactions and calculates physical transport using the General Estuarine Transport Model (GETM). Parameters of the ecosystem module were calibrated using a 0D set-up constrained by available measurements at Helgoland Roads. The comparison between data and simulations shows that the model, despite its simplicity, is capable of reproducing the development of the spring bloom in 2003. We propose a novel application that uses MERIS-derived spatial data to constrain the parameterization of light extinction and compare different scenarios of light attenuation as determined by phytoplankton self-shading, yellow substances and SPM dynamics. Our work highlights the sensitivity of calculated autotrophic growth to water depth, salinity fronts and sediment transport. We found that the accuracy of SPM-forcing is only critical at the onset of the bloom.

**Keywords:** ecosystem model, phytoplankton spring bloom, light attenuation, SPM, remote sensing

## 2.1 Introduction

In eutrophic coastal ecosystems the underwater light conditions play an important role in initiating the phytoplankton spring bloom (Kromkamp et al., 1995; Cloern, 1999; Colijn and Cadée, 2003). In this season, light control is stronger than nutrient limitation, particularly near the coast and in estuaries (Postma, 1982; Cloern, 1987; Gallegos et al., 1990). The rate of vertical light attenuation is primarily determined by turbidity, which is caused by river inputs of dissolved loads, suspended particulate matter (SPM) and/or resuspension of bottom sediments. According to the classical theory, in deep water systems the spring bloom starts only when the upper mixed layer depth is shallower than some critical depth, above which depth-integrated photosynthesis exceeds the depth-integrated phytoplankton losses (e.g. Sverdrup, 1953; Smetacek and Passow, 1990; Nelson and Smith Jr, 1991; Platt et al., 1991; Kirk, 1994). In shallow and turbid areas underwater light is horizontally dependent on spatially distributed SPM and is rapidly attenuated with depth. Photosynthesis is confined to a relatively narrow photic zone and it is still not well understood how depth integrated losses are related to physical factors (e.g. vertical mixing) or grazing control (by zooplankton or filter-feeders). Therefore, the correct prediction of phytoplankton bloom timings with ecosystem models represents a challenging task.

To successfully model the spring bloom in a turbid coastal ecosystem, it is particularly crucial to reproduce with great accuracy the underwater light variability both in space and time (Xu et al., 2005; Allen et al., 2007; Arndt et al., 2007). In shallow waters, absorption and scattering properties are largely governed by phytoplankton with their seasonal cycles and short-term dynamics of SPM (from days to weeks). The relevance of SPM increases when water bodies are exposed to strong winds (Van Duin et al., 2001). However, many studies of phytoplankton production in coastal regions do not put much emphasis on the role of fluctuating light regimes (Ebenhöh et al., 1997; Moll, 1997, 1998; Chen et al., 1999). In particular, the coupling between primary production and sediment dynamics has been overlooked in the past, probably because the study of these processes pertains to scientific disciplines that have largely evolved independently (Desmit et al., 2005). Currently, the interaction between rapid light fluctuations and the seasonal cycle of phytoplankton growth are gaining more attention especially in tidal shallow estuaries (Lucas and Cloern, 2002; Desmit et al., 2005). Some studies focusing on coastal regions have already integrated temporally and/or spatially resolved SPM fields in order to recalibrate depth integrated light availability as an important constraint for autotrophic growth (Pohlmann et al., 1999; Van Duin et al., 2001; Muylaert et al., 2005; Xu and Hood, 2006; Byun et al., 2007).

Remote sensing data provide a unique means of validating model results in a temporally-averaged manner (Lacroix et al., 2007). However, these data have to be interpreted with

caution in turbid coastal waters due to problems connected with (1) atmospheric correction, and (2) absorption from non-algal particles and chromophoric dissolved organic matter (CDOM). In the Bay of Biscay, for instance, SeaWiFS-derived Chl-*a* concentration is considerably overestimated in January and February when SPM is high and light is low (Gohin et al., 2005). Estimates tend to be more realistic in May and June when most of the waters are optically dominated by Chl-*a* (Gohin et al., 2005). For simulating the late winter and spring blooms, Gohin et al. (2005) emphasised the need to assimilate sub-surface light attenuation (represented by  $K_d$ ) through a combination of Chl-*a* and SPM, which can be both observed in situ or assimilated from satellite into a coupled physical-biological model.

In this paper we investigate the importance of SPM and related underwater light climate on the spatial patterns of Chl-*a* and on the phytoplankton bloom timing in the German Bight ecosystem for the year 2003 when remote sensing and time-series data are of high quality. A careful analysis of temperature and salinity profiles showed us that the water column of the German Bight is well mixed during most of the year. Particularly during spring, stratification is extremely unlikely in this shallow system with strong tidal and wind mixing. Since our work concerns the mechanisms determining the onset of the spring bloom, for the sake of simplicity and computing efficiency, we adopted a depth-averaged coupled physical-biological model.

The major assumption of our modelling study is that light controls the spring blooms due to variations in SPM distribution. To evaluate this hypothesis, we performed two major experiments in order to assess:

1. the effect of different parameterizations of light attenuation by SPM;
2. the effect of high-frequency fluctuations in SPM on the development of the spring bloom.

Ecosystem models can be only applied with success if observations are available to constrain their parameterization (Lucas et al., 1999a; Murray and Parslow, 1999; Murray, 2001; Losa et al., 2004). In coastal systems, model validation is still difficult as reliable data for SPM and Chl-*a* with high temporal and spatial resolution are rare (Gallegos et al., 1990; van Raaphorst et al., 1998; Wild-Allen et al., 2002; Gohin et al., 2005; Allen et al., 2007; Lacroix et al., 2007; Krivtsov et al., 2008). We note here that we do not aim to investigate errors and uncertainties in model simulations, but, rather, we use available observations together with model simulations, to further the understanding of the effects of SPM dynamics and to highlight possible improvements of models applied to coastal ecosystems.

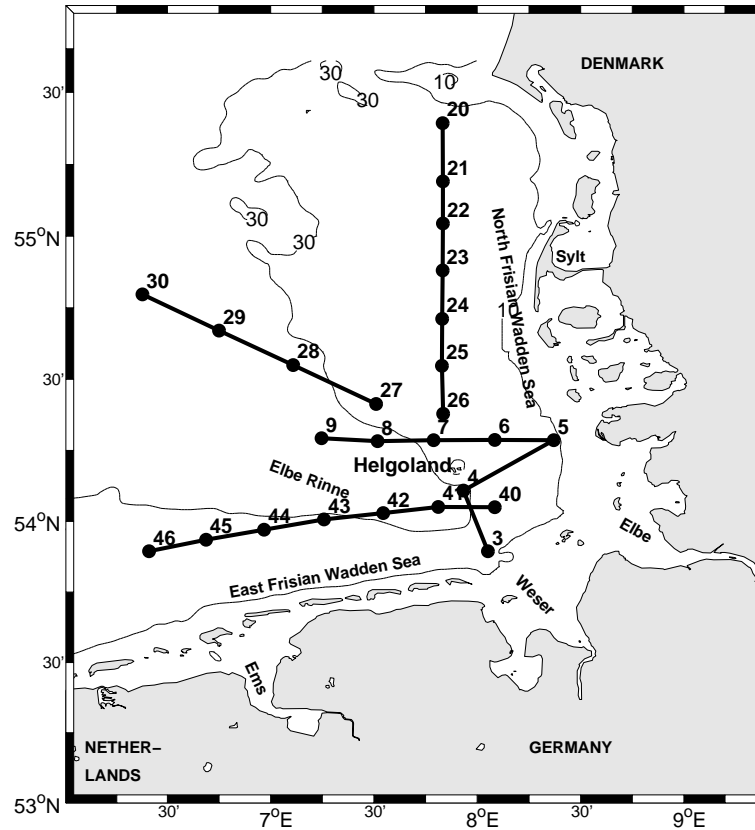


FIGURE 2.1: Map showing the study area (German Bight), with bathymetric contours (m). Four cruise transects are also indicated in the inner German Bight (Stations 3–9), in the North and East Frisian Wadden Sea (Stations 20–26 and 40–46), and in the central German Bight (Stations 27–30).

## 2.2 Methods

### 2.2.1 Characteristics of the German Bight ecosystem

The German Bight (Fig. 2.1) is a relatively shallow, semi-enclosed area of the southern North Sea with a mean depth of about 22 m (Sündermann et al., 1999). Inshore, the German Bight includes the Wadden Sea, characterised by extensive tidal mud flats and stretching along the 10 m isobath. Several large rivers flow into the German Bight, the most important of which are the Ems, the Weser and the Elbe. Tidal currents in the German Bight contribute to a steady exchange of particulate and dissolved matter between the North Sea waters and the Wadden Sea. Large variations in current speed ( $15\text{--}100\text{ cm s}^{-1}$ ) during a tidal cycle result in an alternation of particle settlement and resuspension (Brockmann and Dippner, 1987; Boon and Duineveld, 1996; Stanev et al., 2007). Long-term SPM deposition is observed southeast of Helgoland island ( $54.2^\circ\text{ N}$ ,  $7.9^\circ\text{ E}$ ) and in the Elbe Rinne. In the inner German Bight in the vicinity of the Elbe estuary the particulate matter loads including surface sediment are high. SPM concentration can reach  $50\text{ g m}^{-3}$  in February but it decreases towards April (Gayer et al.,

2006). Large freshwater inputs from the three major rivers contribute to the high levels of inorganic nutrients and the fluctuation of river outflow contributes to salinity fronts (Dippner, 1993). A narrow turbidity zone is always observed just outside the Wadden Sea extending from the Netherlands to Denmark. This distribution reflects the cross-shore salinity gradient along the Dutch and German coasts (Visser et al., 1991; van Raaphorst et al., 1998). By using idealized water column model simulations, Burchard et al. (2008) demonstrated that the difference between high and low SPM concentrations, respectively inside and outside the Wadden Sea, is due to horizontal water density gradients. van Beusekom et al. (2001) have observed that in areas of high SPM concentrations like the Wadden Sea, the pelagic primary production decreases with respect to the open sea due to high water turbidity. The analyses of station data in the German Wadden Sea suggest that underwater irradiance by far exceeds the effects of nutrients on the production of phytoplankton biomass (Tillmann et al., 2000; Colijn and Cadée, 2003). In summary, resuspension of sediment plays a crucial role in phytoplankton dynamics.

### 2.2.2 Model description

Our model represents various important physical characteristics of this coastal environment such as tides, thermohaline stratification and resuspended sediment dynamics and also includes a simple description of the lower trophic levels of the ecosystem. More specifically, the model consists of two coupled components: a box module of four biological compartments is coupled in an off-line mode with a depth-averaged transport model. The latter is based on the General Estuarine Transport Model (GETM). GETM is a free surface, baroclinic hydrostatic model solving salinity, temperature, water-level elevation and velocities in three dimensions (Burchard and Bolding, 2002). The model configuration is based on the nested North Sea-Baltic Sea system with a horizontal resolution of 3 nautical miles, including the German Bight domain ( $53.2^{\circ}$ – $55.6^{\circ}$  N,  $6.0^{\circ}$ – $9.1^{\circ}$  E) with a resolution of 1 km (Staneva et al., 2009). We adopted a four-component ecosystem model of the oceanic upper mixed layer, which includes phytoplankton ( $P$ ), zooplankton ( $Z$ ), nutrients ( $N$ ) and detritus ( $D$ ) based on the model of Fasham et al. (1993) and Popova (1995). In this model the nutrient compartment could refer to dissolved inorganic compounds of nitrogen, phosphorus or silicon. Chl- $a$  is derived from phytoplankton carbon concentration with a fixed ratio. Nutrients are supplied by vertical mixing between the surface mixed layer and the benthic boundary layer (fluffy layer), where the nutrient concentrations are assumed to be constant. All model equations are reported in Appendix A as well as model parameters (Table A.1). Hourly velocity, temperature and salinity fields produced by GETM were averaged through depth and time (to produce daily means). The coupled model system was forced daily on a uniform grid size of 1 km and discretely integrated using a time step of 15 minutes. We adopted the same coupled scheme of Wei et al. (2004) and Tian et al. (2005), and we refer the

TABLE 2.1: Summary of tested scenarios.

Scenarios	Light attenuation formulas ( $K_d$ )	Major causes of light fluctuation
S1 <sup>†</sup>	$K^{S1} = K_b + \varepsilon_{\text{SPM}} \cdot \sqrt{\text{SPM}} + \varepsilon_D \cdot D + \varepsilon_P \cdot P$	SPM dynamics, daily
S2	$K^{S2} = K_w - \varepsilon_{\text{CDOM}} \cdot \text{SAL} + \varepsilon_D \cdot D + \varepsilon_P \cdot P$	Frontal mixing, daily
S3 <sup>‡</sup>	$K^{S3} = \begin{cases} K'_d = K_g + K_{\text{ss}} \cdot P, \text{ for green light;} \\ K''_d = K_r + K_{\text{ss}} \cdot P, \text{ for red light;} \end{cases}$	Seasonal solar radiation, monthly

<sup>†</sup> Standard run

<sup>‡</sup>  $I_Z = \frac{1}{2} I_0 (e^{-K'_d \cdot z} + e^{-K''_d \cdot z})$

TABLE 2.2: Optical parameters in tested scenarios.

Parameter	Symbol	Values	Units	References
Attenuation for background turbidity	$K_b$	0.16	$\text{m}^{-1}$	Jerlov (1968)
Attenuation for pure seawater	$K_w^\dagger$	2.06	$\text{m}^{-1}$	Luyten et al. (1999)
Attenuation for green light	$K_g$	0.058	$\text{m}^{-1}$	Taylor et al. (1991)
Attenuation for red light	$K_r$	0.4	$\text{m}^{-1}$	Taylor et al. (1991)
Phytoplankton self-shading parameter	$K_{\text{ss}}$	0.03	$\text{m}^2 \text{mmol N}^{-1}$	Taylor et al. (1991)
Minimum attenuation coefficients	$K_{\text{min}}$		$\text{m}^{-1}$	
Slope factor in the linear relationship between the attenuation due to CDOM and salinity	$\varepsilon_{\text{CDOM}}$	0.05714	$\text{m}^{-1} \text{psu}^{-1}$	Luyten et al. (1999)
Diffuse attenuation cross section of SPM	$\varepsilon_{\text{SPM}}$	$0.2 \cdot 10^{-4}$	$\text{m}^2 \text{mg}^{-1}$	
Diffuse attenuation cross section of phytoplankton	$\varepsilon_P$	$8.0 \cdot 10^{-4}$	$\text{m}^2 \text{mg C}^{-1}$	
Diffuse attenuation cross section of detritus	$\varepsilon_D$	$2.0 \cdot 10^{-4}$	$\text{m}^2 \text{mg C}^{-1}$	

<sup>†</sup>  $K_w$  together with a linear function of salinity ( $-\varepsilon_{\text{CDOM}} \cdot \text{SAL}$ ) represents background turbidity in Eq. (2.4). The latter is assumed to decrease from coastal to ocean waters with increasing salinity.

reader to these studies for tests on the mass conserving properties. The potential density to determine variations in the MLD was computed from daily profiles with the 3D hydrodynamic model based on a density change from the ocean surface of 0.125 sigma units. The instantaneous production-loss balance in the biological model was vertically integrated over the MLD and divided by the water depth. All biological variables were initially considered uniform over the entire German Bight at values of  $P=0.05$ ,  $Z=0.2$ , and  $D=0.0$  in  $\text{mmol N m}^{-3}$  and  $N=12 \text{ mmol N m}^{-3}$ , roughly consistent with wintertime concentrations as inferred from the World Ocean Database 2005 (Boyer et al., 2006). No flux boundary conditions were applied at the open boundaries. After the 2-year spin-up a baseline simulation was carried out for the period January 2002–December 2005. To highlight the importance of the SPM distribution on the spatio-temporal variation of chlorophyll during spring we implemented a number of different scenarios. These were defined with respect to the choice of different light forcing (listed in Section 2.2.3). Our numerical experiments focused on the year 2003, which offered the best coverage in terms of MERIS imagery (details in Section 2.3.1).



### 2.2.3 Light forcing

The solar irradiance at the top of the atmosphere  $E(\theta, t)$  is a function of the local latitude  $\theta$  and time  $t$  with solar constant set to  $1367.0 \text{ W m}^{-2}$  (Ebenhöh et al., 1997). Photosynthetically active radiation (PAR) in a water body depends on the incident light at the water surface ( $I_0$ ), on the attenuation coefficient ( $K_d$ ) through the water column, and on depth ( $z$ ).  $I_0$  was calculated (Fasham et al., 1993) as

$$I_0(t) = E(\theta, t) \cdot F_c \cdot (1 - a) \cdot (1 - 0.7C). \quad (2.1)$$

where  $F_c$  represents the fraction of total irradiance at PAR wavelength (400-700nm), conventionally ranging from 0.40 and 0.50 (Byun and Cho, 2006),  $a$  represents air-sea transmittance due to albedo and evaporation, ranging from 0.05 to 0.40 (Sverdrup et al., 1942) and  $C$  represents the atmospheric transmittance as a function of cloudiness (Sverdrup et al., 1942). Cloudiness data were obtained at daily intervals from the meteorological climate model REMO (Meinke et al., 2004).  $F_c = 0.47$  and  $a = 0.1$  were chosen after the validation of the simulated  $I_0$  with observation from a land station at Helgoland. The underwater light field  $I_z$  ( $z$  =depth) was calculated by using the Beer-Lambert formula (e.g. Lorenzen, 1972):

$$I_z(t) = I_0(t) \cdot e^{-K_d \cdot z}. \quad (2.2)$$

Light limitation was calculated using a Michaelis-Menten formulation (see Appendix A). This does not account for photoinhibition. However, photoinhibition will rarely occur in turbid coastal waters (Ebenhöh et al., 1997; Ruardij et al., 1997; Tillmann et al., 2000). In most biogeochemical models, e.g. ERSEM (Byun et al., 2007) and COHERENS (Luyten et al., 1999), light attenuation  $K_d$  is taken as a linear combination of various water constituents,

$$K_d = K_b + K_{\text{sus}} \quad (2.3)$$

with

$$K_b = K_w - \varepsilon_{\text{CDOM}} \cdot \text{SAL} \quad (2.4)$$

and with

$$K_{\text{sus}} = \varepsilon_{\text{SPM}} \cdot \text{SPM} + \varepsilon_D \cdot D + \varepsilon_P \cdot P. \quad (2.5)$$

$K_b$  represents the attenuation for background turbidity (i.e. monochromatic light), which mainly accounts for seawater and CDOM. CDOM is constituted by dissolved or very small (non-sinking) particles which behaves conservatively like salinity in some estuaries and coastal systems (Bowers et al., 2004). Following Luyten et al. (1999, Part III), we assumed  $K_b$  to be a linear function of salinity.  $K_{\text{sus}}$  accounts for the attenuation attributed to optically active particles suspended in the water column. The three major components considered here are: SPM concentration ( $\text{mg m}^{-3}$ ), detritus  $D$

( $\text{mg C m}^{-3}$ ) and phytoplankton concentration  $P$  ( $\text{mg C m}^{-3}$ ). The  $\varepsilon$  terms in Eq. (2.5) are diffuse PAR attenuation cross-sections of each type of light attenuator, with units of  $\text{m}^2 \text{mg}^{-1}$ .  $P$  and  $D$  are state variables of the biological module and are assumed vertically homogeneous. The model is forced with surface SPM data because a vertical average would lead to an overestimation of light attenuation due to higher SPM concentration closer to the sea floor (Puls et al., 1999).

By using an empirically derived two-flow approximation (Joseph, 1950), Doerffer and Schiller (2007) developed a bio-optical model to compute the attenuation coefficient for downwelling irradiance ( $K_{\text{opt}}$ ) from MERIS band data:

$$K_{\text{opt}} = \sqrt{a_{\text{tot}}(a_{\text{tot}} + 2b_{b,\text{tot}})}, \quad (2.6)$$

where  $a_{\text{tot}}$  denotes the total absorption coefficient (comprising contributions of water, pigments and yellow substances) and  $b_{b,\text{tot}}$  denotes the backscattering coefficient of pure water and all particles in water. This empirical formulation indicates that absorption outweighs scattering. The linear approach described in Eq.(2.5) may therefore overestimate PAR attenuation when scattering becomes more important than absorption as, for instance, in coastal waters with high SPM loads. To avoid such an unrealistic attenuation of PAR, we considered a square root dependence on SPM, consistently with Eq. (2.6). Thus

$$K_d = K_b + \varepsilon_{\text{SPM}} \cdot \sqrt{\text{SPM}} + \varepsilon_D \cdot D + \varepsilon_P \cdot P. \quad (2.7)$$

In order to quantify the relative importance of SPM dynamics on the spatio-temporal variations of underwater light field, we explored three different scenarios as listed in Table 2.1. In scenario 1 (S1),  $K_b$  was set constant and simulated SPM concentrations (Gayer et al., 2006) were used in the form of daily mean surface values into Eq.(2.7). We considered S1 as the standard run. In scenario 2 (S2),  $K_b$  was explicitly expressed as Eq. (2.4) and the salinity data were supplied at daily intervals. In this case, the term for SPM was not considered in Eq.(2.7). In addition to the non-spectral light attenuation model (Eq.2.2) for S1 and S2, we adopted a conventional two-wave band (red and green) approximation to calculate  $I_z$  (equation see Table 2.1) allowing for the absorption by phytoplankton only (Taylor et al., 1991) in scenario 3 (S3). S1 represents SPM-dominated attenuation while S2 emphasizes turbidity induced by frontal mixing between freshwater and seawater. Both scenarios attempt to account for daily variability of turbidity. S3 can be seen as a reference case with constant turbidity, which is often applied to case 1 waters and when only seasonal variability in phytoplankton self-shading is taken into account. Under scenario 1, we considered three additional cases (S1a, S1b and S1c) aiming at exploring the impact of short-time (hourly) fluctuations in the SPM field. In case S1a we used a hourly model-generated SPM field combined with hourly physical forcing and tidal signals. In case S1b we used a diurnal cycle with maximum

SPM concentration at noon combined with daily physical forcing as for S1. In case S1c we used a diurnal cycle with minimum SPM concentration at noon with daily physical forcing as for S1. In all three cases, a daily mean SPM was considered in accordance to S1 (see inset in Fig. 2.5b). The antiphasing inherent to case S1b and S1c describes two extreme cases and helps exploring possible errors associated with the use of high frequency SPM (model) data.

## 2.2.4 Parameterization of the biological model

The parameter optimization procedure consisted of two steps. In the first step, we looked for the best set of parameter ranges using a 0D set up. In a second step, we looked for the best parameter set (within the previously identified best ranges) using the coupled model setup.

We applied a Monte Carlo-based method of parameter variation (Wirtz and Wiltshire, 2005) to a 0D version of the biological model under attenuation scenario 3. S3 was preferred because it refers to the case of constant turbidity, which does not account for temporal fluctuations driven by either SPM (S1) or salinity (S2). In other words, S3 served as a reference case. In order to choose the best parameter ranges, we recursively used the cost function of Wirtz and Wiltshire (2005) with the aim of minimizing the discrepancy between the simulated time-series of phytoplankton biomass and the observed data from January to May. The best parameter ranges found with this technique were consistent with published values (Wirtz and Wiltshire, 2005).

After having found the best parameter ranges, we recursively run the coupled model (still under scenario 3) to find the best parameter set within these now fixed ranges. At each iteration, the parameters were manually adjusted to obtain the best fit to observed bloom characteristics like maximum, minimum and slope increase in phytoplankton biomass. The final best set of biological parameters (Table A.1) was then used for exploring the other two scenarios with the coupled model.

For the light attenuation scenarios, most of the optical parameters were taken from literature (see Table 2.2) and only  $\varepsilon_{\text{SPM}}$ ,  $\varepsilon_D$  and  $\varepsilon_P$  were fine-tuned within the ranges of values provided by Luyten et al. (1999). To parameterize the specific attenuation coefficients for three major optically active suspended particles ( $K_{\text{sus}}$  in Eq. 2.5), we employed a number of constraints. In early spring, resuspended sediments are the major optical component of the German Bight waters. Water turbidity in March is therefore assumed to be critical to the onset of the spring bloom in April. Organic compounds like phytoplankton ( $P$ ) and detritus ( $D$ ) are negligible in winter. Firstly, we required that the March mean of simulated  $K^{\text{S1}}$  and  $K^{\text{S2}}$  by the coupled model with ready fixed parameters in the biological model was approximately equal to the March mean of the MERIS-derived light attenuation parameter  $K_{\text{min}}$  (see Section 2.3.1 for a definition).

Secondly, in  $K^{S2}$ ,  $\varepsilon_D$  and  $\varepsilon_P$  were tuned within the range from the North Sea modelling study by [Luyten et al. \(1999\)](#). The latter two  $\varepsilon$ -coefficients, thereby, were used to calculate  $K^{S1}$ . The impact due to organic particles was comparable between  $K^{S1}$  and  $K^{S2}$ , hence  $\varepsilon_{SPM}$  was calibrated as a control parameter for  $K^{S1}$ . A complete list of all optical parameters is given in Table 2.2.

## 2.3 Observations

### 2.3.1 Satellite imagery

Remote-sensing data were obtained by the MEdium Resolution Imaging Spectrometer (MERIS) on the ENVISAT satellite launched in 2002 ([Rast et al., 1999](#)). The MERIS sensor possesses certain advantages in detecting Chl-*a* in coastal waters ([Gons et al., 2005](#)). [Schiller and Doerffer \(1999\)](#) developed a neural-network multi-band spectral inversion technique for operational derivation of case 2 water properties from MERIS data, which is referred to as Case 2 Regional Processor. It starts at top of atmosphere radiances, performs atmospheric corrections, and outputs water leaving reflectance, inherent and apparent optical properties of the sea water as scattering lengths, absorption lengths, concentrations of Chl-*a* and total suspended matter (TSM) as well as  $K_{\min}$  ([Doerffer and Brockmann, 2006](#), User Manual).  $K_{\min}$  is calculated as the mean of those 3 bands which have minimum attenuation coefficient  $K_{\text{opt}}$  (Eq. 2.6). Note that direct optical measurements of the total absorption coefficient and of the backscattering coefficient are independent of the retrieval algorithm for water constituents (such as SPM and Chl-*a*). It is important to note here that observed Secchi depth (SD) in the transitional waters of the German Bight shows higher correlation with MERIS  $K_{\min}$  than with SeaWiFS single band  $K_{\text{opt}}$  at wavelength of 490 nm ([R. Doerffer, pers. comm.](#)).

We also focused our study on spring 2003 because a Chl-*a* algorithm was validated for 2003 MERIS imagery in North Sea waters ([Peters et al., 2005](#)). Specifically, for each month in 2003 approximately 35–45 Chl-*a* maps were integrated into monthly composite images at an output resolution of 2 km including parameters such as mean, maximum, minimum, standard deviation and number of images used ([Peters et al., 2005](#)). The monthly mean Chl-*a* images from MERIS represented a powerful data source for biogeochemical model validation in Belgian waters because of the excellent spatial coverage ([Lacroix et al., 2007](#)). We applied the same procedure for binning daily images of TSM and  $K_{\min}$  as it has been applied to obtain monthly mean Chl-*a* images. Monthly composites are compared for the period from February to April 2003 (Fig. 2.2). The cloud cover percentages were 65%, 48% and 33% in February, March and April, respectively. This visual inspection of MERIS images suggests that the German Bight is optically

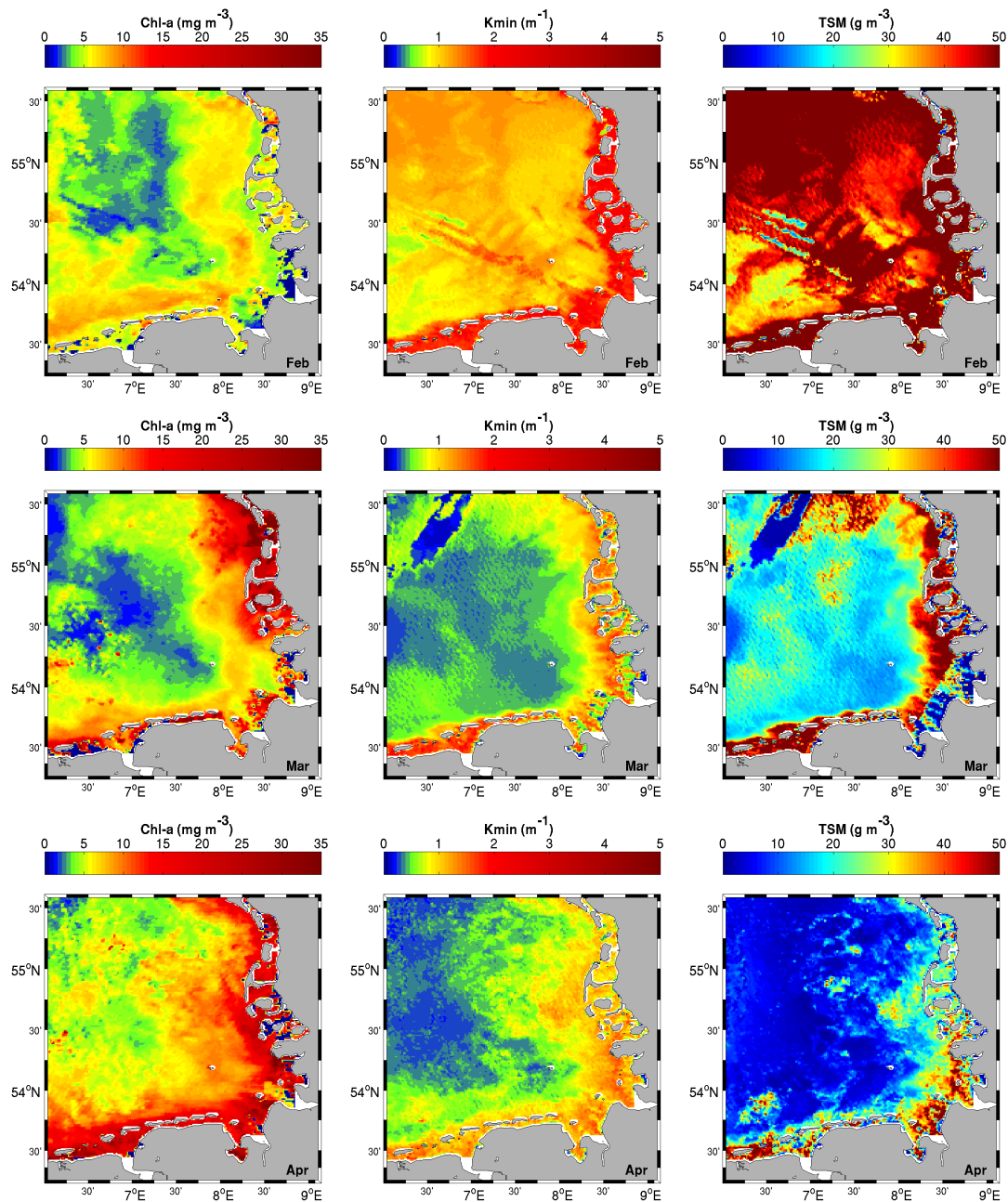


FIGURE 2.2: MERIS images showing (from top to bottom) a monthly evolution (February to April 2003) of Chl-*a* (left panels),  $K_{\min}$  (central panels) and TSM (right panels). The satellite images have been integrated into monthly composites and adapted to  $1 \text{ km} \times 1 \text{ km}$  model resolution.

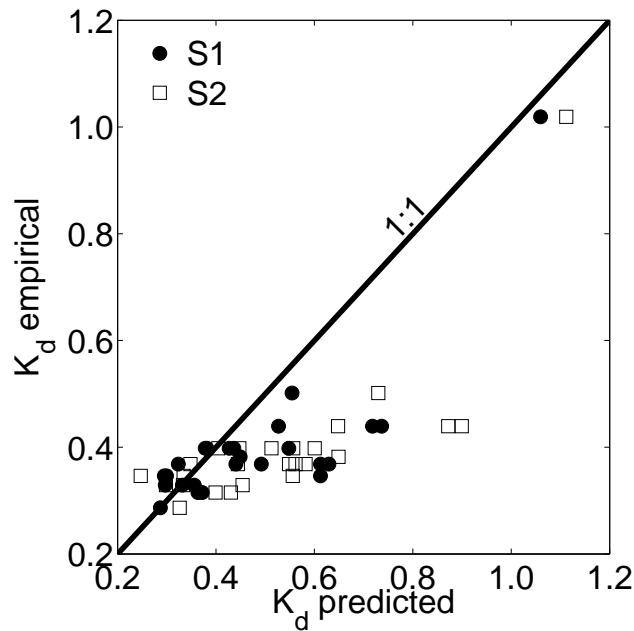


FIGURE 2.3: Phase diagram showing the vertical light attenuation coefficient  $K_d$  empirical (obtained from cruise measurement of Secchi depth, SD, using the empirical relationship  $K_d = 0.191 + 1.242 \cdot SD^{-1}$  of Tillmann et al. 2000) versus  $K_d$  predicted (obtained using Chl-*a*, SPM, detritus and salinity observed during the cruises and according to the formula of  $K^{S1}$  and  $K^{S2}$ , see Table 2.1).

dominated by suspended inorganic material in February and by Chl-*a* in April but is co-dominated by both suspended material and Chl-*a* in March depending on intermittent sediment resuspension driven by tides or wind-induced waves.

### 2.3.2 Cruise observations

In order to validate the  $K_d$  formulations for scenarios 1 and 2 ( $K^{S1}$  and  $K^{S2}$ , respectively), we used data from a measuring campaign that took place in the coastal waters of the North Sea from 22 April to 2 May 2003. Measurements include meteorological data, SD, Chl-*a* concentration, suspended matter and various optical parameters. The campaign covered 25 stations (divided into four transects) within our model domain (Fig. 2.1). At each station, water samples were taken at the surface (0.5–1 m), above/under the pycnocline (if detected) and at the bottom.

We performed a regression analysis between SD and SPM ( $SD^{-1} = 0.08 \cdot SPM + 0.11$  with correlation coefficient  $R = 0.96$ ) and between SD and Chl-*a* ( $SD^{-1} = 0.03 \cdot Chl-a + 0.08$  with correlation coefficient  $R = 0.68$ ). The high correlations suggest that the observed SPM, SD and Chl-*a* can be used to derive a light attenuation coefficient as follows. Tillmann et al. (2000) proposed an empirical formula that relates  $K_d$  to SD ( $K_d = 0.191 + 1.242 \cdot SD^{-1}$ ) for the German Wadden Sea. We used this formula in combination

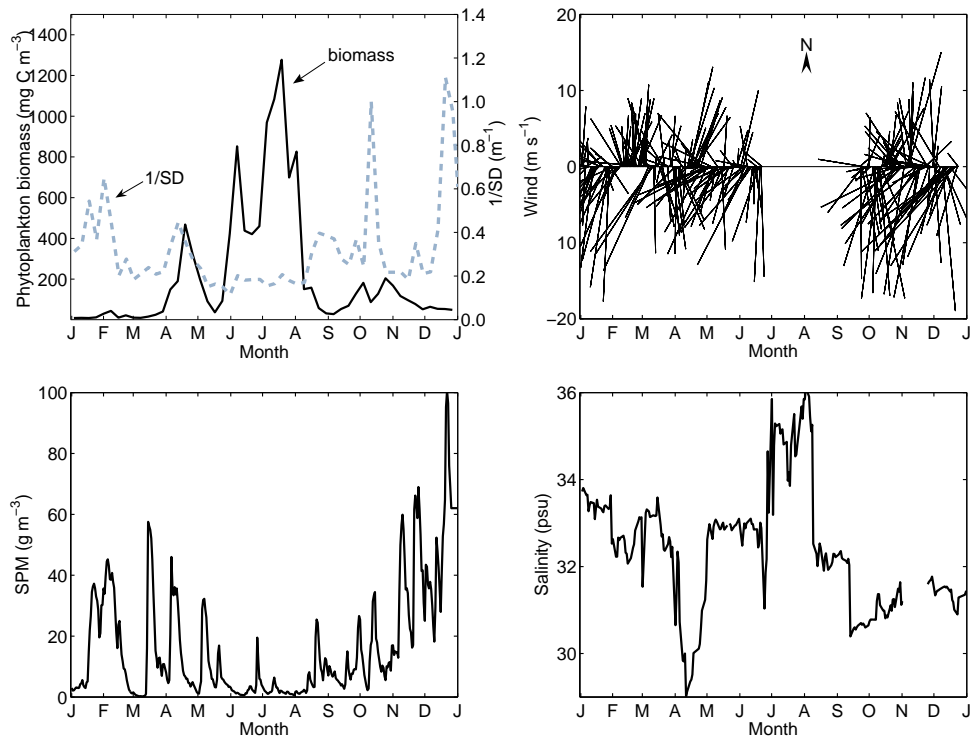


FIGURE 2.4: Helgoland Roads (HR) data for the year 2003. Top panels showing weekly mean of total phytoplankton biomass ( $\text{mg C m}^{-3}$ ) in solid line and inverse of Secchi depth ( $\text{m}^{-1}$ ) in dashed line (left hand) and daily observations of wind speed ( $\text{m s}^{-1}$ ) and direction (right hand); bottom panels showing daily model-derived SPM concentration ( $\text{g m}^{-3}$ ) at surface (right hand) and daily observation of salinity (psu, right hand).

with the observed SD during the cruises in order to obtain a reference attenuation coefficient that we called  $K_d$  empirical.  $K_d$  empirical was then compared with the calculated  $K_d$  (called  $K_d$  predicted) obtained with Chl-*a*, SPM, detritus and salinity observed during the cruises and according to scenarios 1 and 2 (respectively equations for  $K^{S1}$  and  $K^{S2}$  in Table 2.1). The comparison (Fig. 2.3) shows that predicted  $K^{S1}$  and  $K^{S2}$  provide good estimates at low attenuation coefficient values (below  $0.6 \text{ m}^{-1}$ ). At higher values, closer to shallower and turbid waters, the correlation is weaker likely due to higher uncertainties in the visual readings of SD.

### 2.3.3 Helgoland Roads data

A long-term pelagic monitoring program at Helgoland Roads (HR) station provides work-daily data of phytoplankton, zooplankton, salinity, temperature, water transparency, and dissolved nutrients (Wiltshire, 2004; Franke et al., 2004; Wiltshire et al., 2008) from surface water. The site is between 3 and 5 m deep and generally well mixed. Phytoplankton biomass has been estimated on the base of cell counts at species level

and is, thus, subject to inaccuracies (Wiltshire and Dürselen, 2004). However, we do not expect large effects of possible conversion errors on a logarithmic biomass scale.

Being roughly the inverse of the light extinction coefficient, SD reflects an approximate indication of light availability to photosynthesis. The data show a negative relationship between phytoplankton biomass and  $1/SD$  values (Fig. 2.4). The period when light penetrates deeper (i.e.  $1/SD$  declines) through the water column coincides with the time just prior to the spring bloom. Fig. 2.4 also shows observed wind speed, salinity data and modelled SPM data, which likely account for  $1/SD$  fluctuations in early spring as well as phytoplankton responses. The simulated SPM concentration dramatically increases up to  $50 \text{ g m}^{-3}$  just after a few days of strong northern winds in the last week of January. Correspondingly, light extinction ( $1/SD$ ) increases up to a factor of 3. After this event a small peak of phytoplankton biomass develops. SPM concentration decreases again when south winds become dominant in mid-March. In mid-April, salinity is low and SPM concentration is above  $50 \text{ g m}^{-3}$  for a few days. Light extinction increases at the same time and, consequently, the growing phase of phytoplankton ceases, leading to a period of strong fluctuations in biomass.

## 2.4 Results

### 2.4.1 Spring bloom timing

We ran the model for 2 years spin-up prior to 2003. Our simulations were focused on the first 120 days of the year 2003, with an emphasis on the effects of different representations of light attenuation (Table 2.1) on the spring bloom timing. We analysed only the temporal evolution in phytoplankton biomass extracted in a point with a water depth of 17.3 m close to Helgoland Roads Station ( $54.2^\circ \text{ N}$ ,  $7.9^\circ \text{ E}$ ) in order to compare model results with HR data (Fig. 2.5a). The simulations show similar patterns of variability (although mean values may be quite different) in all three scenarios. Scenario 3, which results have been obtained by carefully calibrating all parameters of the biological model, produces a gradual increase in algal biomass from early February with a peak reached in April, anticipating the starting of the spring bloom. By contrast, the uncalibrated scenarios S1 (the standard run) and S2 result in an underestimation of phytoplankton biomass in January, but produce a good agreement with the observed slopes and peaks of biomass from March to April. We suggest that in terms of water turbidity the winter period is better represented either by an explicit SPM field ( $K^{S1}$ ) or by the salinity field ( $K^{S2}$ ).

Fig. 2.5b shows three additional experiments compared to scenario 1. In the first experiment (S1a) the model is forced with hourly physical and light forcing. In the second experiment (S1b) the model is forced with a diurnal cycle with maximum at noon as



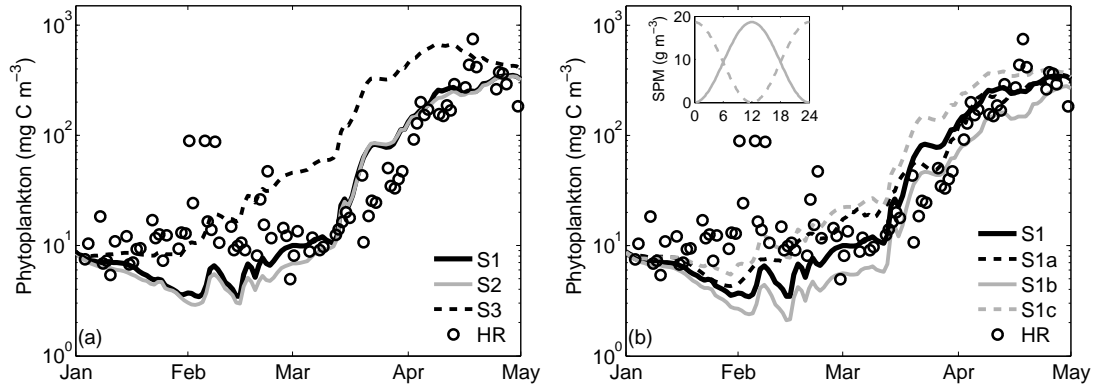


FIGURE 2.5: Helgoland Roads (HR) phytoplankton data (open circles) compared to simulated daily phytoplankton biomass ( $\text{mg C m}^{-3}$ ) for the first 120 days of the year 2003 under two kinds of experiments on  $K_d$  formulations. Panel (a) shows results of three scenarios under which  $K_d$  is dominated by different optical water properties: S1) SPM dynamics (black solid line), which we consider our standard run, S2) CDOM transport (grey solid line) and S3) phytoplankton self-shading (black dashed line). See details in Table 2.1. Panel (b) shows sensitivity tests of  $K^{S1}$  to different temporal fluctuations in SPM concentration. S1 represents the standard run, which is forced with a daily-averaged SPM (black solid line). S1a represents a run forced with hourly SPM concentration combined with hourly physical fields (black dashed line). In the other two cases, SPM fluctuates according to idealised diurnal cycles with maximum (S1b, solid grey line) or minimum (S1c, dashed grey line) values at noon (illustrated in the inset) and in combination with daily physical forcing as for S1.

opposed to a third experiment (S1c) in which the model is forced with a diurnal cycle with minimum at noon. All three experiments are compared to the standard run (i.e. S1 with daily-averaged forcing). We can infer that the case of S1a a minimum SPM at noon produces a higher phytoplankton concentration from February to mid-March with respect to S1c. By contrast, S1a a maximum SPM at noon produces a lower phytoplankton concentration from mid-March onwards with respect to S1b. These exercises suggest that diurnal cycles or hourly frequent fluctuations in SPM concentration play an importance role in initiating the spring bloom.

Using a Taylor diagram (Taylor, 2001), we compared phytoplankton biomass observed at HR station with all six numerical experiments in order to assess the possibility for biases in the model system and to highlight how closely the predicted spring bloom matches observations under different underwater light fields. Unsurprisingly (given no differences in model structure) all simulation tests show similar correlation with the observations, with correlation coefficient  $R = 0.8$  (Fig. 2.6). The exception is represented by S3 ( $R = 0.72$ ) because light limitation is not critical to the initiation of the spring bloom in this scenario (Fig. 2.5a). Good fits were produced under S1 and S2. The similarity between S1 and S2 (Fig. 2.5a) implies that daily variations of  $K^{S1}$  and  $K^{S2}$  are highly correlated. Hourly forcing (S1a) leads to the highest correlation with the observation ( $R = 0.85$ ). This indicates that the model accuracy in predicting biomass variability during spring is connected to the temporal resolution of the light field.

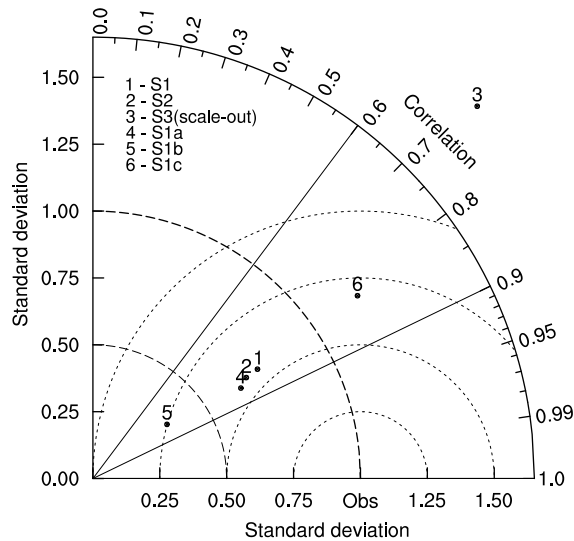


FIGURE 2.6: Taylor diagram assessing the different modelling tests with correlation and normalised standard deviation to Helgoland Roads data (Obs) for the first 120 days in 2003. The sensitivity tests are illustrated in Fig. 2.5 a and b. S3 is out of scale in the diagram with standard deviation  $\sigma = 2.90$  and correlation coefficient  $R = 0.72$ .

In summary, our coupled model was relatively robust in reproducing the spring bloom development in 2003 at Helgoland waters. The correlation between all simulations and observations is persistently high. Noteworthy, only scenario 3, which was previously used for model calibration in a 0D setup, leads to large deviations from the observations. In contrast, the formulation of  $K^{S1}$ , which takes into account SPM dynamics, clearly improved the model performance on initiating the spring bloom.

#### 2.4.2 Horizontal and vertical gradients in Chl-*a*

To characterise the horizontal and vertical distribution of phytoplankton during spring, we used Chl-*a* concentrations for the period from 23 to 30 April 2003 from four cruise transects (Fig. 2.7). The analyses of cruise data reveal three major features. Firstly, along the transect Inner German Bight (IGB, stations 6–9) and East Frisian Wadden Sea (EWS, stations 40, 41 and 46), and station 26 from the transect North Frisian Wadden Sea (NWS), bottom water Chl-*a* concentrations are generally higher than at surface. This implies that benthic processes may play a significant role in the waters surrounding Helgoland, at the end of the Elbe River Valley. Secondly, at stations 29 and 30 Chl-*a* concentrations are, in contrast, much higher at the surface than at the bottom. This suggests that in the Central German Bight (CGB), where water depth is about 40 m, the thermocline determines the vertical distribution of Chl-*a*. Another explanation is that the observed high surface Chl-*a* concentration may originate from the Dutch coastal waters flowing into the German Bight (Joint and Pomroy, 1993). Finally, in the other stations, Chl-*a* concentrations rarely show any vertical gradient, indicating

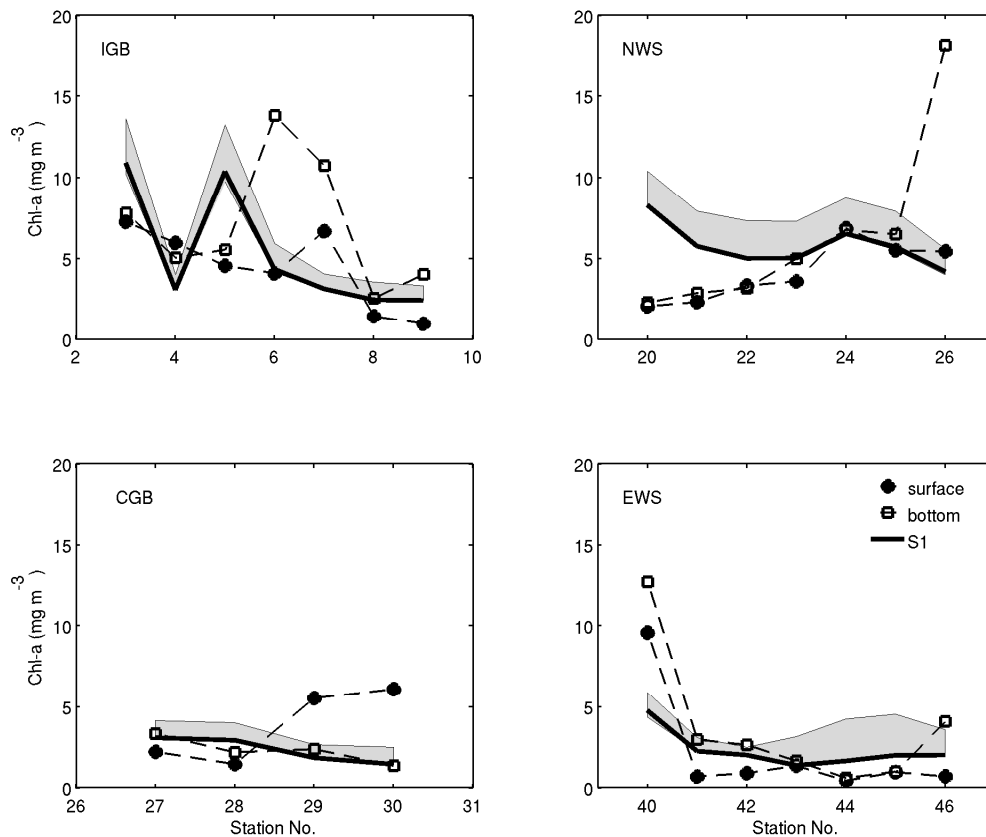


FIGURE 2.7: Simulated spatial distribution of Chl-*a* compared to cruise observations measured in surface (solid circles) and in bottom (open squares) waters during the cruise period from 23 to 30 April 2003. The observations are grouped into four transects covering respectively: the inner German Bight (IGB), the North Frisian Wadden Sea (NWS), the central German Bight (CGB), and the East Frisian Wadden Sea (EWS). The station numbers are reported in Fig. 2.1. The grey shadows mark the maximum and minimum amongst the simulations for S1, S2 and S3. The continuous solid lines represent the results of the standard run (S1).

that the water is well mixed off the NWS (along the 20 m isobath) and off the EWS (along the 25 m isobath).

From model results obtained under three scenarios, we extracted data along cruise transects covering the same temporal period of the observation. The simulated algal biomass ( $P$ ), originally computed in units of nitrogen, was converted into Chl-*a* in order to be compared with fluorescence observations. A constant C:Chl ratio of  $100 \text{ gC} (\text{gChl})^{-1}$  was obtained by fitting the model to the data. We also employed the empirical formula proposed by Cloern et al. (1995) to compute the environment-derived C:Chl ratios along the four transects. The C:Chl conversion factors for all of the stations show rather low spatial variability with a mean  $52.7 \pm 2.4 \text{ gC} (\text{gChl})^{-1}$  and a coefficient of variation of 4.6%. Horizontal gradients in the Chl-*a* concentration derived from our vertically-averaged model results under S1 match spatial differences in observed surface values rather well, particularly in the shallow waters off the Wadden Sea (NWS and EWS).

Exceptions to this general outcome include: (1) an overestimation at station 20 near the northern open boundary of the German Bight domain, and (2) an underestimation at station 40 between the Weser and Elbe River estuaries. For transect IGB, the model appears to perform well at least in the surface waters. A major misfit only arises at station 3 and 5 near the outlet of Weser and Elbe River mouths. As for transect CGB, S1 is able to capture the vertical mean at station 27 and 28, where only small discrepancies between surface and bottom were observed, and bottom observation at stations 29 and 30, where water is probably well stratified. The model has difficulties in reproducing realistic Chl-*a* concentration at stations 26 and 40. The three major scenarios S1, S2 and S3 produce quantitatively similar results especially in deeper waters, e.g. IGB and CGB. Under scenario 3, the simulations overestimate Chl-*a* in the shallow turbid waters, i.e. in all stations along NWS and in stations 43–46 along EWS. We note here that the procedure of finding the best parameter ranges with the 0D biological model (see Section 2.2.4) was applied to scenario 3, which does not account for water turbidity. This might explain the overestimation of Chl-*a* in the turbid Wadden Sea areas.

### 2.4.3 Mesoscale variabilities in $K_d$ and Chl-*a*

The main mesoscale feature in the German Bight is the mixture of the tidal front and plume front in the transitional area between estuaries and sea water. The spatial distributions of  $K_d$  and Chl-*a* also present this mesoscale feature. A central aspect in our work was to distinguish the effect of different spatial gradients produced by various formulations of light attenuation. For all scenarios (S1, S2 and S3), we produced March and April means of simulated light attenuation coefficients and Chl-*a* field (vertically averaged). These spatial maps were compared (Figs. 2.8 and 2.9) to monthly composites MERIS-derived surface Chl-*a* and  $K_{\min}$  (Fig. 2.2). It is worthwhile to point out here that the MERIS March composite is mostly represented by scenes of the second half of the month which had 82% clear skies. Therefore we show the monthly averaged results over the same period (i.e. the second half of March) in Fig. 2.8. Both S1 and S2 predict low Chl-*a* in the deeper waters off the EWS and the CGB. However,  $K_d$  in S1 is a bit higher than that in S2 in CGB. As we see from Fig. 2.5 we can infer that enhanced turbidity in winter imposes strong light limitation on the spring bloom development both in terms of timing and magnitude. A winter storm can raise SPM concentration to values 10 times higher than those under calm conditions (Fig. 2.4), and these effects of sediment movement can extend to the whole German Bight, as seen from satellite image of TSM in February (Fig. 2.2). In S2, light attenuation is approximated on the base of salinity gradients, which reflects the conservative character of salinity but can not present the intermittent sediment resuspension, particularly in the open waters of the German Bight. Although Fig. 2.5a shows the similarity between S1 and S2 at Helgoland water, Chl-*a* concentration in deeper waters appears higher in S2 and the spatial gradient turn out to be smaller compared to under scenario 1, especially in April (Fig. 2.9).

March 2003

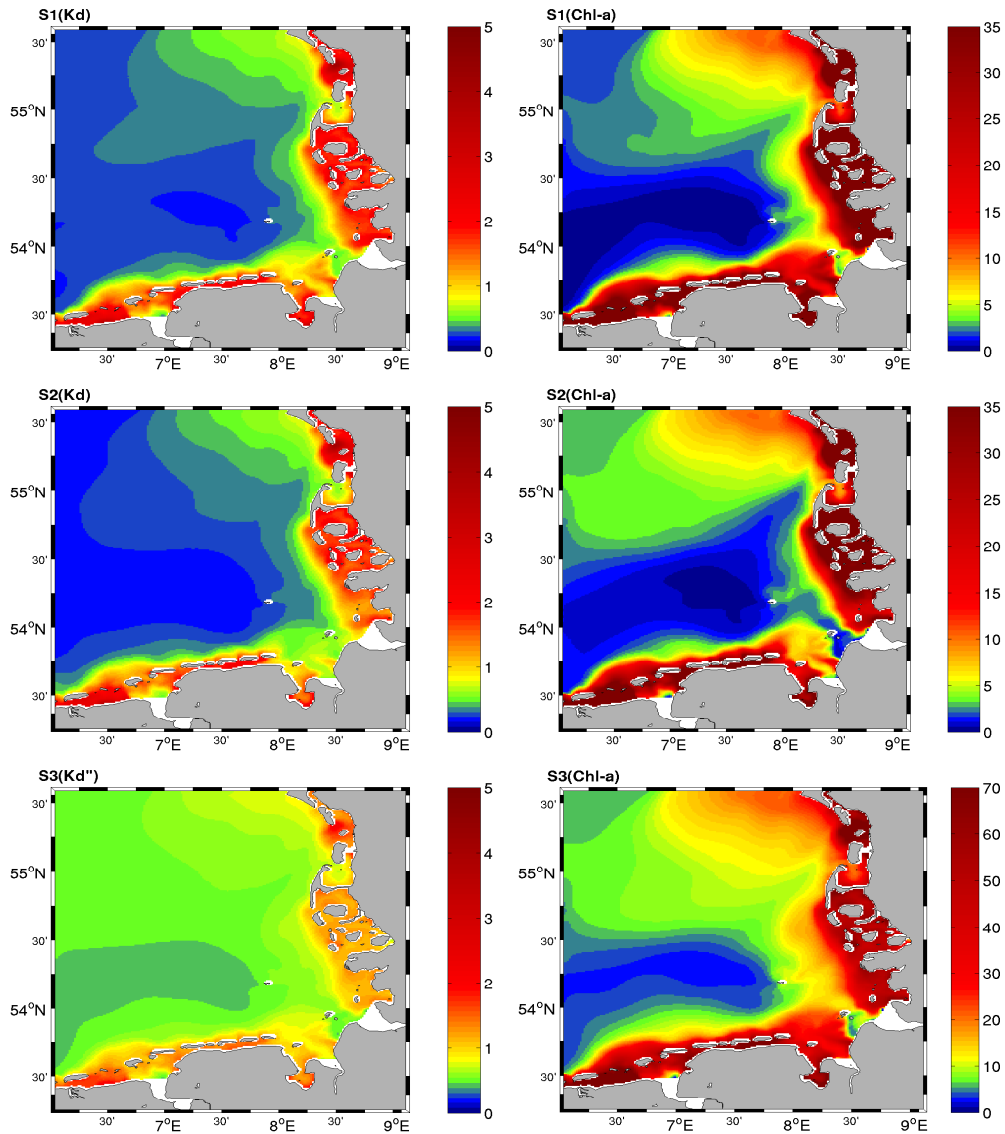


FIGURE 2.8: The left and right panels show the simulated vertical light attenuation coefficient  $K_d$  ( $\text{m}^{-1}$ ) and vertically averaged Chl-*a* concentration ( $\text{mg m}^{-3}$ ) averaged over the second half of March 2003. The simulations of the three scenarios (S1, S2 and S3) are compared from top to bottom. Scenarios are listed in Table 2.1. The remote-sensed data are shown in Fig. 2.2. We note for S3 that  $K_d''$  represents only the contribution of red light and that the color bar for Chl-*a* concentration is two times higher than the ones in S1 and S2.

April 2003

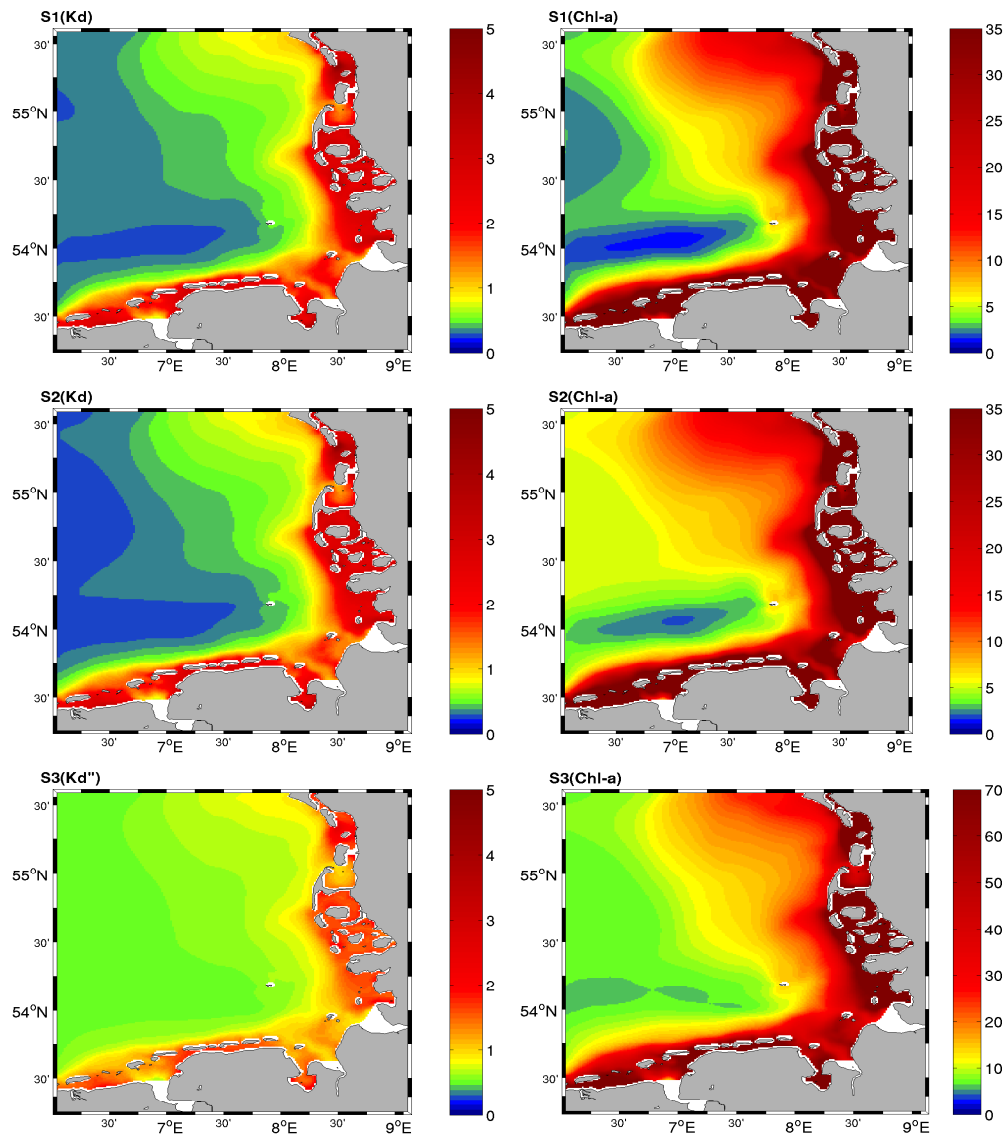


FIGURE 2.9: The left and right panels show the simulated vertical light attenuation coefficient  $K_d$  ( $\text{m}^{-1}$ ) and vertically averaged Chl-a concentration in monthly mean ( $\text{mg m}^{-3}$ ) for April 2003. The simulations of the three scenarios (S1, S2 and S3) are compared from top to bottom. Scenarios are listed in Table 2.1. The remote-sensed data are shown in Fig. 2.2. We note for S3 that  $K_d''$  represents only the contribution of red light and that the color bar for Chl-a concentration is two times higher than the ones in S1 and S2.

S3 produced Chl-*a* concentrations a factor of two higher than the other scenarios. This may be due to the fact that the parameterization of the biological module was optimized in a 0D setup without accounting for water turbidity (see Section 2.2.4). In all scenarios, the horizontal gradients of  $K_d$  and Chl-*a* reflect quite accurately depth-dependent, along the 25 m isobaths (Fig. 2.1), especially in April, also seen from satellite images (Fig. 2.2). However, the spatial gradient in Chl-*a* concentration between the German Wadden Sea and the off-shore water at the 10 m isobath is considerably overestimated in all experiments. Besides, simulated Chl-*a* is too high at the north open boundary and too low at the western open boundary. Also, a strikingly high Chl-*a* plume off the Dutch coast (Fig. 2.2) is not captured. These discrepancies are likely due to the model condition of no flux at the boundary.

## 2.5 Discussion

### 2.5.1 Implications for spatial gradients of Chl-*a*

The three tested scenarios of light attenuation (S1, S2 and S3) produced similar spatial gradients of Chl-*a*, particularly in shallow waters off the Wadden Sea (Figs. 2.8 and 2.9). At a given light extinction coefficient, the depth averaged difference between photosynthesis and respiration in shallow coastal water is always higher than that over the upper mixed layer of off-shore waters because PAR in the water column provides an important link between bathymetry and phytoplankton net growth (Lucas et al., 2009). Hence, the persistently higher Chl-*a* concentrations reproduced by our model in nearshore waters are consistent with the general understanding of the German Bight system. A combined effect of bathymetry and tidal mixing leads to the formation of a tidal front in April along the 25 m isobath (Dippner, 1993). In the German Bight, the tidal front separates the well mixed coastal waters (with higher Chl-*a* concentration) from the stratified off-shore waters (with lower Chl-*a* concentration). Therefore, physical factors (the tidal front in this case) control the chlorophyll spatial pattern in April. However, in shallow waters sediment re-suspension also plays an important role, thus making photosynthesis highly sensitive to light availability on daily timescales.

What process can explain low Chl-*a* concentrations in the CGB? In most temperate marine systems, the development of a stable thermocline is the factor that triggers the onset of the spring bloom, by reducing the effective mixing depth of the water column and thus enhancing the mean light level available to phytoplankton (Townsend et al., 1994; Huisman et al., 1999). However, our modelling exercises focused primarily on pre-bloom before the thermal stratification is formed (Staneva et al., 2009). Furthermore, Iriarte and Purdie (2004) found that mean water column irradiance was the main factor controlling the spring bloom timing based on 5 years observations of main spring bloom events in the Southampton estuary. They also showed that the phenomenon is highly

related to surface incident radiation, which is affected by cloud cover, rainfall levels, and water turbidity rather than water stratification. At a station outside the estuary mouth (station Calshot), the spring bloom (defined as  $\text{Chl-}a \geq 10 \text{ mg m}^{-3}$ ) started only when  $K_d$  had decreased to values of ca.  $0.5 \text{ m}^{-1}$ . Under those conditions, the entire water column (10 m deep) was above the 1% light depth. In the CGB, an entire water column (more than 30 m deep) above the 1% light depth would correspond to a  $K_d$  of 0.15. However,  $K_b$  in  $K^{\text{S1}}$  is set constant to 0.16. Clearly in the region deeper than 30 m, the critical depth ( $\leq 1\%$  light depth) is always within the water column and fluctuates with perturbation in light environment due to sediment resuspension (see Figs. 2.8 and 2.9 for S1). The low Chl-*a* concentrations in CGB may also be related to the use of a single parameter set of the N-based biological module. We suggest that a more realistic spatial representation of Chl-*a* may require variable C, N and Chl stoichiometry (e.g. Cloern et al., 1995; Pahlow, 2005) or the adoption of adaptive-based approaches (Pahlow et al., 2008).

### 2.5.2 SPM dynamics and spring bloom timing

Fig. 2.5a shows that scenarios 1 and 2 produce an unrealistic slight decline in phytoplankton biomass during January but an accurate prediction of the spring bloom timing and peak. In contrast, scenario 3 produces a more realistic result during winter but it fails to predict the correct spring bloom timing and shows a persistent overestimation of phytoplankton concentration through spring. It is also evident that light dependence of phytoplankton growth is better described by turbidity as formulated within S1 and S2 and calibrated using the Heincke cruise data in the Wadden Sea (Fig. 2.7, EWS). Amongst three scenarios the lowest Chl-*a* concentration in the CGB predicted by S1 for March and April (Figs. 2.8 and 2.9) suggests that bloom timing in the deep water may be strongly regulated by sediment re-suspension. These results imply that more realistic light dependencies of phytoplankton growth can be obtained by accounting for the role of turbidity in shallow coastal regions. A daily resolved SPM field in March is therefore critical to accurately reproduce the initial phase of the bloom. By the end of April, when the bloom is fully developed, the effect of SPM distribution is less pronounced (see Figs. 2.2 and 2.5). Therefore, we concluded that light availability played a key role in the initial phase of the spring bloom in 2003.

Waters surrounding HR represent a highly dynamic region. Drift experiments have shown that different water masses (originating from rivers, open North Sea or continental coastal waters all with distinct biological species and biogeochemical signatures) may either pass or mix over Helgoland station depending on meteorological conditions (Brockmann et al., 1997; Schrum, 1997; Schrum et al., 1997). As a result, phytoplankton and zooplankton data in this station exhibit a strong variability. It is unusual for a



spring bloom to be triggered by a stratified water column at HR, because of its shallowness (about 10 m deep) and strong tidal currents (Wiltshire et al., 2008). Our simple approximations for  $K^{S1}$  and  $K^{S2}$  produce good model results for Chl-*a*, with model-data differences limited to only some weeks in January and March. This suggests a close relation between SPM and salinity around Helgoland Station. The physical and biological time-series (Fig. 2.4) show that extreme events such as strong north wind and significant freshwater discharge may induce resuspension of sediments, particularly in winter and early spring. High SPM values will subsequently decrease in a few days under calm conditions. Light extinction fluctuates in a correlated manner. Under these conditions light limitation dominates over other factors in the control of phytoplankton net growth (see Wiltshire et al., 2008). We conclude that SPM transport around Helgoland region is strongly influenced by a salinity front between coastal and ocean waters. The results of all our scenarios indicate that the correct representation of water turbidity, either based on SPM ( $K^{S1}$ ) or on salinity ( $K^{S2}$ ), improves model estimates by decreasing the crucial biomass-building phase and leading to a delayed phytoplankton bloom. This outcome implies that a correct parameterization of light availability may be obtained from salinity fields ( $K^{S2}$ ) at this region. Hence, coastal ecosystem models may be parameterized with relatively accurate salinity fields, if SPM data are not available. The importance of this outcome may be further appreciated when considering the challenges involved in producing reliable 3D SPM fields (often based on computationally expensive model estimates). A correct parameterization of light may also endorse a more confident approach of other important processes such as trophic interactions and inter-annual variability in spring bloom timings (Wiltshire et al., 2008).

### 2.5.3 High frequency light fluctuations

Tidally induced high frequency interactions between light and phytoplankton growth in coastal shallow waters have gained increasing attention in the latest years (Lucas and Cloern, 2002; Desmit et al., 2005; Lunau et al., 2006; Byun et al., 2007). Dring and Lüning (1994) observed that at Helgoland Station during autumn and winter 1990 a strong bi-weekly cycle of daily underwater irradiance coincided with peaks at neap tides and troughs at spring tides in the semi-diurnal tidal regime. May et al. (2003) studied the sensitivity of estuarine phytoplankton dynamics to short-term variations in turbidity in connection to wind-driven sediment resuspension in South San Francisco Bay where tidal forcing was generally weak and insufficient to resuspend sediments. In this particular case, phytoplankton growth was maximized when the sediment fluctuations caused by the daily wind cycle produced a fairly clear water column. Also, the timing of the peak wind affected phytoplankton growth. If the daily peak surface irradiance coincided with the daily turbidity minimum, growth was enhanced compared to a situation where noon coincides with the daily turbidity maximum.

What is the effect of high frequency fluctuations in light attenuation on the spring bloom in the German Bight? Sensitivity analyses on the temporal resolution of SPM concentrations fluctuating either in simple ideal diurnal cycles (S1b and S1c) or in a more realistic manner using hourly assimilated fields (S1a) show that high frequency fluctuations can cause differences in spring bloom timing and S1a captures the observed temporal variability in algal biomass fairly well (Fig. 2.5b). Phytoplankton biomass exhibits similar frequency of fluctuations irrespective of various light forcing. This is due to water-mass movement (investigations not shown here). Light limitation induced by different attenuation functions only affects the amplitude of fluctuations.

#### 2.5.4 Data-model integration

Lacroix et al. (2007) applied seasonal climatology of SeaWiFS-derived TSM data temporally and spatially interpolated to force the light attenuation module (i.e.  $K_d$ ). Their modelling study on turbid waters of the Belgian and Dutch coasts revealed that TSM is a dominant term when computing  $K_d$  as compared to the relative contributions of Chl-*a* and CDOM. Therefore, the temporal coarse resolution of TSM concentrations may have contributed in their study to the deviations in the bloom timing and to the underestimation of simulated Chl-*a*. An important novel aspect of our study is the use of satellite-derived  $K_{\min}$  to constrain the parameterization for obtaining a more realistic light attenuation coefficient. In case 2 waters,  $K_{\min}$  is a more reliable quantity with respect to Chl-*a* concentration. Kratzer et al. (2003) demonstrated that it is possible to estimate the degree of eutrophication in case 2 waters by combining remotely sensed and in situ measured spectral attenuation coefficients with Secchi depth obtained during sea-truth campaigns. Therefore,  $K_{\min}$  can provide a valuable and additional source of information for the validation of models aiming at estimating primary production. Promisingly it would necessitate a high spatial and temporal coverage of  $K_{\min}$  data to force the biological model directly instead of relying on formulating  $K_d$  with a realistic SPM field.

Xu et al. (2005) observed that there are two competing factors controlling the relationship between  $K_d$  and Chl-*a* in Chesapeake Bay. In turbid waters where constituents other than phytoplankton strongly influence  $K_d$ , light controls phytoplankton growth and biomass. This gives rise to a negative correlation between  $K_d$  and Chl-*a*. In clear waters, where phytoplankton growth and biomass are controlled by factors other than light (i.e. nutrients), Chl-*a* strongly influences  $K_d$  leading to a positive correlation between  $K_d$  and Chl-*a*. By relating SPM,  $K_d$  and SD in UK marine waters, Devlin et al. (2008) found that the statistical model prediction of the  $K_d$ -SPM relationship was improved by fitting separate models to data from transitional, coastal and offshore waters. When we emphasise the spatial gradient of light attenuation in the estuary-sea transitional area, adaptive parameterization of assimilation rate for phytoplankton C:Chl

ratio cannot be ignored in this highly dynamic ecosystem. We therefore suggest that future ecosystem modelling studies on dynamic coastal systems should apply more sophisticated assimilation schemes. Strong regional differences in the forcing as well as in the specific biogeochemical response should be also considered more carefully.

In summary, we adopted an integrated model-data approach to perform comprehensive analyses of model performance on hydrodynamics, mass transport, light attenuation and biology. In our opinion, a coupled depth-averaged physical-biological model approach is still a logical first stage to optimize various information on forcing inputs and horizontal distributions of water properties, particularly when addressing spring bloom timing in coastal systems.

## 2.6 Conclusions

Clarifying the physical interactions among estuaries, Wadden Sea and open sea, is a crucial aspect in understanding the functioning of German Bight ecosystem. The transport of matter into and through coastal waters and the subsequent intrusion in the shelf sea are particularly relevant processes in this quest. Although the German Bight zone and its functionality have been already investigated in the past (Sündermann et al., 1999), a high resolution circulation and transport model combined with reconstructed cloudiness and assimilated forcing data (such as model-generated SPM) and with detailed observations offers a new opportunity for a more comprehensive and up-to-dated investigation of coastal ecosystems. Chl-*a* and SPM govern a large part of the absorption and scattering properties of coastal waters. Both quantities, which can be retrieved from remote-sensing data (Gohin et al., 2005), are usually computed separately in numerical models. We have shown, however, that a consistent integration of Chl-*a* and SPM leads to an efficient modelling approach and to a more accurate prediction of magnitude and timing of the 2003 spring bloom in the German Bight area. Our tests with different light attenuation scenarios show that a spatially resolved SPM distribution improves considerably the model performance with respect to Chl-*a* spatial variability at the onset of the spring bloom. Some model-data discrepancies (particularly with respect to cruise data transects) suggest that the spatial variability in Chl-*a* cannot be fully captured by one single parameter set of the N- or C-based biological module, or that improvements on the light attenuation module alone are not sufficient to describe this highly dynamic ecosystem. We expect further model advancements by adopting adaptive-based approaches (Pahlow et al., 2008).

## Acknowledgement

We are grateful to Gunnar Brandt for helping with MLD data, Beate Geyer and Frauke Feser for providing REMO cloudiness, Mikhail Dobrynin and Heinz Günther for providing SPM fields, and Hansjorg L. Krasemann, Roland Doerffer, Dagmar Müller for providing and discussing MERIS data. We thank the scientific crews of the research vessels *Heincke* and *Aade* for their unfailing provision of samples and data. The initiative of the manuscript benefited from useful discussion with Dr. Lacroix, Geneviève and Dr Byun, Do-Seong. We are grateful to two anonymous reviewers for their constructive comments, which improved our manuscript.

## Chapter 3

# Factors controlling the onset of spring blooms in the German Bight 2002–2005: light, wind and stratification

---

**Abstract:** In this study we reconstructed the spring bloom dynamics of a shallow (tidal) ecosystem from 2002 to 2005 by combining three continuous time-series along a nearshore to offshore transect in the German Bight (GB). Our analysis reveals a very different response of phytoplankton growth to different light and mixing regimes in terms of variable bloom timing, P-I relation and Chl:C ratios. Nearshore, the timing and magnitude of the bloom remained nearly constant between years. At further offshore locations, the mechanism controlling the onset of bloom onset was related to water provenance expressed by salinity and tidal front position. 1) The bloom started in early spring before stratification if this transitional zone was characterised by coastal waters. The net change rate of Chl-*a* and the Chl:C ratios both increased with increasing mean water column irradiance,  $I_m$ . 2) The bloom started in late spring after stratification if the water originated from less turbid North Sea water. In this case, the bloom development depended less on  $I_m$ . The Chl:C ratio was negatively correlated to  $I_m$  and fluctuated in a wide range. In both cases, wind-slack events were found to trigger the bloom. Particularly a transient wind slack with  $\leq 5 \text{ m s}^{-1}$  favored the formation of a pronounced bloom. This study demonstrates the critical role of mesoscale spatial variations on coastal plankton dynamics in winter-spring.

**Keywords:** spring bloom, light limitation, tidal front, wind, nearshore-offshore gradient, Helgoland Roads

### 3.1 Introduction

Phytoplankton spring blooms start the production cycle in most temperate aquatic ecosystems. The interannual changes in the timing of the phytoplankton spring bloom lead to the matching or mismatching of phytoplankton to zooplankton and ultimately determine the recruitment success of higher trophic levels like fish (Cushing, 1990). To understand such changes is therefore a central task in the study of highly productive habitats like coastal seas. For the German Bight (GB, part of the southern North Sea), it is often believed that underwater irradiance and lateral advection regulate where and when the spring bloom will be formed in the GB (Colijn and Cadée, 2003; Tian et al., 2009; Brandt and Wirtz, 2010). Those studies suggested that the bloom starts in early spring (late March) in the shallow well-mixed coastal water and in late spring (mid-April) in deep offshore waters. And different light regimes were proposed to regulate the onset of spring blooms from nearshore to offshore caused by bathymetric variations and seasonal tidal mixing front. In the shallow coastal area, underwater light is a function of light intensity and turbidity. Turbidity variations are determined by riverine inputs and sediment resuspension. The spring bloom starts when turbidity drops under a specific threshold ensuring deeper light penetration (Iriarte and Purdie, 2004). In the deeper offshore area, the bloom begins only when the seasonal surface mixed layer depth (MLD) becomes less than a critical depth (Sverdrup, 1953). Only then, an increase of net growth within the MLD promotes the onset of the bloom (Townsend et al., 1994; Lucas et al., 1998).

This general model of the phytoplankton spring bloom in coastal and shelf seas is challenged by recent observations and remote sensing images. These time- or space-continuous data, with increased coverage and reliability in coastal regions, reveal strong variability in Chl-*a* concentration on many spatio-temporal scales (Petersen et al., 2008). In some years, strikingly high Chl-*a* levels extended from nearshore to offshore (Tian et al., 2009) but in other years high Chl-*a* concentrations were restricted nearshore as expressed by a sharp gradient between the coastal and the offshore areas (Petersen et al., 2008). The mechanisms regulating inter-annual variations in the onset of spring blooms and the interactions between shallow and deep water masses before and after the formation of the tidal mixing front have been rarely addressed in the past because the high variability impedes a clear identification of key processes. For example, variability in the timing and magnitude of annual river runoff, in tidal mixing and in wind-driven currents often results in large and multi-scale fluctuations exhibited by river plumes extent and stratification. These fluctuations, in turn, affect the light availability, phytoplankton patchiness and mass transport during bloom events (Furuya et al., 1993; Yin et al., 1997; Seuront, 2005). Accurate representation of how the spring bloom dynamics cope with different light, mixing and advective regimes along a coastal-ocean gradient requires an integration of empirical descriptions into a processes-based view (Cloern and Jassby, 2008; Rixen et al., 2009).

The aim of the present study is to acquire new insights into the interannual changes in the timing and intensity of the spring bloom and to better understand the role of external forcing in coastal marine ecosystems. More specifically, we investigate how the effective mixture of light availability, wind intensity, estuarine/marine water masses, tidal-mixing front position, and phytoplankton physiology (e.g., Chl:C variations) controls the timing of coastal spring blooms. The marine observatory station Helgoland Roads (HR) in the GB represents an estuary-sea transitional area because of its location at the borders of the seasonal tidal mixing (thermal) front and river plumes (Gerlach, 1995; Becker et al., 1999; Wiltshire et al., 2010). Our analysis is therefore primarily based on the long-term observations made at HR. In order to describe different water types around Helgoland, we introduce three continuous time-series data along a nearshore-offshore transect during the period 2002–2005 (corresponding to the best data coverage available) and we use satellite SST data to reconstruct the position of the tidal front along the zonal section crossing Helgoland.

## 3.2 Data and methods

### 3.2.1 Study area

The GB is an estuary-sea transitional area of the southern North Sea (Fig. 3.1). Inshore, the GB includes the Wadden Sea, characterised by tidal flats and shallow water depths. The rivers Elbe ( $700 \text{ m}^3 \text{ s}^{-1}$ ), Weser ( $327 \text{ m}^3 \text{ s}^{-1}$ ), Ems ( $80 \text{ m}^3 \text{ s}^{-1}$ ) and several smaller ones discharge into the GB. Tidal currents contribute to a steady exchange of particulate and dissolved matter between the offshore waters and the Wadden Sea (Staneva et al., 2009). The mean current pattern in the GB is anticlockwise. Oceanic water masses enter the GB from the west and flow northward along the North Frisian coast, but circulation patterns can vary significantly, mostly depending on wind forcing (Becker et al., 1999). There are two distinct frontal systems in the GB: a seasonal tidal mixing front (thermal as well as haline) within the 25 m isobath and a permanent river plume front deriving mainly from the Elbe river in the southeast (Dippner, 1993). In Fig. 3.1, the isohalines of 31.5, calculated as the monthly mean of sea surface salinity from a four-year simulation for 2002–2005 (Staneva et al., 2009) underline the significance of the river plumes to Helgoland waters (Raabe and Wiltshire, 2009). The region around Helgoland is influenced either by coastal and estuarine waters or by waters originating from the stratified central parts of the North Sea, depending on hydrological and meteorological conditions (Greve et al., 1996; Visser et al., 1996).

In this study, we seek to understand the physical and biological impacts of front emergence insofar as relevant for the timing of major spring bloom events. We select the data sets from two fixed and one mobile platforms which cover the offshore water, near-coast water and a transect in between to represent the relation between these highly

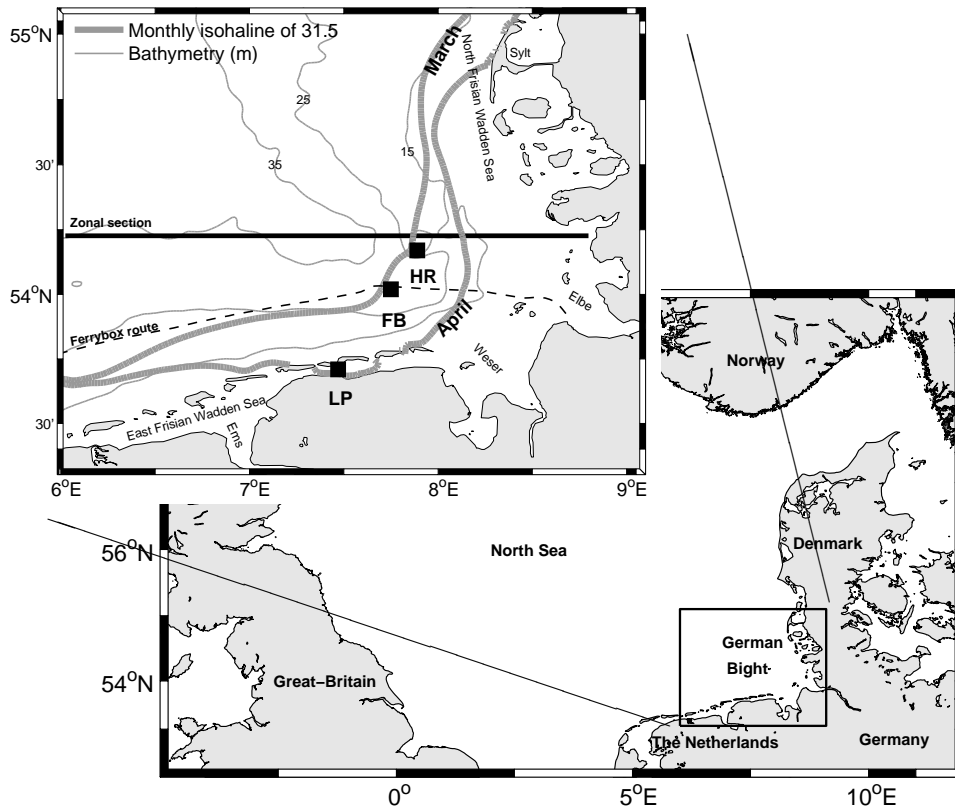


FIGURE 3.1: Study area: the southern North Sea and the German Bight with monitoring locations (squares) at Helgoland Roads (HR), Langeoog pile (LP) station and the extracted data points from the FerryBox (FB) route (dashed line). Bathymetry is shown as contours (m). The isohalines of 31.5 (thick grey lines) depict the significance of the Elbe river plumes in March and in April, calculated as the monthly mean of sea surface salinity from a four-year simulation for 2002–2005. The isohaline retarded to outside of the river mouth by May (not shown).

dynamic environments and to study the effect of lateral gradients in bloom relevant factors (Fig. 3.1).

### 3.2.2 Station data sets

The offshore marine station of HR (54°11'18" N, 7°54' E) provides, among others, work-daily data (Monday-Friday) of phytoplankton biomass, salinity and Secchi depth from surface water. The water column at this site fluctuates between 6 and 10 m and is generally well mixed. Phytoplankton is counted to species level, whereby over 360 species are recognised (Wiltshire et al., 2010). For each species, a size class and corresponding carbon content per cell was given by Wiltshire and Dürselen (2004). The sample



for Chl-*a* measurement is independent of that for carbon estimation. Chl-*a* concentration is extracted from fluorescence data using an algal group analyser (bbe-moldaenke, Germany) after the filtration onto 47-mm GF/F filters (Knefelkamp et al., 2007).

As more coastal oriented references, we refer to the new monitoring and modelling system (COSYNA-Coastal Observation System for Northern and Arctic Seas) which includes an automatic measuring system installed on pile platforms in the German Wadden Sea and on a commercial ferry travelling across German coastal waters. In this study, the Langeoog pile station (LP, 53°43' N, 7°28' E) was selected with underwater sensors installed 1 to 1.5 m above the sea floor. In addition, data are taken from a FerryBox (FB) which, from 2002 to 2005, is installed on a ferry travelling every two days between Cuxhaven (Germany) and Harwich (Great Britain). The extraction location is at the intersect of the ferry route with the transect between HR and LP (Fig. 3.1). The water intake is at a fixed depth (5 m below sea level). The two kinds of platforms (LP and FB) deliver high frequency measurements of salinity and fluorescence. Turbidity (FTU) and Chl-*a* ( $\text{mg m}^{-3}$ ) are determined using a spectrophotometer and a fluorometer (Brandt and Wirtz, 2010). Instrument specifications are given by Onken et al. (2007) and Petersen et al. (2008). The data can be freely accessed at <http://www.coastlab.org/>.

The time series of salinity and the optical parameters (Chl-*a*, Secchi depth and turbidity) at the three stations provide the basis of this data analysis. The availability and quality of the three monitoring systems restrict our study period to the years between 2002 and 2005. To eliminate large, short-term fluctuations, we based our analysis on 7-day averages according to Julian day instead of calendar day. In this way, the 5-day observations per week at HR can be distributed evenly at a 7-day interval from the beginning of each year. Being aware of the difference between the measured Chl-*a* data at HR and fluorescence-derived values from the monitoring system (Petersen et al., 2008; Brandt and Wirtz, 2010), we focused our analyses on distinct temporal variabilities at each station rather than on cross-comparing exact absolute values.

We calculated the net change rate of Chl-*a* concentration ( $\text{mg m}^{-3} \text{d}^{-1}$ ) by

$$R_{chl,n} = \frac{\bar{X}_{n+1} - \bar{X}_n}{7d} \quad (3.1)$$

where  $\bar{X}_n$  is the average Chl-*a* concentration ( $\text{mg m}^{-3}$ ) in week  $n$ . We chose this simple, linear function instead of the more standard relative growth rate (RGR) because the RGR can be more sensitive to the length of the time interval and the size of the population (Hoffmann and Poorter, 2002). In particular, applications of RGR as a measure relies on the idea that growth is based on a local standing stock, while we expect frequent intrusions of different water masses around Helgoland.

To calculate the light attenuation coefficient ( $k$ ,  $\text{m}^{-1}$ ), the Secchi depth ( $Sd$ , m) measured at HR was converted according to  $k = 0.191 + 1.242 \cdot Sd^{-1}$ , which has been

parameterized for GB coastal water by [Tillmann et al. \(2000\)](#). The water turbidity ( $Tb$ , FTU) at FB and LP was empirically converted to  $k = 0.05 + 0.15 \cdot Tb$ , which has been applied to the same coastal region by [Brandt and Wirtz \(2010\)](#).

Following [Sverdrup \(1953\)](#), [Iriarte and Purdie \(2004\)](#) used the depth averaged, vertically integrated irradiance within the MLD as a determinant indicator for the spring bloom onset in coastal waters. We adopted their formula to calculate the daily irradiance averaged over the MLD ( $I_m$ ,  $\text{Einst d}^{-1} \text{m}^{-2}$ ) as

$$I_m = \frac{I_0}{kz} [1 - \exp(-kz)] \quad (3.2)$$

where  $I_0$  is the daily surface irradiance ( $\text{Einst d}^{-1} \text{m}^{-2}$ ),  $k$  is the attenuation coefficient ( $\text{m}^{-1}$ ), and  $z$  is the MLD (m). Meteorological data including  $I_0$  and wind are routinely collected on a land station at Helgoland. Given that the water columns at HR and LP are shallow and vertically well-mixed,  $z$  was set to bottom depth of 8 and 5 m for HR and LP, respectively. The water depth at FB is 30 m and the MLD is approximately 15 m on average during the period of interest, which was calculated from a four-year simulation of 2002–2005 as provided by [Staneva et al. \(2009\)](#). Note that the water monitored at HR originates from deeper areas as the sampling took place at the shallowest part around the Helgoland region. Our calculation may therefore deviate from the real  $I_m$  experienced by the local phytoplankton population.

In order to obtain a physiologically relevant measure for photo-adaptation in bloom species, the Chl:C ratio was calculated from HR samples of Chl-*a* content ( $\text{mg m}^{-3}$ ) and phytoplankton biomass ( $\text{mg C m}^{-3}$ ). There are missing measurements of Chl-*a* between the first week and last week of April 2004 (Fig. 3.2). The weekly averages of Chl-*a* were linearly interpolated to fill the gap. According to the increasing trend of Chl-*a* at FB in the same period, we assume a simultaneous onset of the bloom at HR. This assumption may introduce bias into the assessment of  $R_{chl,n}$ - $I_m$  relations around the period of the actual HR bloom onset.

### 3.2.3 Remote sensed SST and identification of tidal front

We used satellite-derived sea surface temperature (SST) data from the Modular Ocean Data Analysis System (MODAS) ([Kara and Barron, 2007](#)) to infer the position of the tidal front. This high resolution  $1/8^\circ$  daily product is based on Advanced Very-High Resolution Radiometer (AVHRR) satellite measurements. We calculated the maximum temperature gradient along the zonal section of Latitude  $54^\circ 11' 18''$  N. According to [Becker et al. \(1999\)](#), a threshold SST gradient was used to identify tidal fronts between western stratified offshore water and the eastern coastal water masses, the latter in part mixed with Elbe river water (Fig. 3.1). The maximum gradient along the meridional

sections crossing Helgoland was always in the northern direction and undetectable south of the island (not shown).

### 3.3 Results

#### 3.3.1 Interannual changes in the onset of spring bloom

In this work, we defined the (major) spring bloom as the first continuous increase (on a weekly scale) in Chl-*a* concentration within a year with the maximum exceeding  $6 \text{ mg m}^{-3}$  (Fig. 3.2). The first week of this increase was then denoted as the onset of the bloom. According to this definition, the blooms at HR started in late March 2002 and 2003, and around mid-April in 2004 and 2005. The maximum Chl-*a* concentration during the bloom was 9.2 in 2002,  $14.9 \text{ mg m}^{-3}$  in 2003,  $24.0 \text{ mg m}^{-3}$  in 2004 and  $6.5 \text{ mg m}^{-3}$  in 2005. The maximum net change rate of Chl-*a* concentration ( $R_{chl}$ ) during a bloom event always occurred within the first two weeks after the bloom onset. As explained later in more detail, we grouped the early HR spring blooms (2002 and 2003) and the late HR blooms (2004 and 2005) to “coastal” years blooms and “marine” years blooms, respectively.

The evolution of the bloom at the intermediate site FB was similar to that at the more offshore location HR, but reached a higher magnitude in both coastal and marine year blooms. In contrast to HR and FB, the timing and magnitude of the nearshore bloom at LP (inside the East Frisian Wadden Sea) remained nearly constant between 2004 and 2005. There, a minor bloom in late March was followed by a major bloom in late April. Major bloom events reached a maximum Chl-*a* concentration of  $30 \text{ mg m}^{-3}$  in mid-May. Despite the potential overestimation of fluorescence-derived values, the Chl-*a* temporal variability at LP represented the typical characteristics of nearshore coastal blooms.

#### 3.3.2 Processes related to the observed bloom onset

##### Mixing/stratified water masses

We defined a critical gradient of  $0.03^\circ\text{C km}^{-1}$  along the zonal section crossing Helgoland island, above which we assumed the existence of a tidal mixing front separating the eastern well-mixed waters from western stratified waters. This critical value translated to a temperature difference between two grids of  $0.5^\circ\text{C}$  as imposed by the resolution of AVHRR SST data ( $1/8^\circ = 7.5 \text{ n.m.} \approx 13.9 \text{ km}$ ). Before the formation of the tidal front, the maximal SST gradient was below this threshold, indicating well-mixed water dominating the GB (Fig. 3.3). With the focus on the spring bloom onset, we found that the emergence of a tidal front in 2004 and 2005 coincided with the onset of the marine year

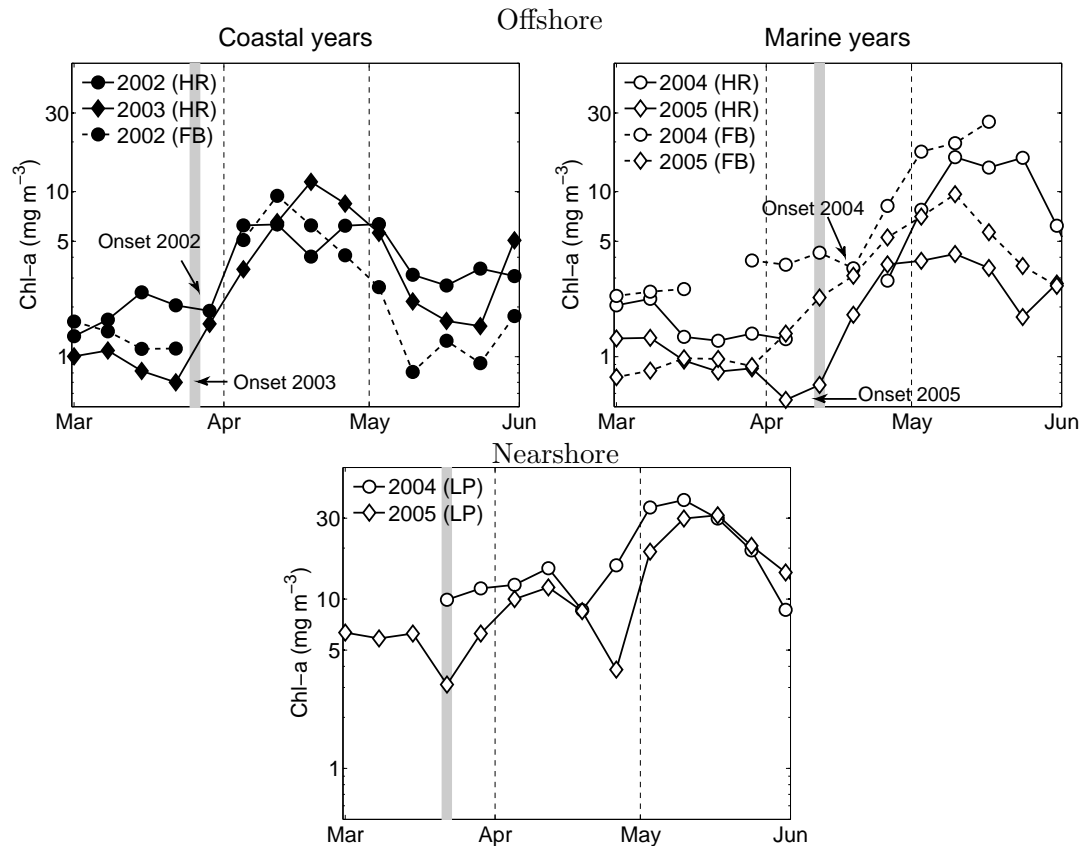


FIGURE 3.2: Weekly mean of Chl-*a* concentration ( $\text{mg m}^{-3}$ ) obtained from HR, FB and LP station between March and May. The onset of the HR spring bloom is defined as the first week of an exponential increase in Chl-*a* concentrations. At the offshore stations, the onset week of coastal year blooms is the last week of March in 2002 and the last second week in 2003; the onset week of marine year blooms is the third week of April in 2004 and the first week in 2005. At the nearshore station, the onset week of the bloom is after the mid-March. The grey line in each panel indicates the average day between two-year bloom onsets at HR. The first day of a month is marked by thin dashed lines.

blooms. The front position east between HR and the nearshore waters suggested that the observed spring blooms in the offshore water (HR and FB) were associated with stratified water. By contrast, no emergence of a tidal front until May in 2002 and 2003 indicated a strong mixing regime associated with the coastal year blooms.

### Estuarine/marine water masses

The GB hydrographic system is typically considered as estuarine when salinity decreases below 31.5 (Raabe and Wiltshire, 2009) and marine at salinity above 33 (Hickel et al., 1993). The salinity at LP was below 31.5 most of time in 2004, which was a clear feature of estuarine water, in contrast to 2005 (Fig. 3.4). In general, salinity at FB co-varied closely with salinity at HR. Offshore salinity variations in March and April reflected a transition from estuarine to marine water in 2002 and from marine to estuarine water

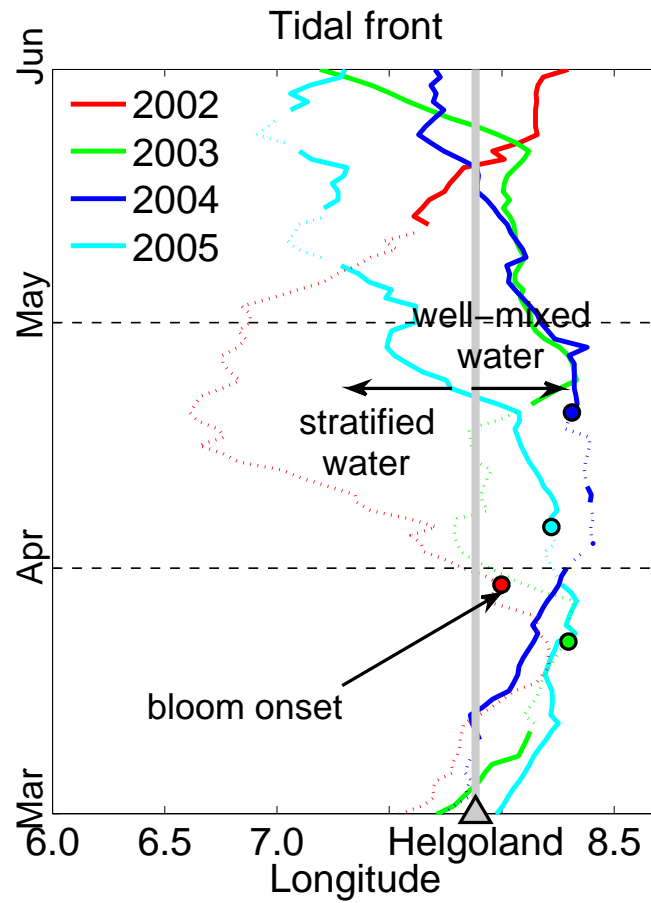


FIGURE 3.3: Time evolution of the daily maximal SST gradient along the zonal section of Latitude  $54^{\circ}11'18''$  N (cf. Fig. 3.1): in color dotted lines if below  $0.03^{\circ}C km^{-1}$  and in color solid lines if above  $0.03^{\circ}C km^{-1}$ . Take the tidal front in 2005 for example that the emergence of tidal front since early April separates the stratified North Sea water in the west (left arrow) and the well-mixed coastal waters in the east (right arrow). The grey line marks the location of Helgoland ( $7^{\circ}54'$  E) and illustrates when Helgoland was surrounded by well-mixed water or stratified water. Color circles note the onset of the HR spring bloom onset in respective years (cf. Fig. 3.2), which tells at that time whether a tidal front is formed already. The thin dashed lines mark the first day of a month.

in April 2003, presumably due to a fresh water inflow event. The salinity gradient between nearshore (LP) and offshore became evident until May in both 2002 and 2003. The early spring blooms therefore coincided with the arrival of estuarine/coastal waters in these two years. In the other two years, salinity rapidly returned to 33 in March, and in most of the spring-time the salinity level remained around 33, reflecting marine water characteristics. The large discrepancy of salinity between offshore and nearshore suggested the existence of river plume (haline) fronts between the ferry route and the East Frisian Wadden Sea, particularly in 2004.

Combining the bloom timing with water provenance expressed by salinity and tidal front, we could confirm the notation introduced in section 3.3.1, with “coastal” years bloom events in 2002 and 2003 and “marine” years blooms in 2004 and 2005. In addition,

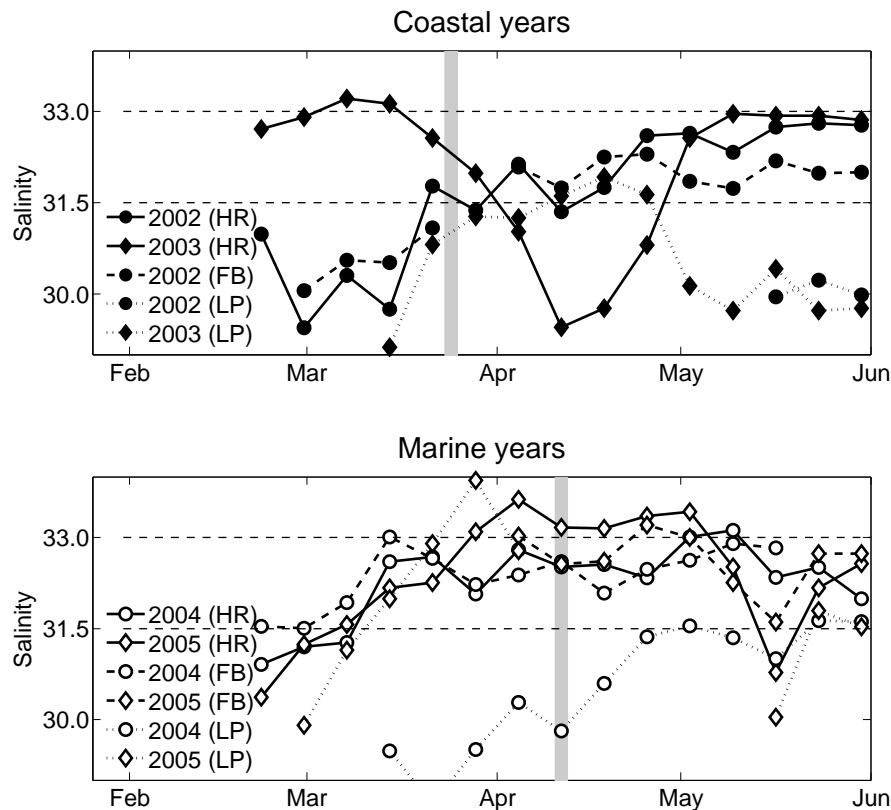


FIGURE 3.4: Evolution of weekly averaged salinity at HR, FB and LP station. The grey thick line indicates the week near the bloom onsets of HR (cf. Fig. 3.2). The thin dashed lines of 31.5 and 33 distinguish estuarine from marine waters.

two anomalous hydrographic conditions prior to the bloom were identified: considerably low salinity in early March 2002 offshore and the high salinity in early April 2005 both nearshore and offshore.

### Light regimes

Turbidity estimated either from Secchi depth or from FTU showed a significant negative correlation with salinity in the bi-weekly period before and after the onset of spring blooms (Fig. 3.5), with  $r^2 \geq 0.55$  at all three stations. We restricted the analysis to the time no later than two weeks after the onset since the rapid increase in Chl-*a* concentration after the onset (Fig. 3.2) already affected light penetration depth. Annual differences in salinity reflected, to some extent, variable influences of fresh water, meaning higher turbidity in the coastal years (Fig. 3.5).

As a result, the mean water column irradiance offshore revealed different light regimes between the coastal and marine year blooms (Fig. 3.5). In turbid well-mixed coastal waters, the bloom started at relatively low  $I_m$ . Corresponding to the extremely high turbidity and low salinity in 2002 at FB and 2004 at LP,  $R_{chl}$  increased rapidly with increasing  $I_m$ . In 2005 with low turbidity and high salinity,  $R_{chl}$  increased slightly over

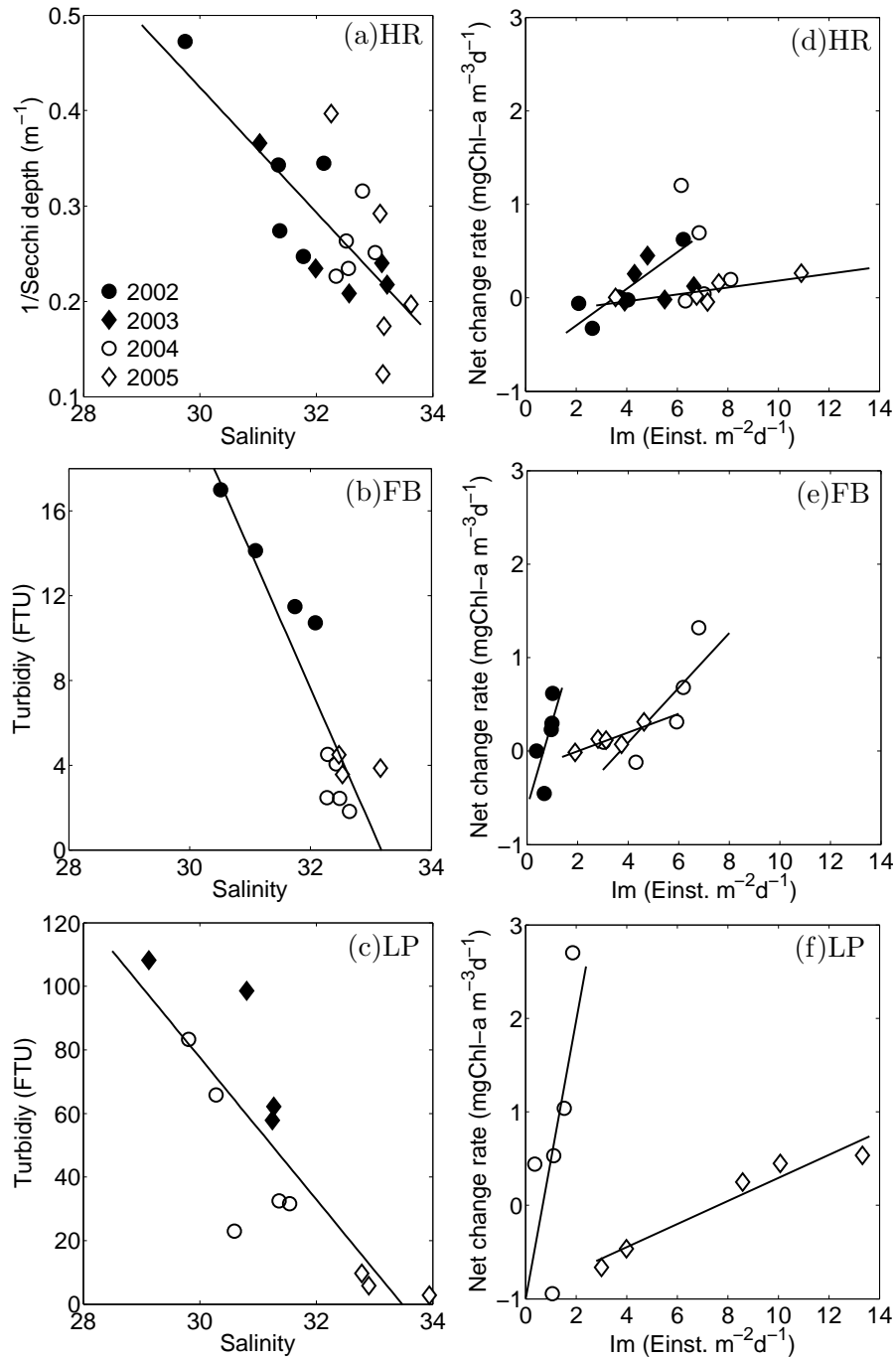


FIGURE 3.5: (a-c): Weekly mean of salinity versus the inverse value of Secchi depth at HR, turbidity at FB and LP, respectively, in the bi-weekly period before and after the bloom onset at HR. The solid lines represent the linear regressions with  $r^2 = 0.55$  and  $p = 0.0002$  at HR,  $r^2 = 0.82$  and  $p = 0.0001$  at FB and  $r^2 = 0.71$  and  $p = 0.0006$  at LP. (d-f): Weekly mean of the net change rate in Chl-*a* concentration versus the daily mean water column irradiance  $I_m$ . Given the small sample sizes involved, the solid lines are used to approximately depict a linear relationship for each year.  $r^2$  and  $p$  values are not taken into account. The legends all refer to the panel (a).

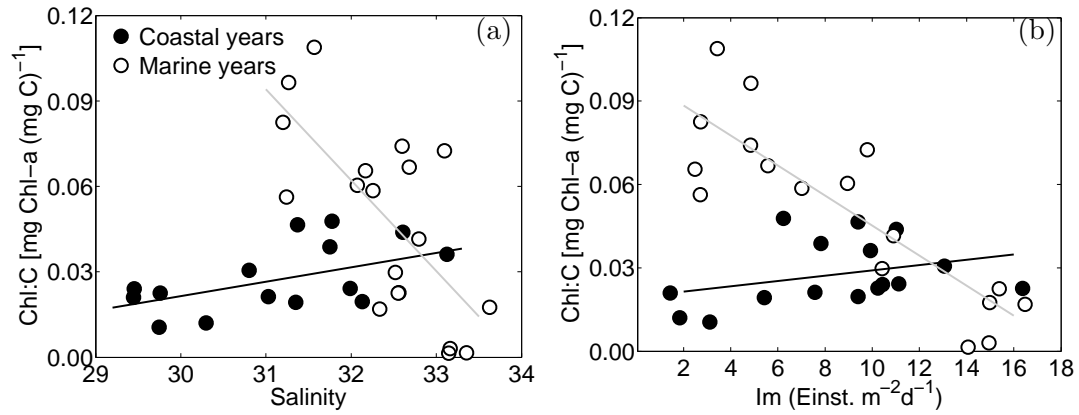


FIGURE 3.6: HR weekly mean of Chl:C ratio versus salinity (a) and the daily mean water column irradiance (b) between March and April. Panel (a): the linear regressions are  $r^2 = 0.26$  and  $p = 0.04$  in the coastal years (black line) and  $r^2 = 0.50$  and  $p = 0.001$  in the marine years (grey line). Panel (b): the linear regressions are  $r^2 = 0.1$  and  $p = 0.2$  in the coastal years (black line) and  $r^2 = 0.77$  and  $p = 0.000001$  in the marine years (grey line).

a wide range of  $I_m$  variations both nearshore and offshore. In 2004, the increase in  $R_{chl}$  with average light occurred at different slopes. Nearshore, at low  $I_m$ , the slope was much higher than offshore, indicating a spatial separation of photosynthetic affinity of phytoplankton in the two regimes.

### 3.3.3 Variations of Chl:C ratio in mixing/light regimes

In March and April,  $I_m$  still appeared to be the prevailing limitation factor in this transitional area, induced by turbid fresh water (i.e. low salinity and low  $I_m$  in Fig. 3.6). We found that water provenance expressed by salinity was clearly linked to phytoplankton physiology as described by Chl:C ratio variations. In the coastal years, Chl:C ratio gradually increased with increasing salinity as well as  $I_m$ . In the marine years, we detected a significant negative correlation between Chl:C ratio and  $I_m$  with  $r^2 = 0.77$ . Not only the trend of Chl:C ratio but also the magnitude differed in the coastal and marine years. Although  $I_m$  varied in the same range, the maximum Chl:C ratio exceeded  $0.1 \text{ mg Chl-a (mg C)}^{-1}$  in the marine years in contrast to  $0.05 \text{ mg Chl-a (mg C)}^{-1}$  in the coastal years.

### 3.3.4 Two effects of alterations in wind intensity

A significant negative correlation ( $r^2 = 0.53$ ) was found between  $R_{chl}$  and average wind speeds in the preceding two weeks (Fig. 3.7). Rapid and intensive blooms ( $R_{chl} > 1.0 \text{ mg Chl-a m}^{-3} \text{ d}^{-1}$ ) arose in the aftermath of a period with low average wind speeds ( $\leq 5 \text{ m s}^{-1}$ ) in both coastal and marine years. On the contrary, the bloom was suppressed ( $R_{chl} < 0.3 \text{ mg Chl-a m}^{-3} \text{ d}^{-1}$ ) by persistently high average wind speeds ( $> 10 \text{ m s}^{-1}$ ).



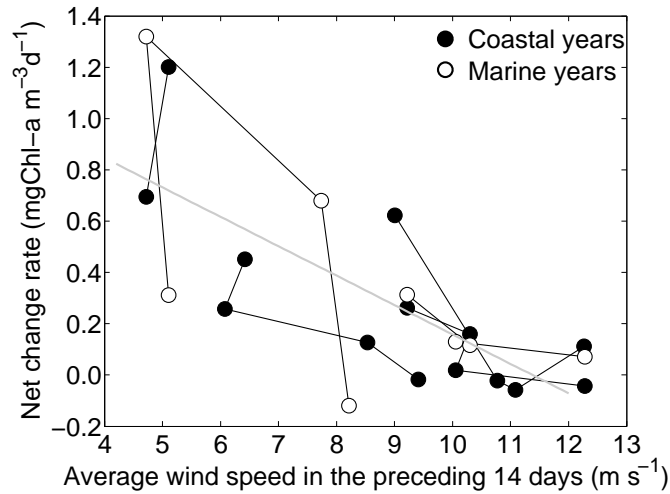


FIGURE 3.7: The net change rate in Chl-*a* ( $\text{mg m}^{-3} \text{d}^{-1}$ ) versus the averaged wind speed ( $\text{m s}^{-1}$ ) in the offshore water (HR and FB) during the development of spring blooms, i.e. two weeks before and after the bloom onset of HR (cf. Fig. 3.2). Wind data ( $\text{m s}^{-1}$ ) averaged over the preceding two weeks are given. The grey thin line represents the linear regressions with  $r^2 = 0.53$  and  $p = 0.0001$ .

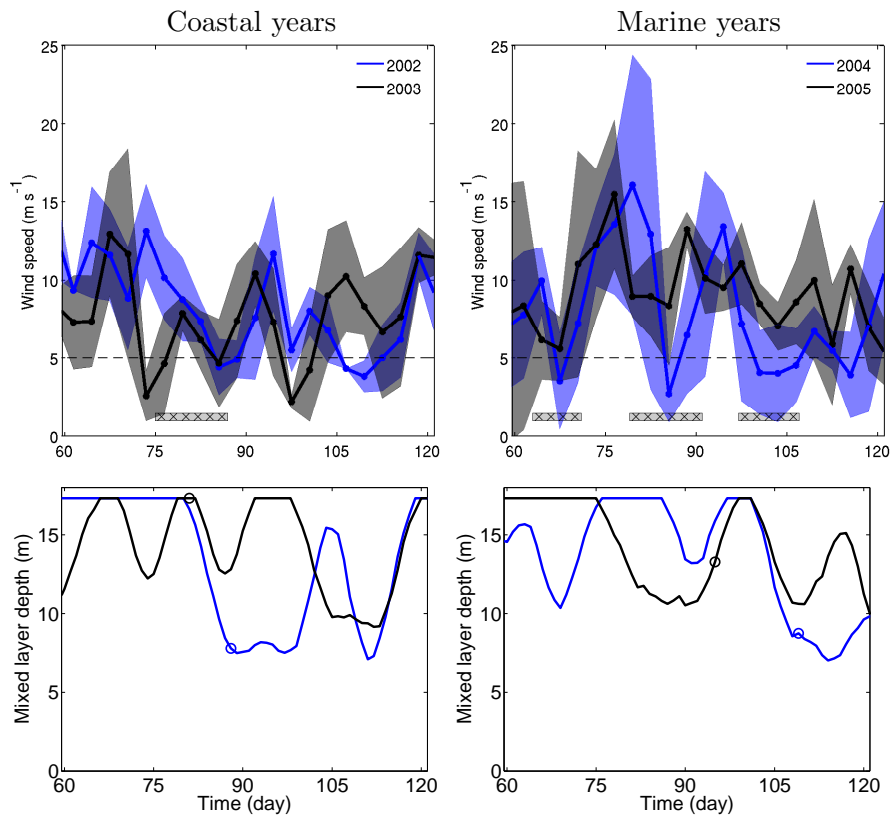


FIGURE 3.8: Upper panels: 3-day mean (solid line) and standard deviation (shadow) of daily wind speed between March and April. The grey meshed bars indicate the occurrences of wind slack preceding the spring bloom. Bottom panels: the modelled MLD extracted from the grid point (depth=17.3 m) nearest to Helgoland. The variations in the MLD were determined by potential density, which was computed from daily profiles with the 3D hydrodynamic model, according to a density change from the ocean surface of 0.125 sigma units. The bloom onset at HR in the respective year is marked by open circle.

As seen from Eq.3.2, wind-driven vertical mixing can affect phytoplankton growth not only through variations in turbidity but also the MLD of the water column (Townsend et al., 1994; Iriarte and Purdie, 2004). These two effects of alterations in wind intensity differed between the mixing or stratified regimes of coastal or marine years, respectively. Overall, there was a strong covariation between wind intensity and the MLD of the surrounding deep water near Helgoland (Fig. 3.8). As seasonal stratification typically forms after April (Becker et al., 1999), we found that the coastal year blooms started in the first break from high wind ( $\approx 15 \text{ m s}^{-1}$ ) to calmer conditions in March. In the marine years, wind speed in March exceeded the one in the coastal years, reaching nearly  $20 \text{ m s}^{-1}$ . The onset of the bloom did not occur in the first event of wind slack in March but followed the co-occurrence of stratification and wind slack in April. To sum-up, wind slack seemed to generally trigger the spring bloom, but in the marine years stratification was an additional prerequisite for the algal spring blooms.

### 3.4 Discussion

Our analysis demonstrates a significant impact of external physical forcing on the spring bloom dynamics in a coastal sea. The forcing is particularly related to wind stress and acts through spatially and temporally distinct light and (lateral as well as vertical) mixing regimes. We could identify clear differences in the sensitivity of phytoplankton growth to these physical factors along a nearshore-offshore gradient and between different years. In the past, a number of studies on the HR time series have documented continuous changes in phytoplankton and zooplankton abundance and composition in connection with the climatic variability like the North Atlantic Ocean Oscillation Index (Edwards and Richardson, 2004; Wiltshire et al., 2008, 2010). Our study is the first to combine information along a continuous transect representing a shallow (tidal) ecosystem from nearshore to offshore. The parallel use of information allows us to understand some of the complex interactions which connect highly fluctuating physical factors with the ecosystem dynamics of coastal seas. For this, we distinguished between water masses of shallow water and of offshore origin which are differently distributed in each year (depending on hydrological and meteorological conditions). This distinction has been a helpful tool to interpret variable co-variations between physical and biological variables before and during the spring bloom.

We note that the estimates for net temporal chlorophyll change  $R_{chl}$  and Chl:C ratios derived from field measurements can not be directly compared to culture experiments. However, we based our analyses on these aggregated measures because they (except phytoplankton carbon measurements) are operationally retrievable observables. The relationships found in this study should therefore be testable also in other (coastal) areas or for different periods of time. In the interpretation of the  $R_{chl}$  we put only little emphasis on feeding losses due to grazing by benthic filter feeders or zooplankton.

Even more, we assumed that zooplankton has no significant impact on the timing of the spring bloom. This has in part been motivated by the analysis of the long-term trend of bloom related variables at HR that considerable interannual changes in the onset and magnitude of the spring bloom contrasts the relative stability in zooplankton phenology (Wiltshire et al., 2008). Much of the variability in spring bloom timing could in this study be explained by changes in light and mixing regimes, without the need to further track possible alterations in loss factors. However, this finding can not be generalized to summer or autumn phytoplankton blooms and we even do not exclude more indirect top-down controls and cascading effects for spring. For example, the delayed bloom in May 2004 was dominated by small microalgae compared to 2003, what may be linked to relatively high zooplankton abundance in April (Wiltshire, unpublished data).

### 3.4.1 Chl:C ratio as a proxy for algal eco-physiology

Variability of the Chl:C ratio is a major source of uncertainty in investigations on photosynthesis in marine unicellular autotrophs (Geider et al., 1998). Large ranges in Chl:C are exhibited by single species phytoplankton species within a few days that is usually referred to as photoacclimation. However, physiological acclimation may also reflect taxonomic composition since major photoacclimation properties are species-specific (Wirtz and Pahlow, 2010). Thus there are evident links between environmental characteristics that regulate photosynthesis and major algal traits such as cell size. These links are often reflected in phytoplankton selection and succession, such as small size algae and low Chl:C in a permanently stratified system but large cell sizes and high Chl:C in a well-mixed coastal system (Moore et al., 2006; Aiken et al., 2008). Many field studies have suggested that gradients in prevailing light or nutrient limitation can be accompanied by changes in both acclimation state and community composition. For example, seasonally large deviations in Chl:C ratios are observed for the southern North Sea (Llewellyn et al., 2005; Muylaert et al., 2006); vertically a linear increase in the phytoplankton Chl:C ratio with depth in the euphotic zone is found in the equatorial Pacific (Le Bouteiller et al., 2003); in the light-limited coastal system of the South San Francisco Bay, the lateral decrease of daily depth-averaged irradiance determines the horizontal increase in Chl:C ratios (Lucas et al., 1999a).

Our analysis identified two distinct mechanisms which regulate the Chl:C stoichiometry in spring phytoplankton. The first is lateral mixing between nearshore and offshore waters and locally adapted algal communities. This lateral transport may override the acclimation response on the cellular level, so that Chl:C becomes insensitive to increasing light levels. Secondly, in the absence of strong advective changes in algal community structure, local populations adaptively lower their Chl:C with increasing light. Lateral mixing of algal community traits may even be a relevant mechanism in “marine” years. In winter-spring 2005 the GB hydrography was characterised by

intrusion of salty and cold water masses, accompanying the extraordinarily low  $R_{chl-I_m}$  slopes. The Lagrangian model of Brandt and Wirtz (2010) hindcasted that this water mass originated from the adjacent Southern Bight entering the west boundary of the GB. This advective processes, presumably, drove algal community composition into the direction of species with relatively low growth rate (albeit their ability the up- and down-regulate Chl:C, see Fig. 3.5d-f and 3.6). A similar phenomenon has been reported from the Otsuchi Bay, Japan where intense water exchange significantly interrupted the formation of spring blooms (Furuya et al., 1993). To sum up, local interannual or lateral coast-offshore shifts in Chl:C ratios can reflect a changing physiological ecology of phytoplankton in coastal seas. These shifts are proposed to be a key for understanding the sensitivity of spring phytoplankton to physical variability.

As previously mentioned, changes in algal community composition could be altered by mesozooplankton grazing. Community structure, in turn, determines feeding conditions for copepods. In the absence of preferred prey species, copepods have to rely on less abundant or nutritious food resources like microzooplankton or detritus (Renz et al., 2008; Gentsch et al., 2009). Consequently, algal composition changes affect the energy flow from primary to fish production (Sommer and Lengfellner, 2008). This means that local and non-local physical factors act on ecosystem dynamics in various ways. They not only determine the timing of the spring bloom as relevant for stage structured consumer species but may also influence the fate of the produced carbon/energy.

### 3.4.2 Wind slack as a spring bloom trigger

In many marine ecosystems, the spring bloom is the dominant seasonal event. Within the nearshore-offshore gradient studied here it appears spatially heterogenous. This feature are highly related to river plumes and the tidal-mixing front, well-known as major agents for mesoscale spatial variations in coastal plankton dynamics in the GB (Becker et al., 1999). In turn, the inclination of the tidal front and salinity stratification is mainly affected by wind field variability (Dippner, 1993; Schrum, 1997; Becker et al., 1999). Thus ultimately determines Helgoland under the influence of either offshore or coastal waters (Greve et al., 1996; Wiltshire et al., 2010). In years when coastal water dominated (with large extent of river plumes), the bloom started as soon as light penetration exceeded some threshold (Iriarte and Purdie, 2004). Whereas in “marine” years, stratification in late spring (with the tidal front) seemed to control the spring bloom onset (Sverdrup, 1953; Townsend et al., 1994). What is the role of wind variability, except in the interplay between river plumes and tidal front, in governing the spring bloom dynamics?

In coastal as well as marine years, wind acted as a major factor for the onset and even the magnitude of the bloom. We found that in all years the spring bloom was preceded by a period of high wind speeds and only developed as wind slackened. Additionally

vertical stratification was always preceded by a wind slack event (Fig. 3.8). Owing to the seasonality of salinity/tidal front and water type indicated by salinity, the wind slack should be associated with event-scale salinity stratification in early spring of “coastal” years whereas with seasonal thermal stratification in late spring of “marine” years. Despite different light regimes governing the spring bloom in coastal and marine years, a sudden period of low wind can effectively ensure deeper light penetration in the shallow coastal waters because of reduced sediment resuspension (May et al., 2003). The concomitant stratification may rapidly increase the net growth within the MLD and trigger the onset of the bloom (Townsend et al., 1994; Lucas et al., 1998).

Furthermore, pronounced blooms were connected to wind speeds below  $5 \text{ m s}^{-1}$  (Fig. 3.7). Recent research in the eastern English Channel found that phytoplankton patchiness increased with decreasing turbulence intensities and this detectable turbulence intermittency was induced by wind speeds below  $4.5 \text{ m s}^{-1}$  in the sampling period (Seuront, 2005). Therefore, the transient wind slack  $\leq 5 \text{ m s}^{-1}$  is proposed to greatly favor the development of phytoplankton bloom and its patchiness formation in this studied transect. Although spring bloom can rise from many different mechanisms of frontal dynamics, stratification and light penetration, our analyses demonstrate wind slack as a direct indicator for the timing and intensity of the spring bloom.

### 3.5 Conclusions

Despite the relatively short time span of the data series used in this study, the large observed interannual variability in phytoplankton spring blooms forms an ideal basis to develop a conceptual model. This study demonstrates a critical role of mesoscale spatial variations on coastal plankton dynamics. Our analysis reveals a very different response of phytoplankton growth (i.e. the bloom timing, P-I relation and Chl:C ratios) to different light and mixing regimes along a nearshore-offshore gradient in the winter-spring transition. Spring blooms were always preceded by strong winds and developed as the winds slackened. Particularly a transient wind slack  $\leq 5 \text{ m s}^{-1}$  favored the formation of the pronounced bloom. This study underlines the importance of integrating nearshore to offshore monitoring systems, which provide a continuous and synoptic environmental state description crossing all relevant sub-compartments at the land-sea interface (Muy-laert et al., 2006; Cloern and Jassby, 2008; Rixen et al., 2009), and the need for future models that include a more realistic representation of algal community traits. Such improved models, by integrating real-time observations, are necessary tools to accurately reproduce and forecast spring bloom phenology and the subsequent ecosystem dynamics on various scales. This is not only of particular interest for the region of the GB but for other coastal regions that are characterised by similarly strong spatio-temporal variability in physical and ecosystem dynamics.

## Acknowledgement

We thank our colleagues W. Petersen who provided FerryBox data and R. Riethmüller to support usage and interpretation of the measurements from the Ferrybox and Langeoog pile station. We thank the scientific crew of the research vessel *Aade* for their provision of samples and data. We also thank A. Merico and T. Pohlmann for their valuable comments on a previous draft. This work was supported by the Helmholtz society via the programme PACES and by the German Research Foundation (DFG) within the Priority Program 1162 “The impact of climate variability on aquatic ecosystems (AQUASHIFT)” (GA 401/7-1, 7-2).

## Chapter 4

# The sensitivity of coastal diatom spring bloom dynamics to meteorological and hydrographic variability

---

**Abstract:** The strong variability of coastal phytoplankton on many spatio-temporal scales still challenges our understanding of temperate shallow-water ecosystems. We investigate the relative importance of local production-loss balance and lateral advection on the spring bloom dynamics along a topography-induced nearshore-offshore gradient in the German Bight (GB). A coupled physical-biological model is used to describe diatom growth (light and silicate-limited) as well as phytoplankton-zooplankton interactions. Lateral transport is calculated by the General Estuarine Transport Model (GETM). The coupled model reproduces very different spring bloom developments in two consecutive years (2003-2004) in near-shore and more central parts of the GB. Direct analysis of the phytoplankton model demonstrates that mean underwater irradiance (PAR) and lateral advection combine to control the pre- and mid-bloom phase as a prevalent role of PAR along the nearshore-offshore transect depends on the formation of a tidal front. In 2003, when the tidal front is absent, the coastal bloom spreads over the transitional zone into the offshore areas. On the contrary, in 2004, low PAR and a strong front (low lateral mixing) both considerably delayed the diatom bloom offshore. The blooming phase is terminated mainly by sedimentation in stratified offshore waters and by grazing in well-mixed coastal waters because there, in our simple model, vertical mixing and higher nutrient availability counteract sedimentation. In scenario runs at elevated temperature, sedimentation becomes less important than temperature-dependent grazing and diatom production is more channeled to the pelagic food web. Enhanced grazing in warmer waters may thus re-organize spatial differences in the diatom production-loss balance along the nearshore-offshore transect. To better represent changing sensitivities to highly variable physical forcings, we suggest a trait based representation of the

plankton in future models. This would widen our capability to understand and deterministically describe the short- and long-term dynamics of complex coastal ecosystems.

**Keywords:** diatom spring bloom, physical-biological model, sedimentation, grazing, nearshore-offshore gradient

## 4.1 Introduction

Phytoplankton spring blooms in temperate aquatic ecosystems reveal a great richness in phenology. They often appear with a strong interannual and spatial variability in the onset, extent, and duration of the bloom (Edwards and Richardson, 2004). Spring bloom phenology gains relevance on the ecosystem scale since, e.g., the subsequent growth of zooplankton is critical for the matching or mismatching of food abundance during the advent of early life stages of consumers, and may thus affect the recruitment success of higher trophic levels like fish (Cushing, 1990). The initiation and evolution of the bloom reflects a delicate balance between the amount of solar radiation received by a phytoplankton population, the availability of nutrients, and the losses of biomass associated with respiration, grazing and sinking (Smetacek and Passow, 1990; Platt et al., 1991; Townsend et al., 1994). The blooming onset in spring is presumably more dependent on light limited photosynthesis than on temperature-mediated physiological responses (Eilertsen et al., 1995). In addition, the population build-up rate mirrors various changes in loss rates (Smetacek, 1999). Diatom sinking rates are influenced by nutrient depletion and post-bloom sinking has been proposed as the principal loss term for the bloom biomass from the water column (Waite et al., 1992a). Also grazing seems to be of high importance (Smetacek, 1999). In the pre, mid-, and post-bloom phase, diatoms will be exposed to different grazing pressures and mixing/sinking regimes (Waite et al., 1992b), but thorough analyses of the factors controlling bloom phenology are scarce. These are further complicated by the spatial openness of most aquatic ecosystems. In addition to the local production-loss balance, lateral advection seems to act as an important factor for how phytoplankton is distributed in time and space (Lucas et al., 1999b).

As a consequence, our knowledge about factors influencing interannual and spatial variability in the spring bloom dynamics is still not sufficient to address relevant research questions like the relative importance and interplay of different growth and loss factors, or on the sensitivity of coastal marine ecosystems to climate changes (which we here primarily reduce to a rise in water temperature). One of the best places to investigate such questions is, given the amount of observations and existing model systems, the southern North Sea (NS) (Brussaard et al., 1995; Ehrenhauss et al., 2004; Lancelot et al., 2005), and more specifically the German Bight (GB, part of the southern NS) (Moll and



Radach, 2003; Wirtz and Wiltshire, 2005; Wiltshire et al., 2008). A special source of information on plankton dynamics is the monitoring station at Helgoland Roads (HR) which is located amid a transitional zone between the Wadden Sea (adjacent to the coast) and offshore, North Sea waters. Previous analyses of long-term trends in ecosystem dynamics at HR revealed considerable interannual changes in the onset and magnitude of the spring bloom, while zooplankton phenology showed a relative high degree of stability (Wiltshire et al., 2008). It can therefore be assumed that zooplankton grazing has no significant impact on the timing of the spring bloom. Much of the variability in spring blooms from nearshore to offshore waters and between years could indeed be explained by changes in light and (lateral as well as vertical) mixing regimes, without the need to further track possible alterations in loss factors (Tian et al., 2010). Still, the ecological role of the planktons in the marine carbon cycle remains poorly understood in this region. This is also reflected by the state of coastal ecosystem modelling. Models have to face a great complexity in the interactions between biological, chemical and physical processes. They, in addition, have to resolve the coupling of atmosphere-ocean, estuarine-offshore and ocean-sediments processes on multiple spatio-temporal scales. An accurate representation of the spring bloom dynamics along a coastal-ocean gradient is hence one of the most challenging aspects of ecosystem modelling (Rixen et al., 2009).

This paper aims to provide a quantitative understanding of how major local- and transport-related processes can influence bloom formation and patchiness (i.e. whether and where a bloom occurs) in a highly variable coastal marine environment. The more general problem is broken down to the following questions: 1) how far does the temporal and spatial variability of spring blooms reflect the interannual variability in light climate and lateral advection? 2) how do predator-prey interactions respond to changes in local (physical) factors like light availability and temperature? 3) To which degree is this response varying between nearshore and offshore habitats, respectively?

We use the GB as a representative case to illustrate the effects of bathymetric variations, turbulence, and transport-related mechanisms on the spatio-temporal distribution of phytoplankton in shallow coastal waters. Although we use data sets of physical forcing and biological parameter ranges that are characteristic for the GB, the purpose of this modelling study is to develop general insights into the drivers and the fate of high primary productivity in a large class of coastal systems. Our focus on two years (2003, 2004) is motivated by the preceding study of Tian et al. (2010) insofar as these years exemplify interannual changes in the development of coastal gradients in phytoplankton biomass (and related ecosystem functioning). Both years differed in the bloom onset (early April in 2003 vs. late April in 2004). In 2003, scales of horizontal patchiness in chlorophyll *a* (Chl-*a*) were much more extensive from nearshore to offshore compared to 2004 (Tian et al., 2010). This study seeks to understand the mechanisms that can give rise to the spatial and temporal differences of the diatom spring bloom between the two years and across the entire GB. The goal of this work is more to explore the sensitivity

of spring bloom dynamics to meteorological and hydrographic variability, as opposed to faithfully reproducing a bloom event in detail under high resolution forcing. This paper presents numerical experiments of phytoplankton population dynamics based on a 3D hydrodynamic model, and uses model validation, analysis and sensitivity test as a source for identifying general mechanisms for coastal algal blooms during winter and spring.

## 4.2 Methods

### 4.2.1 Characteristics of the German Bight ecosystem

The GB is a semi-enclosed area of the southern NS, receiving high loads of inorganic nutrients from riverine discharge (Fig. 4.1). Together with a rather long residence time of water masses due to an anticlockwise circulation pattern, these conditions result in intense algal blooms and an extremely high net input of labile organic matter into the sediment (Luff and Moll, 2004). The combination of weather events, riverine input and physical meso-scale and fine-scale structures, such as coastal currents, fronts and haline stratification induced by freshwater inflow cause high spatio-temporal variability of the plankton system, in particular near Helgoland waters (Radach et al., 1990; Wiltshire et al., 2010; Tian et al., 2010). The forcing acts in a similar way on the distribution of suspended particulate matter (SPM). SPM is, in turn, closely interlinked with primary producers through various processes like light attenuation, aggregation, sinking or coagulation enhancement by exudation (Riebesell, 1991a; Tian et al., 2009; Mäerz and Wirtz, 2009). Strong variations of current speed ( $15\text{--}100\text{ cm s}^{-1}$ ) during a tidal cycle result in an alternation of particle settlement and resuspension (Brockmann and Dippner, 1987; Boon and Duineveld, 1996).

For the GB, it is well established that the spring and pre-summer phytoplankton community consists of over 90% diatoms (Wiltshire et al., 2008). Copepod biomass usually starts to increase in the coastal area of the NS after the first peak of the diatom spring bloom (Krause et al., 2003; Renz et al., 2008). Microzooplankton, as a possible major consumer of primary producers and an important intermediate component between (smaller) algae and copepods in marine foodwebs, are in this region grazing more vigorously nearshore than offshore (Stelfox-Widdicombe et al., 2004; Calbet, 2008).

In the model domain of the GB, the bathymetry typically increases with the distance from the coast (Fig. 4.1). This study is confined to areas that do not exceed a depth of 30 m, where strong tidal mixing impedes stable stratification especially during winter and spring. In order to describe the transect from estuarine coastal to offshore waters we define the three reference points, Inner German Bight (IGB), HR and Central German Bight (CGB), with the average depths of 14.7, 17.3, 31 m, respectively.

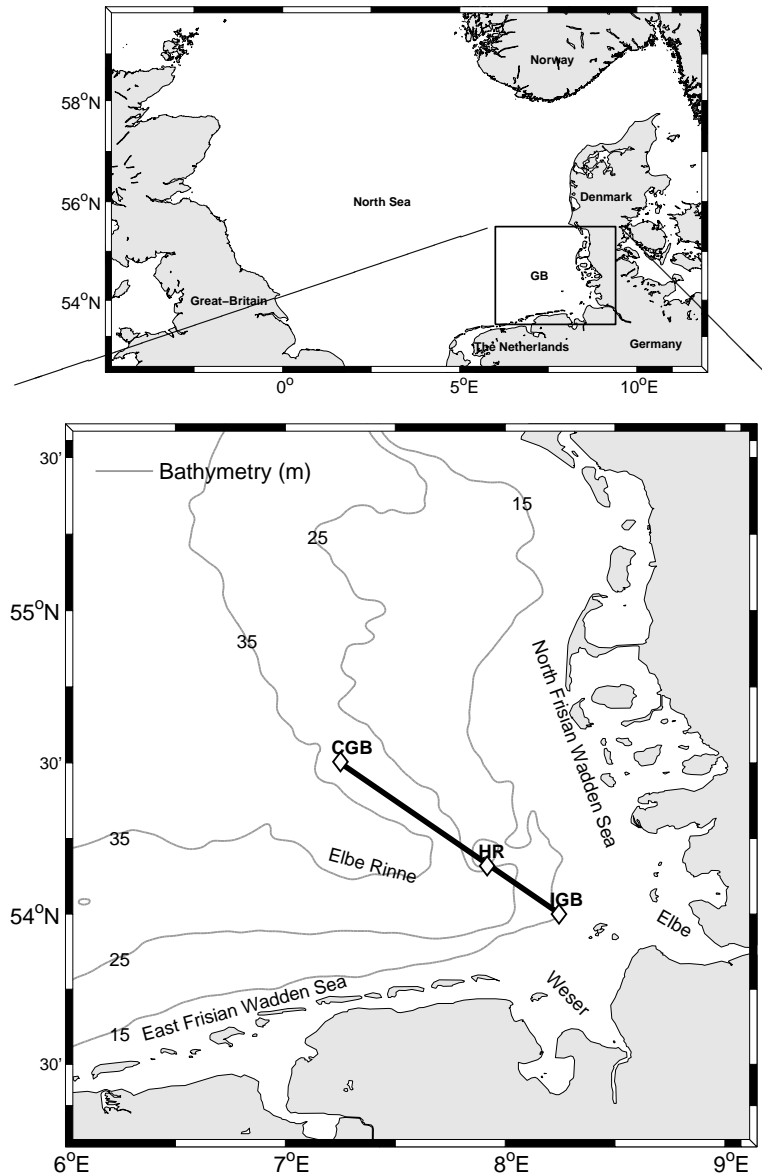


FIGURE 4.1: Study area of the southern North Sea and the model domain of the German Bight (GB). Thin lines show bathymetry (m). Solid thick line represents the transect of interest: from nearshore (IGB) to offshore CGB, crossing the land station, Helgoland Roads (HR). Diamonds represent three selected station points.

#### 4.2.2 Model description

Our general approach is to represent various important physical characteristics of coastal environments and to include key biological processes relevant to bloom development, while aiming at a description with minimal complexity. Physical processes are simulated with the hydrodynamics model GETM, which is a free surface, baroclinic hydrostatic model solving salinity, temperature, water-level elevation and velocities in three dimensions (Burchard and Bolding, 2002). The water column is considered vertically well-mixed in one tidal cycle since stratification is not fully developed yet during spring.

A box model of six biological compartments is coupled in an off-line mode with a depth-averaged transport model based on the 3D output from GETM (see Eq. A.1). If stratification is formed, the mixing rate in the box model is used as an approximation introduced by Fasham et al. (1993) to account for the exchange rate between the upper mixed layer (MLD) and the deep layer. The mixing term is used to import/export material fluxes from/to the bottom boundary at each grid cell, where biological processes are ignored and the nutrient pool is assumed constant.

The biological model originates from an earlier version of Tian et al. (2009) which in turn derives from the models of Popova (1995) or Fasham et al. (1993). The new version includes phytoplankton ( $P$ ), detritus ( $D$ ) and modifies those former models insofar as resolving micro- and meso-zooplankton ( $Z_s$ ,  $Z_l$ ) separately, and two nutrients ( $Si$  and  $N$  for silicate and dissolved inorganic nitrogen, resp.) in order to prescribe two principal loss terms of diatoms as follows.

**Sedimentation:** Diatoms sink at a minimum velocity  $w_s$  which increases at low silicate concentrations (Egge and Aksnes, 1992). Size-dependency of  $w_s$  is neglected in this study since cell size is not resolved as model variable (cf. Fig. 4.3). Sinking rate  $\omega^0$  quantifies the relative loss from the water column (with depth  $h$ ) according to the equation by Tyrrell and Taylor (1996):

$$\omega^0 = \frac{w_s}{h} \left( 1 + w' \cdot \frac{N^* - Si}{N^*} \right) \quad (4.1)$$

Values for the coefficients  $w'$  and  $N^*$  are given in Table 4.2. Assuming that a large fraction of algal cells will die when hitting the ground, only the export flux from the water column to the sea-bed is considered. However, net sedimentation  $\omega$  is frequently affected by high resuspension induced by tidal and wind mixing at the water-seabed interface. Resuspension increases with growing shear stress velocity  $V_t$  ( $\text{m s}^{-1}$ ), calculated from the shear stress and actual water density (Gayer et al., 2006), both taken from the 3D output of GETM. The non-linear decrease in sedimentation with increasing  $V_t$  is expressed following Gayer et al. (2006):

$$\omega = \omega^0 \cdot \max\{0, 1 - (V_t/V_r)^2\} \quad (4.2)$$

with a threshold of  $V_r = 0.01 \text{ m s}^{-1}$ . In this way, sedimentation starts at calm conditions ( $V_t < V_r$ ) and stops at high turbulence ( $V_t > V_r$ ).

**Grazing:** The  $Q_{10}$  law is used in modelling the temperature dependency of the maximum growth rates of zooplankton (Xiao, 2000). The two groups of smaller and larger planktonic consumers  $Z_s$  and  $Z_l$  are assumed to feed according a Holling type III functional response, extended to weighted food preferences (Oguz et al., 2001). Specifically,

$Z_s$  represents heterotrophic flagellates and ciliates, consuming both  $P$  and  $D$ ;  $Z_l$  embraces omnivorous and carnivorous copepods (Broekhuizen et al., 1995), showing selective preference on  $Z_s$  over  $P$ ,  $D$  and  $Z_l$ .

All biological model equations and model parameters are listed in Table 4.1 and 4.2. Major processes and interactions between the model compartments are illustrated in Fig. 4.2. Parameter values are mostly adopted from the previous study of Tian et al. (2009). All biological compartments are thus carried in terms of their nitrogen equivalence by using a constant Redfield ratio for C:N (6.625) and Si:N (15 : 16).

The model configuration was based on the nested North Sea-Baltic Sea system with a horizontal resolution of 3 nm, including the GB domain (53.2°–55.6° N, 6.0°–9.1° E) with a resolution of 1 km (Stanev et al., 2009). In our 2D scheme, the instantaneous production-loss balance in the biological model was vertically integrated over the MLD and divided by the water depth. The variations in the MLD were determined by profiles of potential density computed from the 3D hydrodynamic model, assuming a threshold density change of 0.125 sigma units. The coupled model system was forced by hourly velocity, temperature and salinity fields on a uniform grid size of 1 km and discretely integrated using a time step of 15 minutes. The model has been qualitatively validated using various observations with an emphasis on the spring bloom dynamics in 2003 (Tian et al., 2009). All biological variables were uniformly initialised over the entire GB at values of  $\{N, P, Z_s, Z_l, D\} = \{12.0, 0.05, 0.1, 0.2, 0.0\}$  in  $\text{mmol N m}^{-3}$  and  $\text{Si}=10.0$   $\text{mmol Si m}^{-3}$ . These were roughly consistent with wintertime concentrations as inferred from the World Ocean Database 2005 (Boyer et al., 2006). Fluxes at the open boundaries were set to zero. After a 2-year spin-up the simulation was carried out for the period of 2002–2005. Spatial variability in the light attenuation coefficient  $K_d$  was, due to the lack of SPM fields, reconstructed using salinity (Tian et al., 2009). This approach derived from a high correlation between water turbidity and salinity in the GB (Tian et al., 2010). Incident light was estimated using cloudiness data obtained at daily intervals from the meteorological climate model REMO (Meinke et al., 2004). This setup is in the following termed the standard run (SR).

### 4.2.3 Data integration

HR measurements of temperature and Secchi depth have been taken from surface water, where the water column fluctuates between 6 and 10 m and is generally well-mixed. The mean water column irradiance (PAR) is a function of sea surface irradiance ( $I_0$ ), the attenuation coefficient  $K_d$  and water depth ( $h$ , see Table 4.1).  $I_0$  is routinely collected at the HZG Helgoland land station (www.coastlab.org). Secchi depth ( $Sd$ , m) was converted to light attenuation using the relation  $K_d = 0.191 + 1.242 \cdot Sd^{-1}$ , which has been parameterized for GB coastal waters by Tillmann et al. (2000). Water depth at

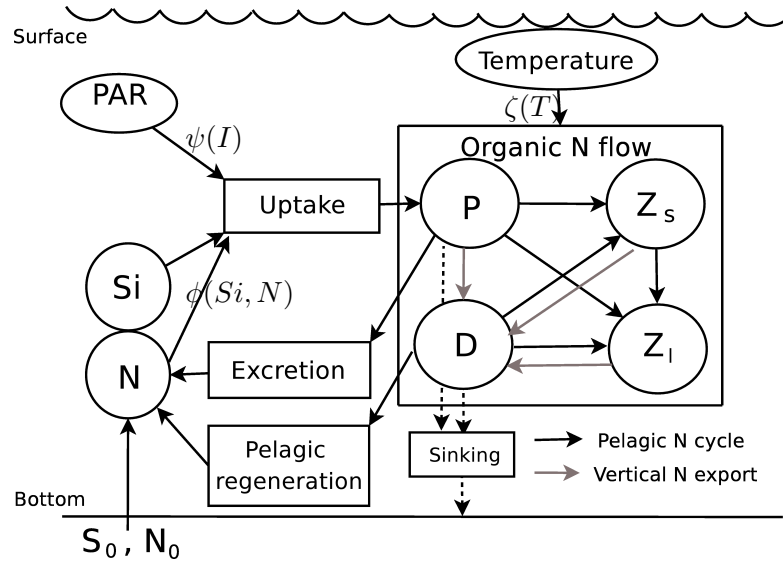


FIGURE 4.2: Schematic diagram of major processes (boxes) and interactions between the model compartments (circles).  $N$ ,  $Si$ ,  $P$ ,  $Z_i$  and  $Z_s$  refer to dissolved inorganic nitrogen, silicate, diatoms, microzooplankton, mesozooplankton, respectively.  $D$  represents pelagic detritus in nitrogen, which later proportionally returns to  $N$ . The forcing data are indicated in ellipses. The equations are presented in Table 4.1.

TABLE 4.1: Biological model equations and process formulations.

$\Re(P) = (1 - \chi)P_P - G_s(P) - G_l(P) - M_P - \omega \cdot P$	
$\Re(Z_s) = \gamma_s[G_s(P) + G_s(D)] - G_l(Z_s) - M_{Z_s}$	
$\Re(Z_i) = \gamma_i[G_l(P) + G_l(D) + G_l(Z_s)] - (1 - \gamma_i)G_l(Z_i) - M_{Z_i}$	
$\Re(D) = \chi \cdot P_P + (1 - \gamma_s)G_s(P) + (1 - \gamma_i)[G_l(P) + G_l(Z_s) + G_l(Z_i)]$ $- \gamma_s \cdot G_s(D) - \gamma_l \cdot G_l(D) + (1 - \beta)(M_{Z_s} + M_{Z_i}) + M_P - M_D - \frac{w_d}{h} \cdot D$	
$\Re(N) = -P_P + \beta(M_{Z_s} + M_{Z_i}) + M_D + \nu \cdot (N_0 - N)$	
$\Re(Si) = -\rho_{S2N} \cdot P_P + \nu \cdot (S_0 - Si)$	
$P_P = \mu_o \cdot \zeta(T) \cdot \psi(I) \cdot \phi(N, Si) \cdot P$	gross primary production
$\zeta(T) = Q_{10}^{\frac{T-10.0}{10}}$	temperature factor to growth function
$\phi(N, Si) = \min\left(\frac{N}{N_H + N}, \frac{Si}{S_H + Si}\right)$	nutrient-limited factor
$\psi(I) = \frac{2}{h} \int_0^h \frac{I_z}{I_H + I_z} dz dt$	mean water column light-limited factor
$I_z(t) = I_0(t) \cdot e^{-K_d \frac{z}{\tau}}$	underwater light at depth $z$
$I_0(t)^\dagger = E(\theta, t) \cdot F_c \cdot (1 - a) \cdot (1 - 0.7C) \cdot W2E$	incident light at sea surface
$K_d = (K_w - \varepsilon_{CDOM} \cdot SAL) + \varepsilon_D \cdot D + \varepsilon_P \cdot P$	light attenuation coefficient
$M_P = \lambda_P \cdot P$	natural mortality
$M_{Z_s} = \lambda_s \cdot Z_s$	excretion term
$M_D = \lambda_D \cdot D$	detritus breakdown to $N$
$M_{Z_i} = \lambda_i \cdot Z_i^2$	mesozooplankton total loss term
$G_s(C_i) = \zeta(T) \cdot \sigma_s \cdot Z_s \frac{ps_i \cdot C_i^2}{R_s + \sum_{i=1}^n ps_i \cdot C_i^2}$	microzooplankton grazing term on $C_i$ (i.e. $P, D$ )
$G_l(C_i) = \zeta(T) \cdot \sigma_l \cdot Z_i \frac{pl_i \cdot C_i^2}{R_l + \sum_{i=1}^n pl_i \cdot C_i^2}$	mesozooplankton grazing on $C_i$ (i.e. $P, D, Z_s, Z_i$ )
$\nu = \begin{cases} \frac{\nu_H}{h} & \text{if } h = \text{water depth} \\ \frac{\nu_M}{h} & \text{if } h = \text{MLD} \end{cases}$	flux rates between surface mixed layer and bottom water interface

$\dagger E(\theta, t)$  denotes the solar irradiance at the top of the atmosphere, a function of the local latitude  $\theta$  and time  $t$  with solar constant set to  $1367.0 \text{ W m}^{-2}$  (Ebenhöh et al., 1997).  $C$  denotes cloudiness.  $\tau$  is the half day length.

TABLE 4.2: Parameters of the ecosystem model and conversion factors.

Parameter	Symbol	Value	Unit
Phytoplankton maximum growth rate	$\mu_o$	1.5	$\text{d}^{-1}$
Temperature coefficient	$Q_{10}$	2.2	
Nutrient half-saturation constant	$N_H, S_H$	1.0, 2.5	$\text{mmol m}^{-3}$
Light half-saturation constant	$I_H$	80.0	$\mu \text{Ein m}^{-2} \text{s}^{-1}$
Half-saturation constant, zooplankton loss rate	$Z_H$	0.2	$\text{mmol N m}^{-3}$
Half-saturation constant, zooplankton grazing	$R_s, R_l$	0.5, 0.5	$\text{mmol N m}^{-3}$
Natural mortality rate	$\lambda_P, \lambda_s$	0.05, 0.1	$\text{d}^{-1}$
Mesozooplankton loss rate	$\lambda_l$	0.25	$\text{d}^{-1}$
Exudation rate	$\chi$	0.05	
Detrital breakdown rate	$\lambda_D$	0.1	$\text{d}^{-1}$
Zooplankton maximum ingestion rate	$\sigma_s, \sigma_l$	0.35, 0.3	$\text{d}^{-1}$
Zooplankton assimilation efficiency	$\gamma_s, \gamma_l$	0.75	
Microzooplankton feeding preferences	$ps_p, ps_d$	0.7, 0.3	
Mesozooplankton feeding preferences	$pl_p, pl_d, pl_{zs}, pl_{zl}$	0.8, 0.2, 1.0, 0.1	
Sinking velocity of diatom and detritus	$w_s, w_g$	0.5, 1.0	$\text{m d}^{-1}$
Diatom sinking factor when silicate deplete	$w', N^*$	5.0, 2.0	
Nitrogen fraction of zooplankton losses	$\beta$	0.3	
Redfield C:N and Si:N ratio	$\rho_{C2N}, \rho_{S2N}$	$\frac{106}{16}, \frac{15}{16}$	
N and Si concentration below surface mixed water	$N_0, S_0$	12.0, 10.0	$\text{mmol m}^{-3}$
Mixing rate	$\nu_M, \nu_H$	0.01, 1.0	$\text{m d}^{-1}$
Fraction of PAR to total solar irradiance	$F_c$	0.47	
Conversion factor from energy to photo content	$W2E$	4.17	$\mu \text{Ein m}^{-2} \text{s}^{-1} (\text{W m}^{-2})^{-1}$
Air-sea transmittance due to albedo and evaporation	$a$	0.1	
Attenuation for pure seawater	$K_w$	2.06	$\text{m}^{-1}$
Factor between the attenuation due to CDOM and salinity	$\varepsilon_{\text{CDOM}}$	0.05714	$\text{m}^{-1} \text{psu}^{-1}$
Diffuse attenuation cross section of phytoplankton	$\varepsilon_P$	$4.0 \cdot 10^{-4}$	$\text{m}^2 \text{mg C}^{-1}$
Diffuse attenuation cross section of detritus	$\varepsilon_D$	$2.0 \cdot 10^{-4}$	$\text{m}^2 \text{mg C}^{-1}$

HR ( $h$ ) was set to 8 m. However, the water monitored at HR originates from deeper areas because the sampling takes place at the shallowest part of the Helgoland region.

The measurements of phytoplankton and dissolved nutrients have been obtained from the HR time series (Wiltshire et al., 2008). A description of sampling techniques and procedures, and of quality control can be found in Wiltshire and Dürselen (2004) and Raabe and Wiltshire (2009). Mesozooplankton abundance has been monitored since 1974 by Greve et al. (2004). Individual counts were transformed to carbon units by assuming a specific weight of  $14 \mu\text{gC/Ind}$  for *Temora longicornis*,  $3.5 \mu\text{gC/Ind}$  for *Acartia clausii*, and  $10 \mu\text{gC/Ind}$  for *Pseudocalanus elongates*, *Paracalanus parvus* or *Centropages* spp. These weights undergo only small variations between March and May (Broekhuizen et al., 1995). We note that this conversion is only an approximation so that biomass values cannot be strictly compared with model results.

To estimate the equivalent spherical diameter (ESD) of diatoms, we divided total cell biovolume by total cell abundance, which gave the mean volume per cell  $V_{dia}$ . Per definition, we had  $\text{ESD} = (\frac{6V_{dia}}{\pi})^{1/3}$ . This simple conversion neglected the exact shape of the diatom cell size distribution. However, alternative formulations that account for typical distribution functions do not yield significantly different estimates for ESD.

Chl-*a* images from the MEdium Resolution Imaging Spectrometer (MERIS) on the EN-VISAT satellite were taken for early April from Tian et al. (2009) for 2003 and from Petersen et al. (2008) for 2004.

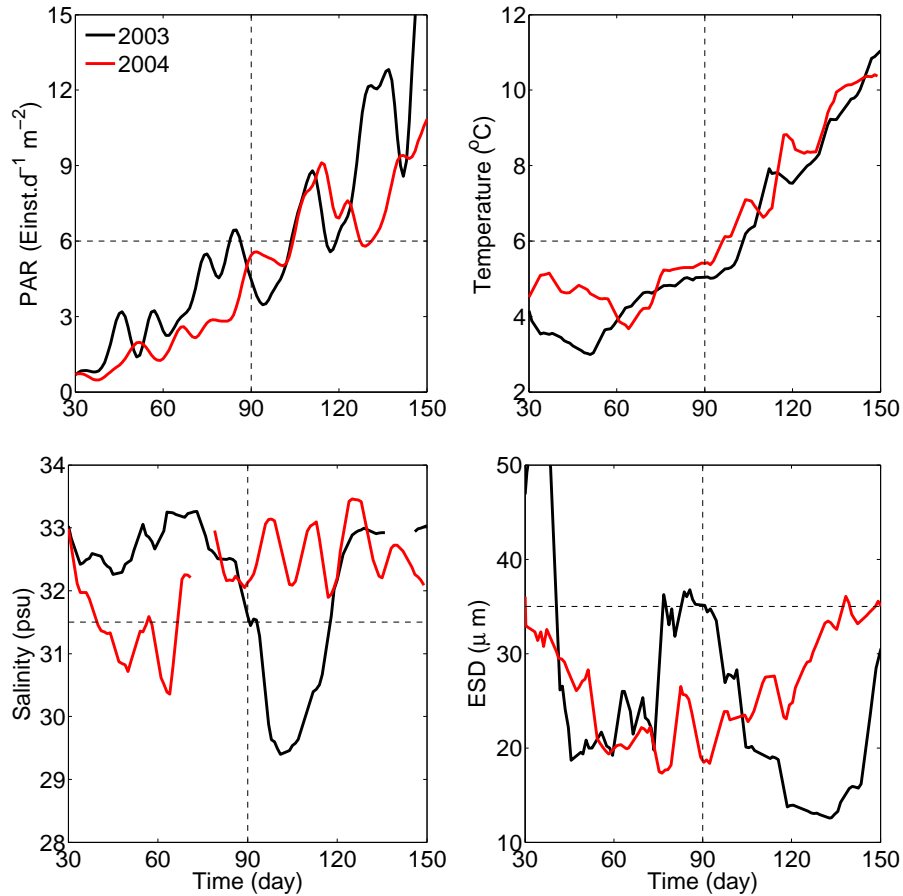


FIGURE 4.3: HR observations in winter-spring of 2003 and 2004: the mean water column irradiance (PAR), salinity, water temperature and the derived ESD of diatom.

#### 4.2.4 Sensitivity tests

We performed sensitivity studies by varying PAR and temperatures in a number of scenario runs and then by examining the effects on the instantaneous growth rates of  $P$  and  $Z$ . The numerical experiments were performed under the realistic circulation patterns of 2003 and 2004, respectively. This way, we aimed to decompose the physical processes into different factors and to differentiate their effects on major biological components at the system-level.

Specifically, lower light intensities were used to force the simulation of 2003 to test whether light forcing combined with lateral advection are the primary drivers leading to a delayed bloom like in 2004. An opposite test for 2004 was used to test reproducibility of an early bloom (like in 2003). In addition, the growth rate of  $P$  and  $Z$  at higher temperatures was tested for both years by adding  $T + 3^\circ\text{C}$ . The value of  $3^\circ\text{C}$  was concerned as the temperature difference between the two-year bloom events (Fig. 4.3).

For the analysis of temperature scenarios, the daily local production-loss balance was expressed as the net diatom growth rate (NDG). We calculated the difference of NDG



between IGB and CGB as an indicator for the potential nearshore-offshore gradient of the spring bloom. Additionally, we calculated the ratio between the loss term of daily production due to grazing and due to particle sinking (sedimentation and natural mortality), both averaged over the entire coastal transect.

## 4.3 Results

### 4.3.1 Sensitivity of the HR bloom to local light and temperature variations

Differences in water provenance are evident from salinity measurements (Fig. 4.3 and 4.4) showing that the diatom spring bloom began in late March 2003, under the dominance of coastal waters, while the late bloom in 2004 (mid-April) occurred at an offshore water prevalence (Tian et al., 2010). Before April (day 90), vertically averaged PAR in 2003 were generally higher than in 2004. Prior to the bloom onset in each year, PAR exceeded  $5 \text{ Ein m}^{-2} \text{ d}^{-1}$  (Fig. 4.3). Maximum diatom biomass occurred in mid-April 2003 when temperature was still below  $6^\circ\text{C}$  in contrast to the temperature of  $9^\circ\text{C}$  in May 2004 at the bloom peak of that year. In the early development of the bloom in 2003, diatoms had mean cell sizes (i.e. ESD) around  $35 \mu\text{m}$ . In the same period of 2004, large diatoms were absent. ESD gradually increased from 20 to  $35 \mu\text{m}$  until May. Dominant blooming species were presumably similar between two years. The bloom peaks were followed by silicate depletion (Fig. 4.4). There was no immediate response of copepod biomass to diatom growth in both years and a substantial increase in copepod biomass was only observed by the end of bloom in 2004.

The model in the standard run (SR) reproduces the bloom onset and termination in 2003 as monitored at HR (Fig. 4.4). The simulation well captures the timing of silicate depletion as well as the increase in copepod biomass, though the latter was systematically overestimated during the entire bloom period. The model in particular fails to describe the post-bloom decline of copepod biomass. The simulation of 2004 reproduces the observed bloom onset, the timing of the diatom biomass maximum on day 120 as well as the bloom termination. Biomass concentrations are, overall, slightly overestimated.

In the sensitivity tests of the simulation for 2003 (Fig. 4.4), the diatom bloom starts earlier and is significantly enhanced after increasing temperature by  $3^\circ\text{C}$ . When reducing PAR by 25%, the simulated bloom starts later and reaches a lower peak value. In both experiments, the magnitude of silicate depletion covaries with the magnitude of the diatom bloom. Simulated copepod biomass directly responds to temperature changes but is insensitive to changes in light intensity. Increasing temperature in the 2004 simulation causes an earlier bloom but does not increase the biomass maximum. A 25% increase in PAR slightly raises diatom growth rates during the pre- and mid-bloom

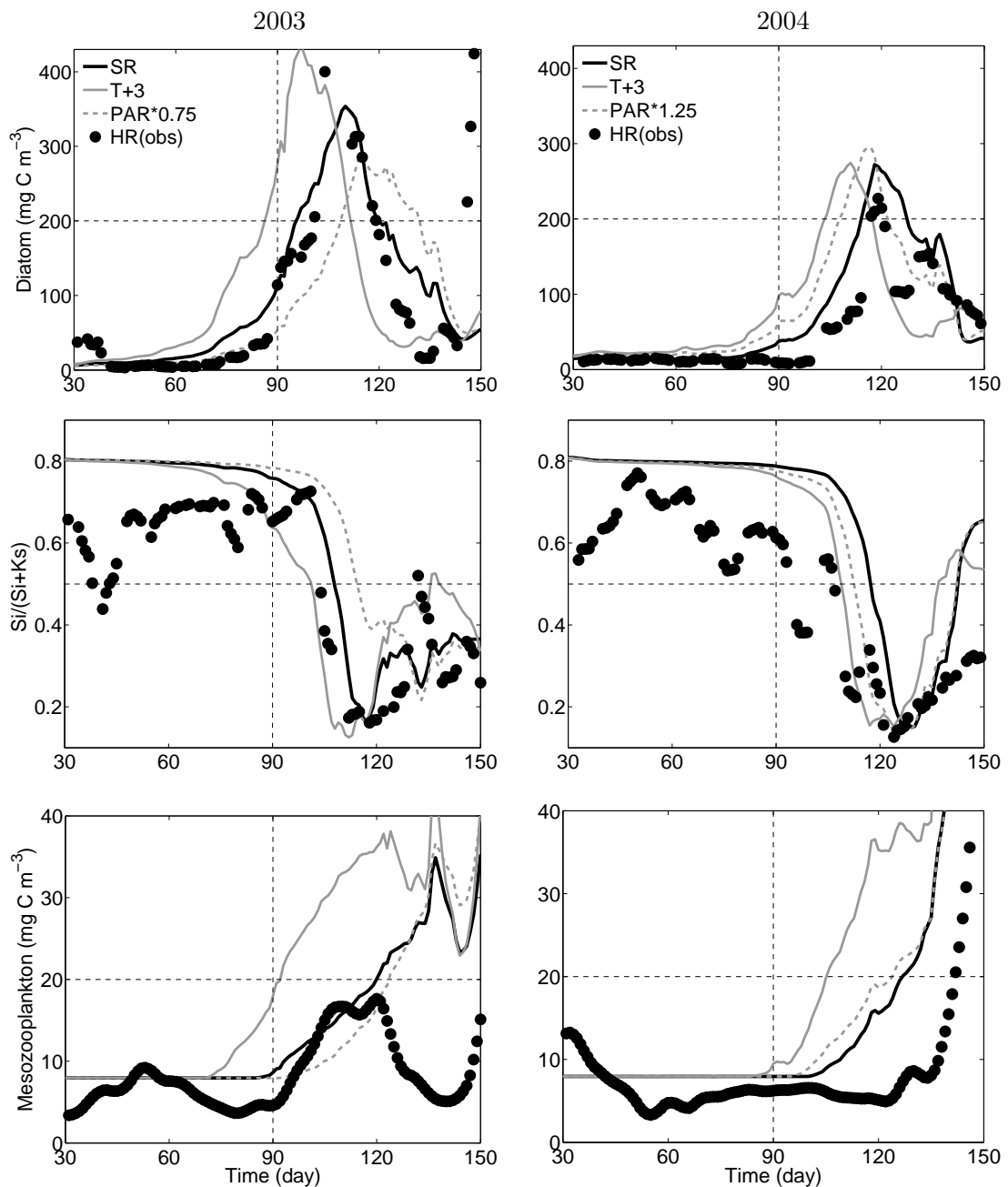


FIGURE 4.4: HR time series are compared with the simulation of silicate limitation, diatom and mesozooplankton biomass for 2003 (left) and 2004 (right). The simulations of SR and sensitivity tests on changing PAR and temperature are compared in the respective years.

but not in the post-bloom phase. Copepod biomass is more sensitive to temperature changes than diatom maximum biomass. The simulation of 2003 with reduced PAR by 25% reveals a similar timing and magnitude of the diatom bloom as in the 2004 SR, while the simulation with the forcing of 2004 and increased PAR by 25% can not reproduce the diatom bloom in the SR for 2003. In other words, the HR spring bloom dynamics turns out to be less sensitive to changing light intensity and temperature in 2004 than in 2003.

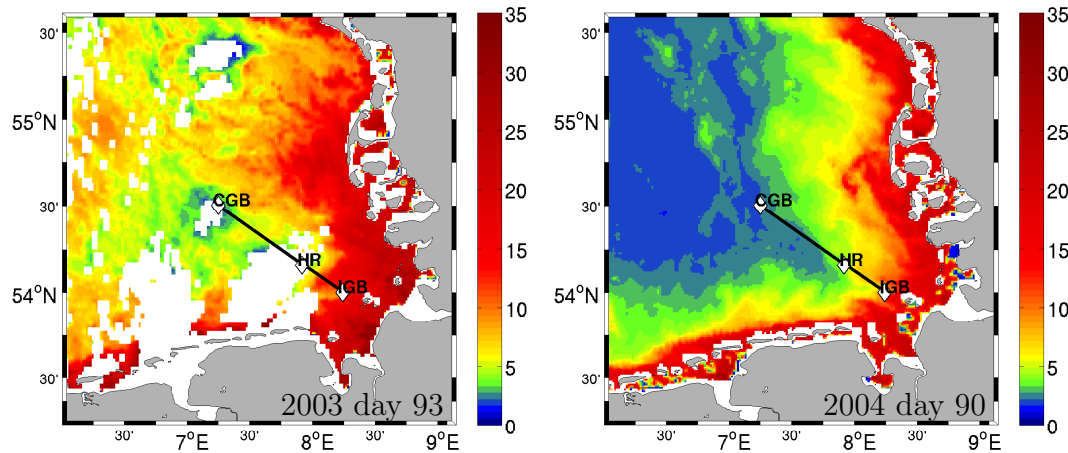


FIGURE 4.5: Spatial distribution of Chl-*a* concentration ( $\text{mg m}^{-3}$ ) in early April 2003 and 2004 from MERIS satellite images.

### 4.3.2 Sensitivity of spatial gradients in Chl-*a* to light and lateral advection

The satellite images show strikingly high Chl-*a* levels extended from nearshore to offshore in early April 2003 (Fig. 4.5). In contrast, high Chl-*a* concentrations were restricted nearshore in 2004 with a sharp gradient from nearshore to offshore. As the coupled model was already tested with respect to major features of lateral Chl-*a* gradients in 2003 by Tian et al. (2009), we here focus on reconstructing and comparing the evolution of the spring bloom along the nearshore-offshore gradient between different years.

We first remove the effect of lateral advection by conducting simulations without the transport model but otherwise using the realistic physical forcing of 2003 and 2004. The resulting evolution of simulated diatom biomass then reflects the local production-loss balance across the coastal topography (Fig. 4.6). Typically, diatom biomass as well as primary productivity decrease with the increasing distance from shallow nearshore to deeper offshore waters. Spring bloom phenology differs between 2003 and 2004, with an earlier onset and higher biomass maximum in 2003, particularly in the offshore stations of HR and CGB. Simulated diatom biomass for the early and mid-bloom at HR and IGB agrees well with the HR observations in 2003. In the 2004 simulation, the biomass evolution at HR is overestimated and the simulated bloom of CGB agrees better with the observations at HR.

Based on our model hindcast, these differences can be explained by light-limitation factors to local growth rate (i.e.  $\psi(I)$  in Table 4.1). The values exceed 0.5 in March 2003 (day 60–90) prior to the blooms at all three stations (Fig. 4.6). In winter-spring 2004, by contrast, HR and IGB are forced by poor light conditions ( $< 0.5$ ) and the bloom at CGB coincides with the light factor surpassing the threshold value of 0.5. The initiation of the early spring bloom in 2003 can therefore be associated with sufficient

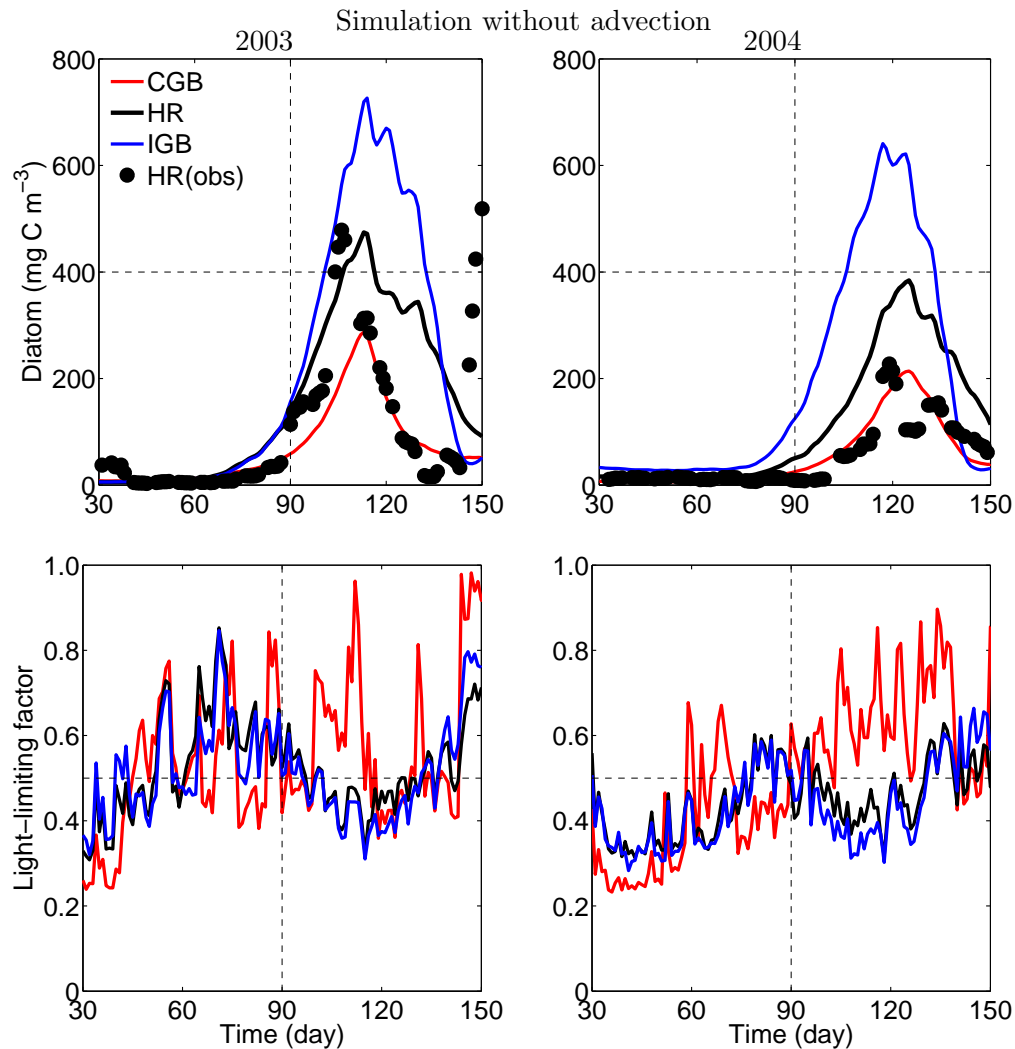


FIGURE 4.6: Evolution of simulated diatom biomass and light factors to local growth rate at three locations based on box model without the transport model in comparison with the HR observation (solid circles). The simulation used the realistic forcing of 2003 and 2004, respectively,

light conditions in that year, and the delayed bloom in 2004 with poor light availability throughout winter-spring. Such critical role of average light availability in the water column for the timing of the spring bloom at HR can also be found in other years (not shown).

How does lateral advection change the position and spatial structure of coastal water masses and thereby translate local growth or loss to spatial patchiness? Simulated Chl-*a* concentrations (derived from diatom carbon) vary along the west-east GB transect between March and April as an effect of lateral advection (Fig. 4.7). In 2003, the bloom initiates as early as day 60 nearshore and then propagates along the transect. The nearshore bloom fully develops until day 90. Chl-*a* concentrations typically decrease from nearshore to offshore and the large extent of high Chl-*a* levels with a small lateral gradient along the transect lasts about one month. The evolution of the bloom

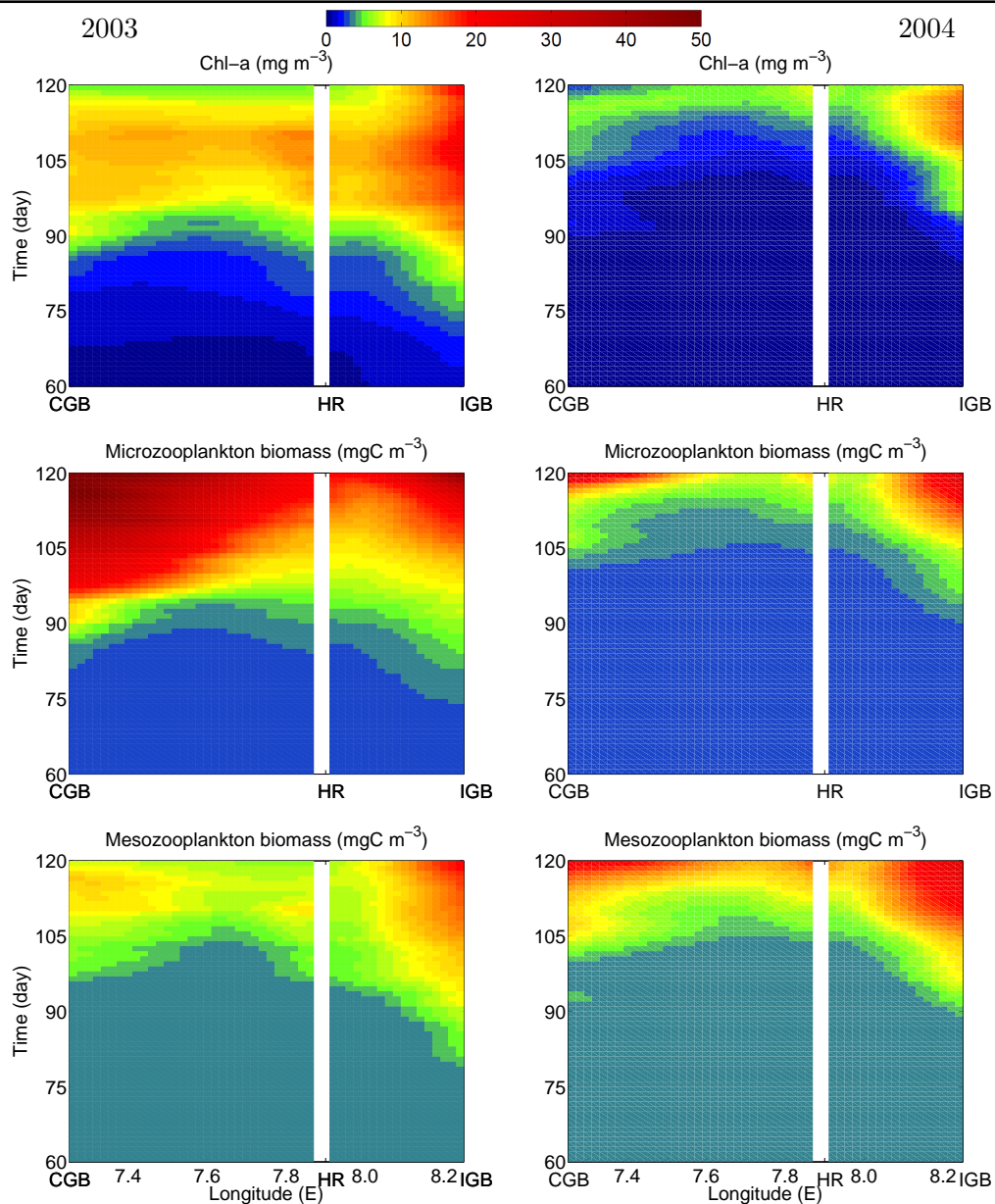


FIGURE 4.7: Evolution of simulated Chl-*a* concentration (drived from diatom carbon) and zooplankton biomass along the transect resulted from the SR for 2003 (left) and 2004 (right). The snap shots of satellite Chl-*a* concentration around day 90 in both years refer to Fig. 4.5. A constant C:Chl ratio of  $40 \text{ g C (g Chl-a)}^{-1}$  is used.

along the transect is accompanied by an increase of microzooplankton biomass. Meso-zooplankton biomass is low until the end of April. A relatively high mesozooplankton biomass nearshore is associated with lower abundance of microzooplankton, in contrast to the relation between meso- and micro-zooplankton biomass offshore. In 2004, the simulated bloom is restricted nearshore, i.e. to the east of HR. To the west of HR, Chl-*a* concentrations remain homogeneously low during March. Chl-*a* concentration in the CGB gradually increases in April and the Chl-*a* gradient offshore (between CGB and HR) seems to be unconnected to the gradient nearshore (IGB). The model results (in Fig. 4.6 and 4.7) show a good agreement with the observations (Fig. 4.3) that the spring

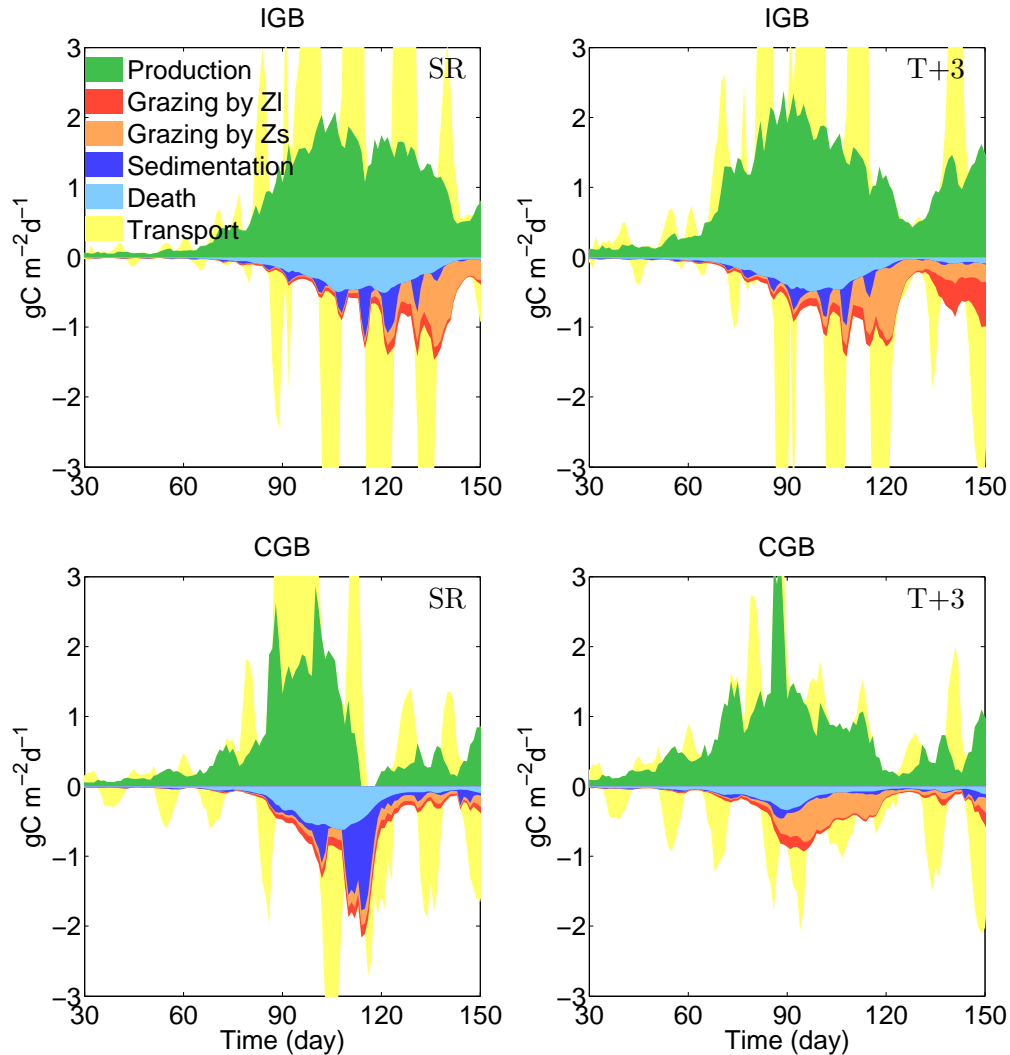


FIGURE 4.8: A comparison of the key components contributed to diatom net growth offshore (CGB) and nearshore (IGB) based on the standard run (SR) in 2003 in contrast to the test with increased temperature by  $3^\circ\text{C}$ .

bloom at HR was more associated with the coastal bloom in 2003 and the offshore bloom in 2004.

### 4.3.3 Sensitivity of diatom production to a warm climate

Our model results describe how the distance to the coast (i.e. bathymetric variations) affects the fate of diatoms during the bloom. The production in the IGB increases from early March and is balanced primarily by natural mortality and by gradually increased microzooplankton grazing until May 2003 (Fig. 4.8). At that time, sedimentation is yet insignificant because vertical mixing and higher nutrient availability counteract sedimentation. The residual current in the IGB is relatively smaller than the open offshore area, resulting in relatively long residence time (Stanev et al., 2009), although instantaneous current transport is high due to the shallowness (Fig. 4.8). All these factors allow the

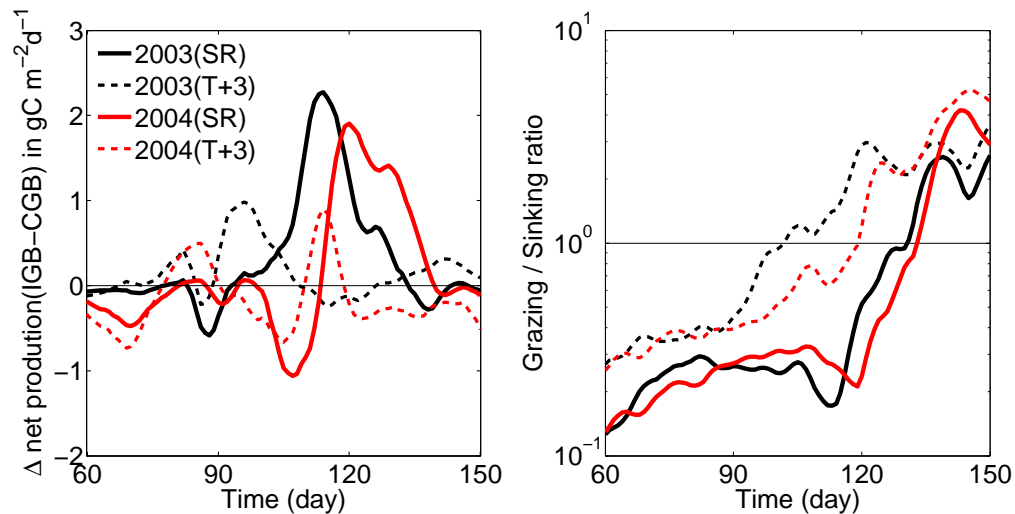


FIGURE 4.9: Comparisons of temperature scenarios by increasing  $3^\circ\text{C}$ : left panel showing the difference of daily diatom net growth between IGB and CGB; right panel showing the ratio between the loss term of daily production due to grazing (by  $Z_1$  and  $Z_s$ ) and due to particle sinking (sedimentation and natural mortality), both averaged over the entire coastal transect.

nearshore bloom to persist for more than two months. The characteristic increase in production at the CGB starts almost at the same time as nearshore and coincides with considerably positive mass transport. Natural mortality and sedimentation are major loss terms in April which terminate the bloom within few weeks. The direct display of the loss terms of diatoms reveals that, in 2004, alike in 2003, the post-bloom production is mainly channelled to microzooplankton grazing nearshore and exported through sedimentation offshore (only shown for 2003). In spring when temperature-dependent grazing are still low, the major mechanism regulating the local production-loss balance, nearshore and offshore, is depth dependent mixing/sinking.

How is the distance to the coast then affecting the sensitivity of spring bloom dynamics to altered physical forcing? Here we only present the high temperature scenario for 2003 as results are similar in 2004. Diatom daily production remarkably differs in its response to temperature changes at the contrasting sites (Fig. 4.8). Production only slightly raises with increased temperature in the IGB, but becomes clearly less intense and more constant in the CGB. High temperatures lead to considerably enhanced microzooplankton grazing in April at both locations. Copepod grazing in May strengthens only nearshore. While offshore, the prevalent importance of sedimentation in the post-bloom is replaced by herbivorous grazing. The large algal biomass inputs due to advection at CGB in the SR simulation vanish in the high temperature scenario.

The net growth difference (NDG) between IGB and CGB aggregates the nearshore-offshore gradient in the spring bloom. Its mostly positive value just reflects typically higher productivity nearshore compared to offshore (Fig. 4.9). High NDG values coincide with the spring bloom events at HR in 2003 and 2004, presumably driven by light

forcing (Fig. 4.6). Interestingly, the maximum NDG does not differ between the two years despite the very different peak biomasses. This again provides evidence that lateral advection played a different quantitative role in the two years in translating local factors to a lateral gradient. However, after increasing temperature by 3 °C, the period of positive NDG is anticipated and the NDG average is much reduced. It even describes a negative spatial difference (i.e. higher offshore production) for a “warm” 2004. The modification from positive to negative spatial difference is concomitant with the increasing ratio of the total grazing loss-term to the total particle sinking loss-term (Fig. 4.9). The NDG gets negative only when the ratio exceeds 1 (Fig. 4.9). This value defines a situation where the diatom production is channeled more to pelagic food webs than to vertical export. This effect of grazing under higher temperature is evident throughout the two-year experiments, appearing independently of yearly differences in light and mass transport.

## 4.4 Discussion

### 4.4.1 Modelling environmental drivers

This paper attempts to search for general mechanistic patterns through which the spring bloom dynamics is regulated in coastal marine environments. For doing so, the study assesses model and observational data on how phytoplankton copes with lateral and interannual changes in physical forcing. We do not aim to investigate errors and uncertainties in model simulations, but, rather, we use available observations together with model simulations, to quantify the effect of different processes dominant in different periods and to advance the understanding of how multiple factors operate together. However, we note that due to the simplification of otherwise complex phenomena the simulation results have to be interpreted with caution.

When re-assessing the parameterization for a simple NPZD model, [Popova \(1995\)](#) found that the variability of light-limited phytoplankton growth through the water column greatly increased the sensitivity of the solution to varying model parameters. Specifically, the parameters controlling the dependence of primary production on PAR and controlling the zooplankton loss and growth rates were the key to improve model predictions with respect to observations. In a coupled physical-biological model, these key parameters can be linked to environmental factors by integrating SPM and salinity fields to recalibrate water column light availability ([Muylaert et al., 2005](#); [Tian et al., 2009](#)) or by introducing a temperature-dependent grazing rate for zooplankton.

High sinking rates of phytoplankton cells has been shown to be important during the spring bloom and tend to be enhanced by the aggregation of living cells with suspended material towards the end of diatom blooms ([Riebesell, 1991b](#); [Brussaard et al., 1995](#);



Smetacek, 1999). Small aggregates are prone to break up under strong turbulence mixing (Riebesell, 1991a). In the GB, where turbulent energy in the water column is repeatedly generated by tidal currents and wind stress, shear can become the dominant mechanism controlling both particle aggregation and break-up. For example, in shallow and tidally dominated coastal regions like the Wadden Sea, particles may rapidly sink down to the seabed during tidal slack and calm wind with sinking velocities of more than  $4 \text{ m h}^{-1}$  (Mäerz and Wirtz, 2009). While otherwise physiologically mediated sinking of alive algae can be of minor importance compared to vertical mixing and particle resuspension (Smayda, 1974). However, in stratified offshore waters, turbulent mixing does not keep diatoms in the upper mixed layer (Raven and Waite, 2004) and tidal mixing becomes largely restrained to the bottom layer (Riebesell, 1991a). The spatial differences in sedimentation rate therefore mainly result from local topography and hydrodynamic (mixing) regimes.

In this hindcast study, we use a uniform set of biological parameters to examine the response of plankton dynamics to realistic environmental gradients in a coastal ecosystem. We identified few key factors comprising the salinity-related light attenuation coefficient, the temperature-mediated grazing rate and the (physiologically and physically determined) sedimentation rate, which are directly or indirectly driven by mesoscale physical processes (i.e. temperature, salinity and mixing regimes). These factors vary seasonally, interannually, and along the nearshore-offshore transect. With their characterization, we attempt to refine ongoing modelling studies that address the dynamics of coastal ecosystems and, in particular, we provide a basis for future models resolving the adaptive behaviour of a phytoplankton population (Wirtz, 2004; Troost et al., 2005).

#### 4.4.2 What governs the HR bloom formation and affects the sensitivity to local forcing?

In light-limited coastal systems like the GB, mean water column irradiance is an important constraint for autotrophic growth (Townsend et al., 1994; Colijn and Cadée, 2003; Iriarte and Purdie, 2004). In the experiment without a transport model, stronger light limitation in 2004 slows down the winter-spring build-up of diatom biomass both nearshore and offshore compared to 2003. At HR, however, the transitional position between nearshore and offshore waters makes large annual difference in the bloom timing very likely. Local light forcing seems to be the primary driver controlling the early- and mid-bloom at HR in 2003 but not exclusively in 2004. The hindcast of diatom biomass along the transect suggests that local growth and loss is linked from nearshore to offshore in 2003 but is separate between nearshore and offshore in 2004.

The HR spring bloom in late April 2004 has earlier been found to be accompanied by a tidal front displacement between nearshore and HR (Tian et al., 2010). The tidal front in the GB typically forms in late April along the 25 m isobath (Dippner, 1993), separating

the well-mixed coastal waters with a higher Chl-*a* concentration from the stratified offshore waters with a lower Chl-*a* concentration (Tian et al., 2009). The coastal area is typically characterized by high nutrient inputs and low water column irradiance due to high SPM concentrations (Tian et al., 2009). The phytoplankton bloom sets in as soon as PAR exceeds a threshold. PAR, in turn, varies with surface incident radiation and water turbidity, so that the threshold is often met (under calm conditions) in early spring (Iriarte and Purdie, 2004). In the offshore area, the development of the thermocline controls the onset of the spring bloom, by reducing the effective mixing depth of the water column and thus enhancing the mean light level available to photosynthesizing phytoplankton cells (Townsend et al., 1994). The influence of lateral transport of high productivity from nearshore to offshore diminishes with the formation of the tidal front in late spring (Dippner, 1993).

The offshore bloom in early spring 2003 can be triggered by sufficient light in the water column despite the absence of stratification due to the large spatial extent of the coastal bloom. On the contrary, given low light and much reduced coastal influence in winter-spring 2004, the bloom offshore only starts after the onset of stratification. Consequently, the spatial gradient in phytoplankton concentration is shaped by the tidal front between the well-mixed coastal and stratified offshore waters. The effects of variations in surface mixed layer depth become more prevalent than changes in light intensity (Tirok and Gaedke, 2006; Berger et al., 2007). Taken together, the interplay of local light limitation, vertical mixing and lateral advection governs the early and mid-bloom in the nearshore-offshore transition. Interannual changes in their spatio-temporal distribution, to a dominant part reflecting alterations in atmospheric forcing, thus also determines the interannual variability in the growth of coastal phytoplankton.

Major features of the spring bloom could be reproduced by our simple model based on a unique parameter set. Though, remaining deviations between model results and observations point to changing sensitivities of coastal phytoplankton to the above mentioned environmental drivers which, so far, had not been resolved. Algal community structure is usually organized along light gradients as, for example, evident from culture competition experiments (Sommer, 1994). Changes in species composition as well as in the physiological state of cells were proposed to explain the significant shift in Chl:C ratios along the salinity/light gradient in our focus area (Tian et al., 2010). According to the HR time series (Fig. 4.3), the decline of salinity in winter-spring coincided with a decrease of diatom ESD. Additionally, strong variations in the light-limitation factor in our model demonstrates a very different light stress from nearshore to offshore. These findings necessitate a further investigation on spatial succession patterns along the nearshore-offshore gradient as an essential internal factor for the development of spring blooms.

### 4.4.3 Can temperature-mediated grazing modify the spatial sensitivity?

Nutrient exhaustion and grazing frequently terminate coastal spring blooms (Waite et al., 1992a). In the post-bloom period, when silicate becomes limiting, strong aggregation of living cells (and detritus) and a rapid decline of the diatom assemblage will occur (Riebesell, 1991b). After the bloom the massive production of copepods in early summer occurs at a considerable time-lag in the GB (Renz et al., 2008), which is also seen from the HR time series (Fig. 4.4). Feeding thresholds which have since long been demonstrated for copepods (Kiorboe and Saiz, 1995) are also assumed by our model. In addition, metabolic rate of copepods is known to be lowered in later winter and early spring in many temperate regions (Townsend et al., 1994). Therefore, our model describes that herbivorous grazing does not play an important role in the early phase of the spring bloom because of low temperature in early April 2003 and low diatom biomass in 2004.

With distance to the coast, diatoms experience different temperature (grazing) and mixing (nutrient, sinking) regimes. The lateral gradient in the ration of those environmental factors, in turn, may determine the fate of the bloom biomass, and, this way, whether the massive productions fuels the pelagic food-web or local benthic biogeochemistry (microbes and their consumers). In shallow coastal waters, the pelagic and benthic subsystems are closely coupled (Greve et al., 2004). Freshly settled phytodetrital organic material is rapidly consumed and incorporated into benthic biomass (bacteria, detritivores, filter feeders, etc), while benthic nutrient mineralization may support a considerable fraction of the pelagic phytoplankton production (Heiskanen and Tallberg, 1999). Moreover, strong tidal mixing may counteract sedimentation, keeping diatom biomass within the water column. The coastal bloom which lasts for more than two months until May (Tiselius and Kuylenstierna, 1996) can then support a massive secondary production with high abundances of copepods (Brussaard et al., 1995; Stelfox-Widdicombe et al., 2004; Sherr and Sherr, 2008). By contrast, in stratified offshore waters, silicate depletion closely follows the bloom development and diatoms are effectively exported by particle sinking within one or two weeks, thus preceding zooplankton production (Riebesell, 1991b). Our sensitivity tests predict that under a warmer climate the time-lag between light-triggered phytoplankton spring bloom and temperature-mediated zooplankton production will be reduced. Diatom production will be increasingly channeled to the pelagic food web rather than to vertical export, particularly offshore. The spatial gradient of high productivity from nearshore to offshore can also be impaired by enhanced grazing.

Sinking and grazing impacts both lead to a shift in the phytoplankton size spectrum into the same direction. Under strong sedimentation loss, large diatoms rapidly disappear such that the mean community cell size moves to smaller values (Riebesell, 1991b).

Moreover, the aggregation process may be very species specific, leading to sequential sedimentation of different diatom species from the water column during the blooms (Riebesell, 1991b; Alldredge et al., 1995). Copepod grazing has a similar effect. Mesocosm and *in vitro* experiments have documented that high selective copepod grazing pressure causes a downward shift in the phytoplankton size structure (Stelfox-Widdicombe et al., 2004; Sommer and Lengfellner, 2008; Gaedke et al., 2010). The succession of sedimenting diatom species may explain the decrease of diatom ESD during the bloom 2003 while diatom biomass was still high (Fig. 4.3 and 4.4). Top-down control can be another reason for the delayed diatom bloom in May 2004: the dominance of small microalgae coincided with relatively high zooplankton abundance in April (Wiltshire, K. unpublished data).

Over the last decades there has been a species shift in the NS toward marine organisms with an affinity to higher temperature habitats (Planque and Fromentin, 1996; Kröncke et al., 1998). Since changes in a single trait (temperature optimum) will be likely linked to changes in other traits through trade-offs (Litchman and Klausmeier, 2008), our scenarios based on a simple representation of the plankton may not be representative for long-term changes in spring bloom phenology. Still, we believe that the prominent role of light for the bloom initialization, the sensitivity to non-local physical factors, and the intricate balance between grazing and sedimentation losses in the second bloom phase may also persist under an altered algal community composition. Both observations and our numerical experiments thus underline the needs for a realistic representation of algal communities and, more specifically, phytoplankton traits to improve such predictions. This trait representation together with the modelling framework presented here may better describe the variable sensitivity of ecosystem dynamics on local and non-local factors along the coastal-ocean gradient.

## 4.5 Conclusions

This study on coastal spring blooms sets the focus on the intercomparison of two consecutive years along a nearshore-offshore transect in the German Bight. The significant differences in spatio-temporal bloom patterns, here explained by a variable interplay of physical and ecological driving forces, however, already allows for a tentative extrapolation of our results to the long-term bloom phenology in coastal ecosystems. The integration of observations and a numerical model thus provides a robust basis to develop future process-oriented (trait based) models which are able to predict long-term changes in the spring phenology, probably not only of coastal phytoplankton. Our model demonstrates a critical role of mesoscale spatial variations in coastal plankton dynamics. The physical control, exerting through local light limitation, vertical export and lateral advection, regulates the nearshore-offshore gradient in the early and mid-bloom phase. Different circulation patterns, mediated by atmospheric forcing in shallow-water systems like the GB, induce large interannual differences not only in the timing of the

spring bloom but also its distribution from nearshore to offshore waters. The blooming phase is mainly terminated by sedimentation in stratified offshore waters and by grazing in well-mixed coastal waters. The scenario runs at elevated temperature predict that the spatial difference of the diatom production-loss balance between nearshore and offshore can be impaired by temperature-dependent grazing effects under a warmer climate. Large changes in ESD from HR time series suggest that species succession in different stages of the bloom might occur when selective sinking was significant under the stress by light- or nutrient-limitation or when more intensive grazing anticipated. To better represent these processes acting on a varying phytoplankton community, we suggest a more mechanistic and trait based representation of the coastal phytoplankton. The ability to simulate how plankton traits adapt along the coastal-ocean gradient would improve model accuracy especially with respect to the sensitivity of the ecosystem dynamics to external forcings (e.g. currents, temperature, turbulence and light availability). Future models that acknowledge spatial variations in plankton traits then will extend the concepts presented in this study, revealing the integral impacts of short- or long-term changes in physical conditions on phytoplankton community and the related food-web relationships in temperate coastal ecosystems.

## Acknowledgement

This work was in part supported by the Deutsche Forschungsgemeinschaft (DFG priority program 1162 “AQUASHIFT”). We thank the crew of the R.V. Aade and the scientists and technicians at Helgoland for their support. Especially, we thank K. H. Wiltshire for providing the HR time series and S. Janisch for information on phytoplankton taxonomy. We are grateful to W. Greve for providing copepod data and J. Staneva for the GETM model output.



## Chapter 5

# Conclusions and perspectives

---

Spring blooms in temperate coastal ecosystems display large spatial gradients and rapid temporal evolution of those spatial patterns as a result of spatial (bathymetric) variations in population dynamics and variable horizontal transport (tidal and wind-driven) of water and plankton. The use of a coupled physical-biological model is still a logical first stage to integrate various information on forcing inputs and horizontal distributions of water properties, particularly when addressing spring bloom dynamics in shallow coastal systems like the GB. The central interest is to understand the mechanisms that can give rise to the spatial and temporal variability of the spring bloom and to examine the sensitivity to meteorological and hydrographic variability. This understanding is strongly connected to set-up, test, and analyse a model, but deliberately differs from the attempt to accurately reproduce observed bloom events in great detail.

Even a process-oriented model validation necessitates the compilation of a large amount of available observations. The integrated use of observations and models, however, enables a comprehensive assessment of model sensitivities on hydrodynamics, mass transport, light fluctuation and biological processes. In the thesis, it is in particular found that a more accurate prediction of timing and magnitude of the spring bloom in the GB area critically relates to a realistic account of the spatio-temporal distribution of SPM concentration, as described in chapter 2. An important novelty is the use of satellite-derived light attenuation  $K_d$  data. Technically speaking,  $K_d$  is a more reliable quantity than satellite-derived SPM and Chl-*a* concentration in case 2 waters. The reconstructed  $K_d$  data by integrating continuous SPM fields from a sediment transport model to a light attenuation module are demonstrated to be an important constraint to simulate light-limited phytoplankton growth in the GB ecosystem.

In nearshore areas of the GB, the onset of the spring bloom depends presumably only on photoperiodic control, thus remaining nearly constant between different years. At further offshore locations, if well-mixed coastal waters dominate, underwater light is determined by light intensity and light penetration depth. A sudden period of low wind can effectively ensure deeper light penetration because of reduced sediment resuspension. If the North Sea water dominates, spring bloom dynamics is primarily controlled by the development of seasonal stratification. Time continuous observations reveal two distinct responses of phytoplankton growth (i.e. the bloom timing, P-I relation and

Chl:C ratios) to light variations in the coastal or marine waters dominated blooms, as described in chapter 3. The transient wind slack is identified as an important trigger for the rapid development of spring blooms. Intermittent turbulence induced by wind slack is suggested to be a structuring agent of phytoplankton patchiness. Numerical experiments documented in chapter 4 show that in the offshore water within the 30 m isobath, 1) the bloom in early spring is often triggered by mean water column light ( $I_m$ ) level when stratification is absent, 2) and also benefits from a large spatial extension of the coastal bloom along the nearshore-offshore gradient; 3) on the contrary, the bloom in late spring is delayed by low  $I_m$  throughout winter-spring and develops only when stratification is formed; 4) the spatial gradient in phytoplankton abundance is mostly determined by a tidal front between well-mixed coastal and stratified offshore waters. By means of an integrated data-modelling approach, the spring bloom dynamics of the GB is reconstructed for multiple years, suggesting that various physical controls, exerting through local light limitation, vertical mixing and lateral advection, govern the interannual variability of the phytoplankton distribution in the early- and mid-bloom phases. In turn, environmental gradients may also determine the fate of primary production. Numerical experiments show that the blooming phase is terminated mainly by sedimentation in stratified offshore waters and by grazing in well-mixed coastal waters because there vertical mixing and higher nutrient availability counteract sinking and burial of viable cells. In scenario runs at elevated temperature, sedimentation becomes less important than temperature-dependent grazing and diatom production will be increasingly channeled to the pelagic food web rather than to vertical export, particularly offshore. The spatial gradient of high productivity from nearshore to offshore may thus be impaired by enhanced grazing in warmer waters.

As most information in this study derives from fluorescence measurements, the work has to specifically consider often large variations in the Chl:C ratio within algal cells. I identified two distinct mechanisms which regulate the Chl:C ratio before and during the spring bloom. The relevance of these mechanisms alternates between the years which are dominated either by coastal or by marine waters. In highly light-limited coastal systems the Chl:C ratio tends to be down-regulated, leading to a correlation between salinity and Chl:C in transitional waters. In deeper parts of the GB, I found a significant negative correlation between the Chl:C ratio and  $I_m$ , reflecting photoadaptation in the phytoplankton community. Some model-data discrepancies appearing in my study suggest that the spatial variability in Chl-*a* cannot be fully captured by a uniform set of biological parameters. Hence, to describe highly dynamic coastal marine ecosystem we need to better resolve adaptation processes on a number of scales. On shorter time scales and small vertical and lateral scales, a dynamic photoacclimation model is required to simulate the response to changing gradients in light- or nutrient-limitation. Furthermore, deviations between simulation results and data suggest that a shifting phytoplankton community composition can be driven by advective processes or intensive grazing during



the spring bloom. This shift may alter feeding conditions for copepods and in particular impairs energy transfer efficiency from primary to fish production. Consequently, future models should include a more realistic representation of algal community traits for accurately reproducing and forecasting spring bloom phenology and the subsequent ecosystem dynamics.

Overall, both data-analysis and numerical experiments underline the demand for combining plankton traits to process-oriented mechanistic representation of marine (near-shore) ecosystems. Set-up and validation of such models require not only an accurate account of strong variations in currents, temperature, turbulence and light availability, but also of how plankton traits are affected by those factors. By integrating observed interannual variability of phytoplankton spring blooms into numerical experiments, and by careful interpretation of matches and mis-matches between data and model, this approach provides a methodical basis for future models which resolve variability in key ecosystem variables on a larger spectrum of spatial and temporal scales. In order to reduce the uncertainty in investigations of primary production and the ecological role of the planktons in the marine carbon cycle, and to test improved models, my study encourages to intensify the development and use of the cross-shore integrated monitoring systems, which provide a continuous and synoptic environmental state description crossing all relevant sub-compartments at the land-sea interface. This is not only of particular interest for the region of the GB but for other coastal regions that are characterized by similarly strong spatio-temporal variability in physical and biological processes.



# Appendix A

## Biological model equations

In this NPZD-model, phytoplankton ( $P$ ) growth is limited by irradiance and dissolved inorganic nutrients ( $N$ ), zooplankton ( $Z$ ) graze on phytoplankton and the all system is closed with a higher order mortality in the equation for zooplankton. Waste products and dead material form the detritus ( $D$ ) pool, a part of which is assumed to remineralise quickly into nutrient ( $N$ ). All losses due to natural mortality and growth inefficiencies are assumed to be exported to the bottom (Brockmann et al., 1999; Moll, 1997; Radach and Moll, 1993). The equations of the four component ecosystem model take into account turbulent fluxes  $F_i$  ( $i \in \{1, 2, 3, 4\}$ ) of state variables at the lower MLD boundary, sinking of detritus with velocity  $w_g$  and inner biological sources and sinks  $B_i$ , can be written as

$$\frac{\partial}{\partial t} C_i + (u \frac{\partial}{\partial x} + v \frac{\partial}{\partial y}) C_i - (\frac{\partial}{\partial x} k_x \frac{\partial}{\partial x} + \frac{\partial}{\partial y} k_y \frac{\partial}{\partial y}) C_i = B_i - F_i - \frac{w_g}{h} C_3, \quad (\text{A.1})$$

where  $\{C_1, C_2, C_3, C_4\} = \{P, Z, D, N\}$ ,  $t$  is time, and  $h$  is the thickness of the surface mixed layer (column height of the box model). Concentrations of all ecosystem components expressed in  $\text{mmol N m}^{-3}$ .

Biological sources and sinks ( $B_i$ ) and mixing terms  $F_i$  are given by as

$$\left. \begin{aligned} B_1 - F_1 &= (1 - \chi) P_P - G_P - D_P \\ B_2 &= \alpha \cdot G_P + \alpha \cdot G_D - D_Z \\ B_3 - F_3 &= \chi \cdot P_P + (1 - \alpha) G_P + D_P - \alpha \cdot G_D - D_D \\ B_4 - F_4 &= -P_P + \beta \cdot D_Z + D_D - V \cdot (N - N_0) \end{aligned} \right\}, \quad (\text{A.2})$$

where  $P_P = \mu_o \cdot \varphi(T) \cdot \psi(I) \cdot \phi(N) \cdot P$  is the average daily phytoplankton growth rate,  $\varphi(T)$  is the temperature-limited growth function,  $\psi(I)$  is the light-limited growth rate,  $\phi(N)$  is a non-dimensional factor (we assume that nutrients are not limiting given special focus on the spring pre-bloom conditions). The mixing terms are represented as follows:

$$V = \begin{cases} \frac{\nu_H}{h} & \text{if } h = \text{water depth} \\ \frac{\nu_M}{h} & \text{if } h = \text{MLD} \end{cases}$$

The mixing rate considered here is an approximation introduced by Fasham et al. (1993) to account for the exchange rate between the upper-mixed layer and the deep layer in

the box model. Note that this mixing rate does not refer to turbulence diffusivity of the 3D hydrodynamic model. In a 2D scheme for mass transport, the mixing rate is used to import/export material fluxes from/to the bottom boundary at each grid cell.

$G_P$  and  $G_D$  are the grazing rates of zooplankton on phytoplankton and detritus respectively, and  $\alpha$  is the respective assimilation efficiency.  $D_P$  is the rate of the phytoplankton natural mortality,  $D_Z$  is the rate of zooplankton losses due to excretion, natural mortality and higher order predation,  $D_D$  is the rate of breakdown of detritus to inorganic nutrient, and  $\beta$  is a fraction of the zooplankton losses transformed into nitrogen. The remaining part  $1 - \beta$  is assumed to be instantly exported to the bottom waters. Following [Fasham et al. \(1993\)](#), functions  $\varphi(T)$ ,  $\psi(I)$ ,  $\phi(N)$ ,  $D_P$  and  $D_D$  are given by

$$\varphi(T) = Q_{10}^{\frac{T-10.0}{10.0}},$$

$$\psi(I) = \frac{2}{h} \int_0^\tau \int_0^h \frac{I_z}{I_H + I_z} dz dt,$$

$$\phi(N) = \frac{N}{N_H + N},$$

$$D_P = m_P \cdot P, \text{ and } D_D = m_D \cdot D,$$

where  $T$  is the water temperature and  $\varphi(T)$  changes according to a  $Q_{10}$  law, with the maximal growth rate at 10.0 °C. The underwater irradiance at depth  $z$ ,  $I_z$ , is given in Eq.(2.2) and  $\tau$  is the half day length.  $N_H, I_H, Z_H, G_H, m_{P,Z,D}, \mu_o, w_g, \alpha$  and  $\beta$  are model parameters and set to constant values (as reported in Table A.1).

In the case of a biharmonic regime, the ecosystem dynamics is controlled by the zooplankton loss term ([Steele and Henderson, 1992](#)). Here, following ([Fasham et al., 1993](#)), we assume that the processes controlling zooplankton losses can be described by the following expression

$$D_Z = \frac{m_Z \cdot Z^2}{Z_H + Z},$$

where  $m_Z$  and  $Z_H$  are the specific mortality rate and the mortality half-saturation constant. This parameterization better accounts for the differences in seasonal variability of the ecosystem ([Popova, 1995](#)). Zooplankton grazing is parameterized according to a Holling type III function extended to the case of two resources (i.e. phytoplankton and zooplankton):

TABLE A.1: Parameters of the ecosystem model and conversion factors.

Parameter	Symbol	Value	Unit
Phytoplankton maximum growth rate at 10.0 °C	$\mu_o$	1.50	d <sup>-1</sup>
Temperature coefficient	$Q_{10}$	2.20	
Nitrogen half-saturation constant	$N_H$	1.0	mmol N m <sup>-3</sup>
Light half-saturation constant	$I_H$	80.0	$\mu\text{Ein m}^{-2}\text{ s}^{-1}$
Half-saturation constant for Zooplankton loss rate	$Z_H$	0.20	d <sup>-1</sup>
Half-saturation constant for Zooplankton grazing	$G_H$	2.50	mmol N m <sup>-3</sup>
Phytoplankton specific mortality rate	$m_P$	0.05	d <sup>-1</sup>
Phytoplankton exudation rate	$\chi$	0.05	
Zooplankton loss rate	$m_Z$	0.25	d <sup>-1</sup>
Detrital breakdown rate	$m_D$	0.10	d <sup>-1</sup>
Zooplankton maximum specific grazing rate	$g$	0.30	d <sup>-1</sup>
Zooplankton assimilation efficiency	$\alpha$	0.75	
Zooplankton feeding preferences	$p_1, p_2$	0.70, 0.30	
Detrital sinking velocity	$w_g$	1.0	m d <sup>-1</sup>
Nitrogen fraction of zooplankton losses	$\beta$	0.30	
Carbon to Chl ratio	$g_C$	40.0	gC (gChl) <sup>-1</sup>
Carbon to nitrogen ratio	$C:N$	6.625	
Nitrogen concentration below surface mixed water	$N_0$	12.0	mmol N m <sup>-3</sup>
Mixing rate cross the thermocline	$\nu_M$	0.01	m h <sup>-1</sup>
Mixing rate cross water/benthic interface	$\nu_H$	1.0	m h <sup>-1</sup>

$$G_P = \varphi(T) \frac{p_1 \cdot P^2 (g \cdot Z)}{G_H + p_1 \cdot P^2 + p_2 \cdot D^2}, \quad G_D = \varphi(T) \frac{p_2 \cdot D^2 (g \cdot Z)}{G_H + p_1 \cdot P^2 + p_2 \cdot D^2},$$

where  $p_1$  and  $p_2$  are the weighted preferences for phytoplankton and detritus, respectively. Accordingly, the maximum specific grazing rate  $g$  is controlled by the temperature (Oguz et al., 2001), half-saturation constant  $G_H$  and food preference (i.e., food capture efficiency).



# Appendix B

## Abbreviations

---

AVHRR	Advanced Very High Resolution Radiometer
CDOM	Chromophoric dissolved organic matter
CGB	Central German Bight
Chl- <i>a</i>	Chlorophyll- <i>a</i>
COSYNA	Coastal Observing System for Northern and Arctic Seas
ESD	Equivalent spherical diameter
FB	Ferry box
GB	German Bight
GETM	General Estuarine Transport Model
HR	Helgoland Roads
IGB	Inner German Bight
LP	Langeoog pile
MERIS	Medium resolution imaging spectrometer
MODAS	Modular Ocean Data Analysis System
NS	North Sea
PAR	Photosynthetically active radiation
SPM	Suspended particulate matter
SST	Sea surface temperature
TSM	Total suspended matter





# Bibliography

- Aberle, N., Lengfellner, K., Sommer, U., 2007. Spring bloom succession, grazing impact and herbivore selectivity of ciliate communities in response to winter warming. *Oecologia* 150 (4), 668–681.
- Aiken, J., Hardman-Mountford, N., Barlow, R., Fishwick, J., Hirata, T., Smyth, T., 2008. Functional links between bioenergetics and bio-optical traits of phytoplankton taxonomic groups: an overarching hypothesis with applications for ocean colour remote sensing. *J. Plankton Res.* 30 (2), 165.
- Allredge, A., Gotschalk, C., Passow, U., Riebesell, U., 1995. Mass aggregation of diatom blooms: Insights from a mesocosm study. *Deep Sea Res. II* 42 (1), 9–27.
- Allen, J., Holt, J., Blackford, J., Proctor, R., 2007. Error quantification of a high-resolution coupled hydrodynamic-ecosystem coastal-ocean model: Part 2. Chlorophyll-a, nutrients and SPM. *J. Mar. Syst.* 68 (3-4), 381–404.
- Arndt, S., Vanderborght, J., Regnier, P., 2007. Diatom growth response to physical forcing in a macrotidal estuary: coupling hydrodynamics, sediment transport, and biogeochemistry. *J. Geophys. Res.* O 112 (C5), c05045.
- Beck, M., Köster, J., Engelen, B., Holstein, J., Gittel, A., Könneke, M., Riedel, T., Wirtz, K., Cypionka, H., Rullkötter, J., et al., 2009. Deep pore water profiles reflect enhanced microbial activity towards tidal flat margins. *Ocean Dyn.* 59 (2), 371–383.
- Becker, G., Giese, H., Isert, K., König, P., Langenberg, H., Pohlmann, T., Schrum, C., 1999. Mesoscale structures, fluxes and water mass variability in the German Bight as exemplified in the KUSTOS-experiments and numerical models. *Ocean Dyn.* 51 (2/3), 155–179.
- Berger, S., Diehl, S., Stibor, H., Trommer, G., Ruhlenstroth, M., Wild, A., Weigert, A., Jäger, C., Striebel, M., 2007. Water temperature and mixing depth affect timing and magnitude of events during spring succession of the plankton. *Oecologia* 150 (4), 643–654.
- Boon, A., Duineveld, G., 1996. Phytopigments and fatty acids as molecular markers for the quality of near-bottom particulate organic matter in the North Sea. *J. Sea Res.* 35 (4), 279–291.

- Bowers, D., Evans, D., Thomas, D., Ellis, K., Williams, P., 2004. Interpreting the colour of an estuary. *Estuarine Coastal Shelf Sci.* 59, 13–20.
- Boyer, T., Antonov, J., Garcia, H., Johnson, D., Locamini, R., Mishonov, A., Pitcher, M., Baranova, O., Smolyar, I., 2006. World ocean database 2005. Tech. rep., US Department of Commerce, National Oceanic and Atmospheric Administration, National Environmental Satellite, Data, and Information Service.
- Brandt, G., Wirtz, K., 2010. Interannual variability of alongshore spring bloom dynamics in a coastal sea caused by the differential influence of hydrodynamics and light climate. *Biogeosci.* 7, 371–386.
- Bricaud, A., Morel, A., Barale, V., 1999. MERIS potential for ocean colour studies in the open ocean. *Int. J. Remote sensing* 20 (9), 1757–1769.
- Brockmann, C., Dippner, J., 1987. Tidal correction of hydrographic measurements. *Ocean Dyn.* 40 (6), 241–260.
- Brockmann, U., Raabe, T., Hesse, K., Viehweger, K., Rick, S., Starke, A., Fabiszisky, B., TopÇu, D., Heller, R., 1999. Seasonal budgets of the nutrient elements N and P at the surface of the German Bight during winter 1996, spring 1995, and summer 1994. *Ocean Dyn.* 51 (2), 267–291.
- Brockmann, U. H., Raabe, T., Nagel, K., Haarich, M., 1997. Measurement strategy of prisma: design and realisation. *Mar. Ecol. Progr. Ser.* 156, 245–254.
- Broekhuizen, N., Heath, M., Hay, S., Gurney, W., 1995. Modelling the dynamics of the North Sea's mesozooplankton. *J. Sea Res.* 33 (3-4), 381–406.
- Brussaard, C., Riegman, R., Noordeloos, A., Cadee, G., Witte, H., Kop, A., Nieuwland, G., Van Duyl, F., Bak, R., 1995. Effects of grazing, sedimentation and phytoplankton cell lysis on the structure of a coastal pelagic food web. *Mar. Ecol. Progr. Ser.* 123 (1), 259–271.
- Burchard, H., Bolding, K., 2002. GETM- a general estuarine transport model. Scientific Documentation Tech Rep EUR 20253 EN European Commission, 157 pp.
- Burchard, H., Flöser, G., Staneva, J. V., Badewien, T. H., Riethmüller, R., 2008. Impact of density gradients on net sediment transport into the Wadden Sea. *J. Phys. Oceanogr.* 38, 566–587.
- Byun, D. S., Cho, Y. K., 2006. Estimation of the PAR irradiance ratio and its variability under clear-sky conditions at ieodo in the east china sea. *Ocean Sci. J.* 41, 235–244.
- Byun, D. S., Wang, X. H., Zavatarelli, M., Cho, Y. K., 2007. Effects of resuspended sediments and vertical mixing on phytoplankton spring bloom dynamics in a tidal estuarine embayment. *J. Mar. Syst.* 67 (1-2), 102–118.

- Calbet, A., 2008. The trophic roles of microzooplankton in marine systems. *ICES J. Mar. Sci.* 65 (3), 325.
- Chen, C., Ji, R., Zheng, L., Zhu, M., Rawson, M., 1999. Influences of physical processes on the ecosystem in Jiaozhou Bay: a coupled physical and biological model experiment. *J. Geophys. Res.* 104 (12), 29925–29949.
- Cloern, J., 1996. Phytoplankton bloom dynamics in coastal ecosystems: A review with some general lessons from sustained investigation of San Francisco Bay, California. *Rev. Geophys.* 34 (2), 127–168.
- Cloern, J., 1999. The relative importance of light and nutrient limitation of phytoplankton growth: a simple index of coastal ecosystem sensitivity to nutrient enrichment. *Aquat. Ecol.* 33 (1), 3–16.
- Cloern, J., Grenz, C., Videgar-Lucas, L., 1995. An empirical model of the phytoplankton chlorophyll: carbon ratio—the conversion factor between productivity and growth rate. *Limnol. Oceanogr.* 40 (7), 1313–1321.
- Cloern, J., Jassby, A., 2008. Complex seasonal patterns of primary producers at the land–sea interface. *Ecol. Lett.* 11 (12), 1294–1303.
- Cloern, J., Jassby, A., 2009. Patterns and Scales of Phytoplankton Variability in Estuarine–Coastal Ecosystems. *Estuaries Coasts*, 1–12.
- Cloern, J. E., 1987. Turbidity as a control on phytoplankton biomass and productivity in estuaries. *Continental Shelf Res.* 7 (11-12), 1367–1381.
- Colijn, F., 1982. Light absorption in the waters of the Ems-Dollard estuary and its consequences for the growth of phytoplankton and microphytobenthos. *J. Sea Res.* 15 (2), 196–216.
- Colijn, F., Cadée, G., 2003. Is phytoplankton growth in the Wadden Sea light or nitrogen limited? *J. Sea Res.* 49 (2), 83–93.
- Cushing, D., 1990. Plankton production and year-class strength in fish populations: an update of the match/mismatch hypothesis. *Advances in Marine Biology* 26, 249–293.
- Desmit, X., Vanderborcht, J. P., Regnier, P., Wollast, R., 2005. Control of phytoplankton production by physical forcing in a strongly tidal, well-mixed estuary. *Biogeosci.* 2 (2), 205–218.
- Devlin, M.J. and Barry, J., Mills, D., Gowen, R., Foden, J., Sivyer, D., Tett, P., 2008. Relationships between suspended particulate material, light attenuation and secchi depth in UK marine waters. *Estuarine Coastal Shelf Sci.* 79, 429–439.
- Dippner, J. W., 1993. A frontal-resolving model for the German Bight. *Continental Shelf Res.* 13 (1), 49–66.

- Dobrynin, M., 2009. Investigating the dynamics of suspended particulate matter in the north sea using a hydrodynamic transport model and satellite data assimilation. Ph.D. thesis, University of Hamburg.
- Doerffer, R., 2007. The Meris Case 2 water algorithm. *Int. J. Remote sensing* 28 (3), 517–535.
- Doerffer, R., Brockmann, C., 2006. MERIS Case 2 regional processor user manual-version 1.1.  
URL <http://www.brockmann-consult.de/beam/plugins.html>
- Doerffer, R., Schiller, H., 2007. Algorithm theoretical basis document (ATBD): MERIS lake water algorithm for BEAM.  
URL <http://www.brockmann-consult.de/beam/>
- Dring, M. J., Lüning, K., 1994. Influence of spring-neap tidal cycles on the light available for photosynthesis by benthic marine plants. *Mar. Ecol. Progr. Ser.* 104 (1-2), 131–137.
- Ebenhöh, W., Baretta-Bekker, J. G., Baretta, J. W., 1997. The primary production module in the marine ecosystem model ERSEM II, with emphasis on the light forcing. *J. Sea Res.* 38 (3-4), 173–193.
- Edwards, M., Richardson, A., 2004. Impact of climate change on marine pelagic phenology and trophic mismatch. *Nature* 430 (7002), 881–884.
- Egge, J., Aksnes, D., 1992. Silicate as regulating nutrient in phytoplankton competition. *Mar. Ecol. Progr. Ser.* 83 (2), 281–289.
- Ehrenhauss, S., Witte, U., Buhring, S., Huettel, M., 2004. Effect of advective pore water transport on distribution and degradation of diatoms in permeable North Sea sediments. *Mar. Ecol. Progr. Ser.* 271, 99–111.
- Eilertsen, H., Sandberg, S., Tøllefsen, H., 1995. Photoperiodic control of diatom spore growth: a theory to explain the onset of phytoplankton blooms. *Mar. Ecol. Progr. Ser.* 116 (1), 303–307.
- Fasham, M., Sarmiento, J., Slater, R., Ducklow, H., Williams, R., 1993. Ecosystem behavior at Bermuda Station “S” and ocean weather station “India”: A general circulation model and observational analysis. *Global Biogeochem. Cycles* 7 (2), 379–416.
- Franke, H., Buchholz, F., Wiltshire, K., 2004. Ecological long-term research at Helgoland (german bight, north sea): retrospect and prospect-an introduction. *Helgoland Mar. Res.* 58 (4), 223–229.
- Furuya, K., Takahashi, K., Iizumi, H., 1993. Wind-dependent formation of phytoplankton spring bloom in Otsuchi Bay, a ria in Sanriku, Japan. *J. Oceanogr.* 49 (4), 459–475.

- Gaedke, U., Ruhlenstroth-Bauer, M., Wiegand, I., Tirok, K., Aberle, N., Breithaupt, P., Lengfellner, K., Wohlers, J., Sommer, U., 2010. Biotic interactions may overrule direct climate effects on spring phytoplankton dynamics. *Global Change Biol.* 16 (3), 1122–1136.
- Gallegos, C., Correll, D., Pierce, J., 1990. Modeling spectral diffuse attenuation, absorption, and scattering coefficients in a turbid estuary. *Limnol. Oceanogr.* 35 (7), 1486–1502.
- Gayer, G., Dick, S., Pleskachevsky, A., Rosenthal, W., 2006. Numerical modeling of suspended matter transport in the North Sea. *Ocean Dyn.* 56 (1), 62–77.
- Geider, R. J., MacIntyre, H. L., Kana, T. M., 1998. A dynamic regulatory model of phytoplanktonic acclimation to light, nutrients, and temperature. *Limnol. Oceanogr.* 43 (4), 679–694.
- Gentsch, E., Kreibich, T., Hagen, W., Niehoff, B., 2009. Dietary shifts in the copepod *Temora longicornis* during spring: evidence from stable isotope signatures, fatty acid biomarkers and feeding experiments. *J. Plankton Res.* 31 (1), 45–60.
- Gerlach, S., 1995. North Sea research: Where might it go? *Helgoland Mar. Res.* 49 (1), 703–707.
- Gohin, F., Loyer, S., Lunven, M., Labry, C., Froidefond, J., Delmas, D., Huret, M., Herbland, A., 2005. Satellite-derived parameters for biological modelling in coastal waters: Illustration over the eastern continental shelf of the Bay of Biscay. *Remote Sens. Environ.* 95 (1), 29–46.
- Gons, H., Rijkeboer, M., Ruddick, K., 2005. Effect of a waveband shift on chlorophyll retrieval from MERIS imagery of inland and coastal waters. *J. Plankton Res.* 27 (1), 125–127.
- Greve, W., Reiners, F., Nast, J., 1996. Biocoenotic changes of the zooplankton in the German Bight: the possible effects of eutrophication and climate. *ICES J. Mar. Sci.* 53 (6), 951–956.
- Greve, W., Reiners, F., Nast, J., Hoffmann, S., 2004. Helgoland Roads meso- and macrozooplankton time-series 1974 to 2004: lessons from 30 years of single spot, high frequency sampling at the only off-shore island of the North Sea. *Helgoland Mar. Res.* 58 (4), 274–288.
- Hansen, P., 1992. Prey size selection, feeding rates and growth dynamics of heterotrophic dinoflagellates with special emphasis on *Gyrodinium spirale*. *Mar. Biol.* 114 (2), 327–334.
- Harding, L., Program, M. S. G. C., 1994. Long-term trends in the distribution of phytoplankton in Chesapeake Bay: roles of light, nutrients and streamflow. *Mar. Ecol. Progr. Ser.* 104, 267–267.

- Heiskanen, A., Tallberg, P., 1999. Sedimentation and particulate nutrient dynamics along a coastal gradient from a fjord-like bay to the open sea. *Hydrobiologia* 393, 127–140.
- Hickel, W., Mangelsdorf, P., Berg, J., 1993. The human impact in the German Bight: Eutrophication during three decades (1962–1991). *Helgoland Mar. Res.* 47 (3), 243–263.
- Hoffmann, W., Poorter, H., 2002. Avoiding bias in calculations of relative growth rate. *Ann. Bot.* 90 (1), 37–42.
- Holstein, J., Wirz, K., 2010. On the origin of highly active biogeochemistry in deeper coastal sediments—inverse model studies. *Biogeosci.* 7, 2065–2097.
- Hoppenrath, M., 2004. A revised checklist of planktonic diatoms and dinoflagellates from Helgoland (North Sea, German Bight). *Helgoland Mar. Res.* 58 (4), 243–251.
- Huisman, J., van Oostveen, P., Weissing, F., 1999. Critical depth and critical turbulence: two different mechanisms for the development of phytoplankton blooms. *Limnol. Oceanogr.* 44 (7), 1781–1787.
- Iriarte, A., Purdie, D., 2004. Factors controlling the timing of major spring bloom events in an UK south coast estuary. *Estuarine Coastal Shelf Sci.* 61 (4), 679–690.
- Jerlov, N., 1968. *Optical Oceanography*. Elsevier Publishing Co, Amsterdam, 194 pp.
- Joint, I., Pomroy, A., 1993. Phytoplankton biomass and production in the southern North Sea. *Mar. Ecol. Progr. Ser.* 99, 169–169.
- Jonsson, P., 1986. Particle size selection, feeding rates and growth dynamics of marine planktonic oligotrichous ciliates (Ciliophora: Oligotrichina). *Mar. Ecol. Progr. Ser.* 33, 265–277.
- Joseph, J., 1950. Untersuchungen über ober-und unterlichtmessungen im meere und über ihren zusammenhang mit durchsichtigkeitsmessungen. *Ocean Dyn.* 3 (5), 324–335.
- Kara, A. B., Barron, C. N., 2007. Fine-resolution satellite-based daily sea surface temperatures over the global ocean. *J. Geophys. Res.* O 112.
- Kiorboe, T., Saiz, E., 1995. Planktivorous feeding in calm and turbulent environments, with emphasis on copepods. *Mar. Ecol. Progr. Ser.* 122, 135–145.
- Kirk, J., 1994. *Light and photosynthesis in aquatic ecosystems*. Cambridge University Press, 509 pp.
- Knefelkamp, B., Carstens, K., Wiltshire, K., 2007. Comparison of different filter types on chlorophyll-a retention and nutrient measurements. *J. Experimental Mar. Biol. Ecol.* 345 (1), 61–70.

- Kratzer, S., Hakansson, B., Sahlin, C., 2003. Assessing secchi and photic zone depth in the Baltic Sea from satellite data. *Ambio* 32 (8), 577–585.
- Krause, M., Fock, H., Greve, W., Winkler, G., 2003. North Sea Zooplankton: a review. *Senckenbergiana Maritima* 33 (1-2), 71–204.
- Krivtsov, V., Howarth, M., Jones, S., Souza, A., Jago, C., 2008. Monitoring and modelling of the Irish Sea and Liverpool Bay: An overview and an SPM case study. *Ecol. Model.* 212 (1-2), 37–52.
- Kromkamp, J., Peene, J., Rijswijk, P., Sandee, A., Goosen, N., 1995. Nutrients, light and primary production by phytoplankton and microphytobenthos in the eutrophic, turbid Westerschelde estuary (the netherlands). *Hydrobiologia* 311 (1), 9–19.
- Kröncke, I., Dippner, J., Heyen, H., Zeiss, B., 1998. Long-term changes in macrofaunal communities off Norderney (East Frisia, Germany) in relation to climate variability. *Mar. Ecol. Progr. Ser.* 167, 25–36.
- Lacroix, G., Ruddick, K., Park, Y., Gypens, N., Lancelot, C., 2007. Validation of the 3D biogeochemical model MIRO&CO with field nutrient and phytoplankton data and MERIS-derived surface chlorophyll a images. *J. Mar. Syst.* 64 (1-4), 66–88.
- Lancelot, C., Spitz, Y., Gypens, N., Ruddick, K., Becquevort, S., Rousseau, V., Lacroix, G., Billen, G., 2005. Modelling diatom and *Phaeocystis* blooms and nutrient cycles in the Southern Bight of the North Sea: the MIRO model. *Mar. Ecol. Progr. Ser.* 289, 63–78.
- Langenberg, H., 1998. Features of coastal current instabilities in the North Sea: Results of a numerical model. *J. Geophys. Res.* O 103 (C4).
- Le Bouteiller, A., Leynaert, A., Landry, M., Le Borgne, R., Neveux, J., Rodier, M., Blanchot, J., Brown, S., 2003. Primary production, new production, and growth rate in the equatorial Pacific: Changes from mesotrophic to oligotrophic regime. *J. Geophys. Res.* 108 (C12), 8141.
- Litchman, E., Klausmeier, C., 2008. Trait-based community ecology of phytoplankton. *Ann. Rev. Ecol. Evol. Syst.* 39, 615–639.
- Llewellyn, C., Fishwick, J., Blackford, J., 2005. Phytoplankton community assemblage in the english channel: a comparison using chlorophyll a derived from HPLC-CHEMTAX and carbon derived from microscopy cell counts. *J. Plankton Res.* 27 (1), 103–119.
- Lorenzen, C., 1972. Extinction of light in the ocean by phytoplankton. *ICES J. Mar. Sci.* 34 (2), 262–267.
- Losa, S., Kivman, G., Ryabchenko, V., 2004. Weak constraint parameter estimation for a simple ocean ecosystem model: what can we learn about the model and data? *J. Mar. Syst.* 45 (1-2), 1–20.

- Lucas, L., Cloern, J., Koseff, J., Monismith, S., Thompson, J., 1998. Does the Sverdrup critical depth model explain bloom dynamics in estuaries? *J. Mar. Res.* 56 (2), 375–415.
- Lucas, L. V., Cloern, J. E., 2002. Effects of tidal shallowing and deepening on phytoplankton production dynamics: A modeling study. *Estuaries* 25 (4A), 497–507.
- Lucas, L. V., Koseff, J. R., Cloern, J. E., Monismith, S. G., Thompson, J. K., 1999a. Processes governing phytoplankton blooms in estuaries. i: the local production-loss balance. *Mar. Ecol. Progr. Ser.* 187, 1–15.
- Lucas, L. V., Koseff, J. R., Monismith, S. G., Cloern, J. E., Thompson, J. K., 1999b. Processes governing phytoplankton blooms in estuaries. ii: The role of horizontal transport. *Mar. Ecol. Progr. Ser.* 187, 17–30.
- Lucas, L. V., Koseff, J. R., Monismith, S. G., Thompson, J. K., 2009. Shallow water processes govern system-wide phytoplankton bloom dynamics: a modeling study. *J. Mar. Syst.* 75, 70–86.
- Luff, R., Moll, A., 2004. Seasonal dynamics of the North Sea sediments using a three-dimensional coupled sediment-water model system. *Continental Shelf Res.* 24 (10), 1099–1127.
- Luff, R., Pohlmann, T., 1995. Calculation of water exchange times in the ICES-boxes with a eulerian dispersion model using a half-life time approach. *Ocean Dyn.* 47 (4), 287–299.
- Lunau, M., Lemke, A., Dellwig, O., Simon, M., 2006. Physical and biogeochemical controls of microaggregate dynamics in a tidally affected coastal ecosystem. *Limnol. Oceanogr.* 51 (2), 847–859.
- Luyten, P., Jones, J., Proctor, R., Tabor, A., Tett, P., Wild-Allen, K., 1999. Coherens a coupled hydrodynamical–ecological model for regional and shelf seas: user documentation. MUMM report, management unit of the mathematical models of the North Sea, 914 pp.
- Mäerz, J., Wirtz, K., 2009. Resolving physically and biologically driven suspended particulate matter dynamics in a tidal basin with a distribution-based model. *Estuarine Coastal Shelf Sci.* 84 (1), 128–138.
- May, C., Koseff, J., Lucas, L., Cloern, J., Schoellhamer, D., 2003. Effects of spatial and temporal variability of turbidity on phytoplankton blooms. *Mar. Ecol. Progr. Ser.* 254, 111–128.
- Meinke, I., von Storch, H., Feser, F., 2004. A validation of the cloud parameterization in the regional model sn-remo. *J. Geophys. Res.* A 109, D13205.



- Moll, A., 1997. Phosphate and plankton dynamics during a drift experiment in the German Bight: simulation of phosphorus-related plankton production. *Mar. Ecol. Progr. Ser.* 156, 289–297.
- Moll, A., 1998. Regional distribution of primary production in the North Sea simulated by a three-dimensional model. *J. Mar. Syst.* 16 (1-2), 151–170.
- Moll, A., Radach, G., 2003. Review of three-dimensional ecological modelling related to the North Sea shelf system part 1: models and their results. *Progr. Oceanogr.* 57 (2), 175–217.
- Moore, C., Suggett, D., Hickman, A., Kim, Y., Tweddle, J., Sharples, J., Geider, R., Holligan, P., 2006. Phytoplankton photoacclimation and photoadaptation in response to environmental gradients in a shelf sea. *Limnol. Oceanogr.* 51 (2), 936–949.
- Murray, A. G., 2001. The use of simple models in the design and calibration of a dynamic 2D model of a semi-enclosed Australian Bay. *Ecol. Model.* 136 (1), 15–30.
- Murray, A. G., Parslow, J. S., 1999. The analysis of alternative formulations in a simple model of a coastal ecosystem. *Ecol. Model.* 119 (2-3), 149–166.
- Muylaert, K., Gonzales, R., Franck, M., Lionard, M., Van der Zee, C., Catrijsse, A., Sabbe, K., Chou, L., Vyverman, W., 2006. Spatial variation in phytoplankton dynamics in the Belgian coastal zone of the North Sea studied by microscopy, HPLC-CHEMTAX and underway fluorescence recordings. *J. Sea Res.* 55 (4), 253–265.
- Muylaert, K., Tackx, M., Vyverman, W., 2005. Phytoplankton growth rates in the freshwater tidal reaches of the Schelde estuary (belgium) estimated using a simple light-limited primary production model. *Hydrobiologia* 540, 127–140.
- Nelson, D., Smith Jr, W., 1991. Sverdrup revisited: Critical depths, maximum chlorophyll levels, and the control of Southern Ocean productivity by the irradiance-mixing regime. *Limnol. Oceanogr.* 36 (8), 1650–1661.
- Oguz, T., Ducklow, H., Purcell, J., Malanotte-Rizzoli, P., 2001. Modeling the response of top-down control exerted by gelatinous carnivores on the Black Sea pelagic food web. *J. Geophys. Res.* 106, 4543–4564.
- Onken, R., Callies, U., Vaessen, B., Riethmüller, R., 2007. Indirect determination of the heat budget of tidal flats. *Continental Shelf Res.* 27 (12), 1656–1676.
- Pahlow, M., 2005. Linking chlorophyll-nutrient dynamics to the Redfield N: C ratio with a model of optimal phytoplankton growth. *Mar. Ecol. Progr. Ser.* 287, 33–43.
- Pahlow, M., Vézina, A., Casault, B., Maass, H., Malloch, L., Wright, D., Lu, Y., 2008. Adaptive model of plankton dynamics for the north atlantic. *Progr. Oceanogr.* 76 (2), 151–191.

- Passow, U., Alldredge, A., 1995. Aggregation of a diatom bloom in a mesocosm: The role of transparent exopolymer particles (TEP). *Deep Sea Res. II* 42 (1), 99–109.
- Patsch, J., Radach, G., 1997. Long-term simulation of the eutrophication of the North Sea: temporal development of nutrients, chlorophyll and primary production in comparison to observations. *J. Sea Res.* 38 (3-4), 275–310.
- Peters, S., Eleveld, M., Pasterkamp, R., van der Woerd, H., Devolder, M., Jans, S., Park, Y., Ruddick, K., Block, T., Brockmann, C., Doerffer, R., Krasemann, H., Röttgers, R., Schönfeld, W., Jørgensen, P., Tilstone, G., Martinez-Vicente, V., Moore, G., Sørensen, K., Høkedal, J., Johnsen, T., Lømsland, E., Aas, E., 2005. Atlas of chlorophyll-a concentration for the North Sea based on MERIS imagery of 2003. IVM report, Vrije Universiteit, Amsterdam, 117 pp. ISBN 90-5192-026-1.
- Petersen, W., Wehde, H., Krasemann, H., Colijn, F., Schroeder, F., 2008. Ferrybox and MERIS—Assessment of coastal and shelf sea ecosystems by combining in situ and remotely sensed data. *Estuarine Coastal Shelf Sci.* 77, 296–307.
- Planque, B., Fromentin, J., 1996. Calanus and environment in the eastern North Atlantic. I. Spatial and temporal patterns of *C. finmarchicus* and *C. helgolandicus*. *Mar. Ecol. Progr. Ser.* 134, 101–109.
- Platt, T., Bird, D., Sathyendranath, S., 1991. Critical depth and marine primary production. *Proc. Biol. Sci.* 246 (1317), 205–217.
- Pohlmann, T., Raabe, T., Doerffer, R., Beddig, S., Brockmann, U., Dick, S., Engel, M., Hesse, K., König, P., Mayer, B., et al., 1999. Combined analysis of field and model data: A case study of the phosphate dynamics in the German Bight in summer 1994. *Ocean Dyn.* 51 (2), 331–353.
- Popova, E., 1995. Non-universal sensitivity of a robust ecosystem model of the ocean upper mixed layer. *Ocean Model.* 109, 2–5.
- Postma, H., 1982. Sediment transport and sedimentation. *Chem. Biochem. Estuaries*, 153–186.
- Puls, W., van Beusekom, J., Brockmann, U., Doerffer, R., Hentschke, U., König, P., Murphy, D., Mayer, B., Müller, A., Pohlmann, T., Reimer, A., Schmidt-Nia, R., J., S., 1999. Spm concentrations in the German Bight: comparison between a model simulation and measurements. *Ocean Dyn.* 51 (2/3), 221–244.
- Raabe, T., Wiltshire, K., 2009. Quality control and analyses of the long-term nutrient data from Helgoland Roads, North Sea. *J. Sea Res.* 61, 3–16.
- Radach, G., Berg, J., Hagmeier, E., 1990. Long-term changes of the annual cycles of meteorological, hydrographic, nutrient and phytoplankton time-series at Helgoland and at LV Elbe 1 in the German Bight. *Continental Shelf Res.* 10 (4), 305–328.

- Radach, G., Moll, A., 1993. Estimation of the variability of production by simulating annual cycles of phytoplankton in the central North Sea. *Progr. Oceanogr.* 31 (4), 339–419.
- Rast, M., Bezy, J., Bruzzi, S., 1999. The ESA Medium Resolution Imaging Spectrometer MERIS a review of the instrument and its mission. *Int. J. Remote sensing* 20 (9), 1681–1702.
- Raven, J., Waite, A., 2004. The evolution of silicification in diatoms: inescapable sinking and sinking as escape? *New Phytologist* 162 (1), 45–61.
- Reid, P., Lancelot, C., Gieskes, W., Hagmeier, E., Weichart, G., 1990. Phytoplankton of the North Sea and its dynamics: a review. *J. Sea Res.* 26 (2-4), 295–331.
- Renz, J., Mengedoht, D., Hirche, H., 2008. Reproduction, growth and secondary production of *Pseudocalanus elongatus* Boeck (Copepoda, Calanoida) in the southern North Sea. *J. Plankton Res.* 30 (5), 511–528.
- Reynolds, C., 2006. *Ecology of phytoplankton*. Cambridge Univ Pr.
- Riebesell, U., 1991a. Particle aggregation during a diatom bloom. I. Physical aspects. *Mar. Ecol. Progr. Ser.* 69 (3), 273–280.
- Riebesell, U., 1991b. Particle aggregation during a diatom bloom. II. Biological aspects. *Mar. Ecol. Progr. Ser.* 69 (3), 281–291.
- Rixen, M., Book, J., Orlic, M., 2009. Coastal processes: Challenges for monitoring and prediction. *J. Mar. Syst.* 78, S1–S2.
- Ruardij, P., Van Haren, H., Ridderinkhof, H., 1997. The impact of thermal stratification on phytoplankton and nutrient dynamics in shelf seas: a model study. *J. Sea Res.* 38 (3-4), 311–331.
- Schartau, M., Oschlies, A., 2003. Simultaneous data-based optimization of a 1D-ecosystem model at three locations in the North Atlantic Ocean: Part 1. Method and parameter estimates. *J. Mar. Res.* 61 (6), 765–793.
- Schiller, H., Doerffer, R., 1999. Neural network for emulation of an inverse model operational derivation of case II water properties from MERIS data. *Int. J. Remote sensing* 20 (9), 1735–1746.
- Schrum, C., 1997. Thermohaline stratification and instabilities at tidal mixing fronts: Results of an eddy resolving model for the German Bight. *Continental Shelf Res.* 17 (6), 689–716.
- Schrum, C., König, P., Michaelsen, K., Niemeier, U., Pohlmann, T., 1997. Meteorological and oceanographic situation in the German Bight from 23 to 29 april 1991. *Mar. Ecol. Progr. Ser.* 156, 263–273.

- Seuront, L., 2005. Hydrodynamic and tidal controls of small-scale phytoplankton patchiness. *Mar. Ecol. Progr. Ser.* 302, 93–101.
- Sherr, E., Sherr, B., 2008. Heterotrophic dinoflagellates: a significant component of microzooplankton biomass and major grazers of diatoms in the sea. *Mar. Ecol. Progr. Ser.* 352, 187–197.
- Smayda, T., 1974. Some experiments on the sinking characteristics of two freshwater diatoms. *Limnol. Oceanogr.* 19 (4), 628–635.
- Smetacek, V., 1999. Diatoms and the ocean carbon cycle. *Protist* 150 (1), 25–32.
- Smetacek, V., Passow, U., 1990. Spring bloom initiation and sverdrup critical-depth model. *Limnol. Oceanogr.* 35 (1), 228–234.
- Sommer, U., 1994. The impact of light intensity and daylength on silicate and nitrate competition among marine phytoplankton. *Limnol. Oceanogr.* 39 (7), 1680–1688.
- Sommer, U., Lengfellner, K., 2008. Climate change and the timing, magnitude, and composition of the phytoplankton spring bloom. *Global Change Biol.* 14 (6), 1199–1208.
- Stanev, E., Brink-Spalink, G., Wolff, J., 2007. Sediment dynamics in tidally dominated environments controlled by transport and turbulence: A case study for the east Frisian Wadden sea. *J. Geophys. Res. O* 112 (C4), c04018.
- Stanev, E., Dobrynin, M., Pleskachevsky, A., Grayek, S., Günther, H., 2009. Bed shear stress in the southern north sea as an important driver for suspended sediment dynamics. *Ocean Dyn.* 59, 183–194.
- Staneva, J., Stanev, E., Wolff, J.-O., Badewien, T., Reuter, R., Flemming, B., Bartholomä, A., Bolding, K., 2009. Hydrodynamics and sediment dynamics in the German Bight. a focus on observations and numerical modelling in the east Frisian Wadden Sea. *Continental Shelf Res.* 29 (1), 302–319.
- Steele, J., Henderson, E., 1992. The role of predation in plankton models. *J. Plankton Res.* 14 (1), 157–172.
- Stelfox-Widdicombe, C., Archer, S., Burkill, P., Stefels, J., 2004. Microzooplankton grazing in *Phaeocystis* and diatom-dominated waters in the southern North Sea in spring. *J. Sea Res.* 51 (1), 37–51.
- Sündermann, J., Hesse, K., Beddig, S., 1999. Coastal mass and energy fluxes in the southeastern North Sea. *Ocean Dyn.* 51 (2), 113–132.
- Sverdrup, H., 1953. On conditions for the vernal blooming of phytoplankton. *ICES J. Mar. Sci.* 18 (3), 287–295.

- Sverdrup, H., Johnson, M., Fleming, R., et al., 1942. The oceans, their physics, chemistry, and general biology. Prentice-Hall, New York, 1087pp.
- Taylor, A., Watson, A., Ainsworth, M., Robertson, J., Turner, D., 1991. A modeling investigation of the role of phytoplankton in the balance of carbon at the surface of the North Atlantic. *Global Biogeochem. Cycles* 5 (2), 151–171.
- Taylor, K. E., 2001. Summarizing multiple aspects of model performance in a single diagram. *J. Geophys. Res. A* 106 (D7), 7183–7192.
- Tian, T., Merico, A., Su, J., Staneva, J., Wiltshire, K., Wirtz, K., 2009. Importance of resuspended sediment dynamics for the phytoplankton spring bloom in a coastal marine ecosystem. *J. Sea Res.* 62 (4), 214–228.
- Tian, T., Su, J., Flöser, G., Wiltshire, K., Wirtz, K., 2010. Factors controlling the onset of spring blooms in the German Bight 2002–2005: light, wind and stratification. *Continental Shelf Res.* Under the 2nd round of reviews.
- Tian, T., Wei, H., Su, J., Chung, C., 2005. Simulations of annual cycle of phytoplankton production and the utilization of nitrogen in the yellow sea. *J. Oceanogr.* 61 (2), 343–357.
- Tiedje, B., Moll, A., Kaleschke, L., 2010. Comparison of temporal and spatial structures of chlorophyll derived from MODIS satellite data and ECOHAM3 model data in the North Sea. *J. Sea Res.* 64, 250–259.
- Tillmann, U., Hesse, K., 1998. On the quantitative importance of heterotrophic microplankton in the northern German Wadden Sea. *Estuaries Coasts* 21 (4), 585–596.
- Tillmann, U., Hesse, K., Colijn, F., 2000. Planktonic primary production in the german Wadden Sea. *J. Plankton Res.* 22 (7), 1253–1276.
- Tirok, K., Gaedke, U., 2006. Spring weather determines the relative importance of ciliates, rotifers and crustaceans for the initiation of the clear-water phase in a large, deep lake. *J. Plankton Res.* 28 (4), 361.
- Tiselius, P., Kuylenstierna, B., 1996. Growth and decline of a diatom spring bloom phytoplankton species composition, formation of marine snow and the role of heterotrophic dinoflagellates. *J. Plankton Res.* 18 (2), 133–155.
- Townsend, D., Cammen, L., Holligan, P., Campbell, D., Pettigrew, N., 1994. Causes and consequences of variability in the timing of spring phytoplankton blooms. *Deep Sea Res. I* 41 (5), 747–765.
- Troost, T., Kooi, B., Kooijman, S., 2005. Ecological specialization of mixotrophic plankton in a mixed water column. *Am. Nat.* 166, E45–E61.

- Tyrrell, T., Taylor, A., 1996. A modelling study of *Emiliania huxleyi* in the NE atlantic. *J. Mar. Syst.* 9 (1-2), 83–112.
- van Beusekom, J., Fock, H., de Jong, F., Diehl-Christiansen, S., Christiansen, B., 2001. Wadden Sea specific eutrophication criteria. Tech. rep., Wadden Sea Ecosystem No.14. Common Wadden Sea Secretariat, Wilhelmshaven, Germany.
- Van Duin, E. H. S., Blom, G., Los, F. J., Maffione, R., Zimmerman, R., Cerco, C. F., Dortch, M., Best, E. P. H., 2001. Modeling underwater light climate in relation to sedimentation, resuspension, water quality and autotrophic growth. *Hydrobiologia* 444 (1-3), 25–42.
- van Raaphorst, W., Philippart, C., Smit, J., Dijkstra, F., Malschaert, J., 1998. Distribution of suspended particulate matter in the North Sea as inferred from NOAA/AVHRR reflectance images and in situ observations. *J. Sea Res.* 39 (3-4), 197–215.
- Visser, M., Batten, S., Becker, G., Bot, P., Colijn, F., Damm, P., Danielssen, D., Van den Eynde, D., Føyn, L., Frohse, A., et al., 1996. Time series analysis of monthly mean data of temperature, salinity, nutrients, suspended matter, phyto-and zooplankton at eight locations on the Northwest European shelf. *Ocean Dyn.* 48 (3), 299–323.
- Visser, M., de Ruijter, W., Postma, L., 1991. The distribution of suspended matter in the dutch coastal zone. *J. Sea Res.* 27 (2), 127–143.
- Waite, A., Bienfang, P., Harrison, P., 1992a. Spring bloom sedimentation in a subarctic ecosystem. I: Nutrient sensitivity. *Mar. Biol.* 114 (1), 119–129.
- Waite, A., Bienfang, P., Harrison, P., 1992b. Spring bloom sedimentation in a subarctic ecosystem. II: Succession and sedimentation. *Mar. Biol.* 114 (1), 131–138.
- Wei, H., Sun, J., Moll, A., Zhao, L., 2004. Phytoplankton dynamics in the Bohai Sea observations and modelling. *J. Mar. Syst.* 44 (3-4), 233–251.
- Wild-Allen, K., Lane, A., Tett, P., 2002. Phytoplankton, sediment and optical observations in netherlands coastal water in spring. *J. Sea Res.* 47 (3-4), 303–315.
- Wiltshire, K., 2004. Time-series and project data of the biological institute on helgoland. URL <http://www.pangaea.de/Projects/BAH/data.html>
- Wiltshire, K., Dürselen, C., 2004. Revision and quality analyses of the Helgoland Reede long-term phytoplankton data archive. *Helgoland Mar. Res.* 58 (4), 252–268.
- Wiltshire, K., Kraberg, A., Bartsch, I., Boersma, M., Franke, H., Freund, J., Gebühr, C., Gerds, G., Stockmann, K., Wichels, A., 2010. Helgoland Roads, North Sea: 45 Years of Change. *Estuaries Coasts* 33, 295–310.

- Wiltshire, K., Malzahn, A., Wirtz, K., Greve, W., Janisch, S., Mangelsdorf, P., Manly, B., Boersma, M., 2008. Resilience of North Sea phytoplankton spring bloom dynamics: an analysis of long-term data at Helgoland roads. *Limnol. Oceanogr.* 53 (4), 1294–1302.
- Wiltshire, K., Manly, B., 2004. The warming trend at Helgoland roads, North Sea: phytoplankton response. *Helgoland Mar. Res.* 58 (4), 269–273.
- Wirtz, K. W., 2004. A generalized model for adaptation and stress reaction in biosystems. Habilitation thesis, Faculty of mathematics and natural sciences, Carl-von-Ossietzky University Oldenburg.
- Wirtz, K. W., Pahlow, M., 2010. Dynamic chlorophyll and nitrogen:carbon regulation in algae optimizes instantaneous growth rate. *Mar. Ecol. Progr. Ser.* 402, 81–96.
- Wirtz, K. W., Wiltshire, K., 2005. Long-term shifts in marine ecosystem functioning detected by inverse modeling of the Helgoland roads time-series. *J. Mar. Syst.* 56 (3-4), 262–282.
- Xiao, Y., 2000. Modelling temperature-dependency in biology by generalizing temperature coefficient Q10. *Ecol. Model.* 127 (2-3), 283–290.
- Xu, J., Hood, R., 2006. Modeling biogeochemical cycles in Chesapeake Bay with a coupled physical-biological model. *Estuarine Coastal Shelf Sci.* 69 (1-2), 19–46.
- Xu, J., Hood, R., Chao, S., 2005. A simple empirical optical model for simulating light attenuation variability in a partially mixed estuary. *Estuaries Coasts* 28 (4), 572–580.
- Yin, K., Harrison, P., Goldblatt, R., St John, M., Beamish, R., 1997. Factors controlling the timing of the spring bloom in the strait of Georgia estuary, British Columbia, Canada. *Can. J. Fisheries Aquat. Sci.* 54 (9), 1985–1995.





## Acknowledgements

---

Gratitude is dedicated to Prof. Dr. Kai W. Wirtz for his constant encouragement, support and excellent scientific supervision. His scientific creativity and enthusiasm were as instructive as inspiring. Thanks to Prof. Dr. Andreas Oschlies for his second opinion assessment. Many thanks to Prof. Dr. Agostino Merico for kindly being my second supervisor. This research and PhD studies received kind support of Prof. Dr. Francisco Colijn, former director of Institute for Coastal Research at HZG. Respectfully thank him. Additionally I should thank my new boss, Dr. Nicolai Kliem, head of Section for Regional Oceanography, and Dr. Erik Buch, head of Centre for Ocean and Ice at DMI, for their kind encouragements to continue my PhD study.

I thank my officemate, Merja, and my colleagues in the former research group of Ecosystem Modelling at HZG, namely Bettina, Carole, Carsten, Daniela, Gunnar, Jian, Markus Kreuz and Markus Schartau. Particular acknowledgement is made to former colleagues in the other research groups for providing their database and friendly cooperation, namely Joanna Staneva, Mikhail Dobrynin, Gisbert Breitbach, Dagmar Müller, Roland Doerffer, Hajo Krasemann, Rolf Riethmüller, Götz Flöser, Wilhelm Petersen, Ulrich Callies, Mirco Scharfe and Feser Frauke as well as Karen Wiltshire from Biologische Anstalt Helgoland, Alfred Wegener Institute for Polar and Marine Research. I would like to express my appreciation to Dr. P. Thomas and Dr. A. Moll from University of Hamburg, Dr. G. Lacroix from Royal Belgian Institute for Natural Sciences, Dr. D.S. Byun from National Oceanographic Research Institute, South Korea, and Dr. B.A. Kelly-Gerreyn from Southampton Oceanography Centre for giving valuable advices on my scientific articles.

I owe my thanks to my colleague at DMI, Jens Murawski, for translating the abstract in German, and to Jan M Holstein from Bremen and to Vittorio Saggiomo from Netherland for sharing their successful experiences on the dissertation. Many thanks to the administration staff at HZG, Miss Arndt, Miss Hartmann and Mr. Kummerow for facilitating my work. My thanks also owe to Chinese fellows at HZG and my friends, Miss Kong Qi, Miss Tang Xiaohui, Miss Zhu Xiuhua and Mr. Mu Lin.

I owe gratitude to my parents and parents-in-law, Tian, Shuben, Jin, Rong, Su, Haixing and Wang, Jianfen for their patience and encouragement. A whole-hearted thank my husband Dr. Jian Su (i.e. my classmate at College and colleague at HZG) who provides a continuous motivation and support for my study.

Last but not least, I would like to express my deepest thanks to Prof. Dr. Alice Newton, chair coordinator for Erasmus Mundus European Joint Master in Water and Coastal Management, for providing me the opportunity to study in Europe and to broaden my own vision on science and life.



## Curriculum Vitae

---

**Name:** Tian Tian  
**Birth date:** 24.08.1978  
**Birth place:** Liaoning  
**Nationality:** Chinese

12/2008–           Scientist in ecological modelling  
                          Section for Regional Oceanography, Center for Ocean and Ice  
                          Danish Meteorological Institute (DMI), Denmark

06/2008            Accepted as a doctoral candidate  
                          Faculty of Mathematics and Natural Sciences, University of Kiel

04/2006–11/2008   Research assistant  
                          Ecosystem Modelling Group, Institute for Coastal Research  
                          Helmholtz-Zentrum Geesthacht (HZG), Germany

12/2004–03/2006   M.Sc. in Water and Coastal Management  
                          Erasmus Mundus European Joint Master  
                          University of Algarve, Portugal and University of Bergen, Norway

2000–2004         Graduate research assistant  
                          Shallow Seas Group, Institute of Physical Oceanography, OUC

1996–2000         B.S. in Oceanography, Ocean University of China (OUC), China

---



Anlage zur Dissertation

Tian Tian  
Hyltebjerg Allé 38A  
2720 Vanløse

### **Eidesstattliche Erklärung**

Hiermit erkläre ich, Tian Tian, an Eides statt, dass ich die vorliegende Dissertation selbstndig und nur mit den angegebenen Hilfsmitteln angefertigt habe. Die Arbeit ist nach Inhalt und Form, abgesehen von der Beratung durch meinen Betreuer, durch mich eigenständig erarbeitet und verfasst worden. Die Arbeit entstand unter Einhaltung der Regeln guter wissenschaftlicher Praxis der Deutschen Forschungsgemeinschaft. Weder die gesamte Arbeit noch Teile davon wurden von mir an anderer Stelle im Rahmen eines Prüfungsverfahrens eingereicht. Dies ist mein erster Promotionsversuch.

Copenhagen, 12 December 2010

